

Hamburg University of Applied Sciences
Faculty of Life Sciences

Mechanical Design of a Soft Palm and a Tendon-Driven Thumb for an Anthropomorphic Robotic Hand

Master's Thesis

in the study programme
Biomedical Engineering (M.Sc.)

submitted by
Lena Sophie Ewering,
Matr.-Nr. [REDACTED]

Hamburg – Bergedorf
on May 30, 2025

Reviewer: Prof. Dr. Nicholas Bishop (HAW Hamburg)
Reviewer: M.Sc. Oliver Neumann (DLR Oberpfaffenhofen)

The thesis was supervised and prepared in the laboratory
of the German Aerospace Center (DLR), Oberpfaffenhofen

Abstract

Anthropomorphic hands can be useful in many robotic applications, e. g. limb replacement, humanoid service robots, or terrain exploration. Current robotic hands achieve impressive performance in power grasping, but fall short of replicating human dexterity, for which the thumb's mobility and the palm flexion are essential aspects. This work investigates how a robotic hand can benefit from a third degree of freedom in the trapezio-metacarpal joint (TMC) and the use of soft material in the palm. In a kinematic model, three variations of a biaxial TMC did not sufficiently approximate human performance in two common benchmarks, the Total Opposition Test and the GRASP taxonomy, when a newly proposed criterion for fingertip orientation was applied. FEM simulations of the soft material indicated that the palm's structural stiffness can be modulated by notching the soft matrix between the metacarpal bones and by increasing the tendon's lever arm. A 3D-printed, hybrid soft-rigid prototype was built, integrating a custom ball joint for the TMC and a compliant palm with embedded bones. A starting point for the tendon-driven actuation was included in the design but needs elaboration. Further evaluation and iteration of the concept would greatly benefit from a control system for the hand. The prototype developed here is the first anthropomorphic hand featuring an active flexible palm with embedded bones.

Keywords: soft robotics, biomimetics, Kapandji test, GRASP taxonomy, FEM, structural stiffness

Zusammenfassung

In vielen robotischen Anwendungen können anthropomorphe Hände nützlich sein, bspw. als Ersatz eines Körperteils, in humanoiden Service-Robotern, oder in der Geländeerforschung. Bisherige robotische Hände erzielen beeindruckende Leistungen im kraftvollen Greifen, doch erreichen nicht die menschliche Geschicklichkeit, für welche die Beweglichkeit des Daumens und die Beugung der Handfläche essenziell sind. Diese Arbeit untersucht, welche Vorteile ein dritter Freiheitsgrad im Daumengelenk (TMC) und die Verwendung von weichem Material in der Handfläche haben. Die Ergebnisse von drei Varianten eines kinematischen Modells mit biaxialen TMC in zwei verbreiteten Benchmark-Tests, unter Anwendung eines neuen Kriteriums für die Fingerausrichtung, waren keine ausreichende Annäherung der menschlichen Leistung. FEM-Simulationen zum flexiblen Material zeigten, dass die Struktursteifigkeit der Handfläche durch Aussparungen zwischen den Knochen sowie einen größeren Hebelarm der Sehnenaktuierung verringert werden kann. Ein 3D-gedruckter Prototyp wurde erarbeitet, der ein Kugelgelenk im TMC und eine biegsame Handfläche mit eingebetteten Knochen vereint. Ansatzpunkte für die Seilaktuierung wurde im Design berücksichtigt, erfordern jedoch genauere Ausarbeitung. Für die Weiterentwicklung des Konzepts wäre eine Regelung des Handmodells hilfreich. Der hier entwickelte Prototyp ist die erste anthropomorphe Hand, die sich durch eine aktiv-flexible Handfläche mit eingelagerten Knochen auszeichnet.

Stichworte: weiche Robotik, Bionik, Kapandji Test, GRASP Taxonomie, FEM, Struktursteifigkeit

Contents

| | |
|--|-----------|
| List of Figures | ix |
| List of Tables | xi |
| List of Abbreviations | xiii |
| 1 Introduction | 1 |
| 1.1 Motivation and Context | 2 |
| 1.2 Contribution | 3 |
| 2 Background and Related Work | 5 |
| 2.1 The Biomimetic Principle | 5 |
| 2.2 The Human Hand | 5 |
| 2.3 Compliance and Robustness in Robotics | 9 |
| 2.4 State of the Art in Robotic Hands | 10 |
| 3 Thumb Kinematics and Palm Compliance | 15 |
| 3.1 Analysis of Thumb Kinematics | 15 |
| 3.1.1 Evaluation Metrics | 16 |
| 3.1.2 Kinematic Model | 21 |
| 3.1.3 Evaluation Results | 26 |
| 3.2 Linking Kinematics to Structure: The Case for a Compliant Palm | 28 |
| 3.3 Soft Palm – Material and Structural Analysis | 28 |
| 3.3.1 Material Contact Stress Behaviour | 29 |
| 3.3.2 Structural Behaviour | 37 |
| 3.4 Integrated Discussion | 46 |
| 4 Prototype Design and Evaluation | 49 |
| 4.1 Design Process and Criteria | 49 |
| 4.2 Prototype Description | 55 |
| 4.3 Evaluation | 55 |
| 4.4 Discussion | 59 |
| 5 Conclusion and Future Work | 63 |
| Bibliography | 65 |
| A Kinematic Model - Design and Construction | 73 |
| B Evaluation Metrics | 77 |
| B.1 Kinematic Model | 77 |
| B.2 Prototype | 82 |
| C FEM - Ansys Settings | 85 |

| | |
|-------------------------------------|----|
| D Mechanical Drawing Tendon Spindle | 87 |
| E Digital Appendix | 89 |

List of Figures

| | | |
|------|---|----|
| 1.1 | Hand functions in human use | 1 |
| 1.2 | Thesis structure | 4 |
| 2.1 | Anatomy nomenclature | 6 |
| 2.2 | Thumb neutral position and axes | 8 |
| 2.3 | Overview robotic hands | 13 |
| 3.1 | Total Opposition Test description | 17 |
| 3.2 | GRASP taxonomy, reduced set | 18 |
| 3.3 | Opposition angle evaluation | 20 |
| 3.4 | Kinematic model, final version | 22 |
| 3.5 | Kinematic scheme | 23 |
| 3.6 | Hertzian contact, analytical approximation | 32 |
| 3.7 | Parametric study material behaviour | 34 |
| 3.8 | Material behaviour results | 36 |
| 3.9 | Idealised model of palm cross-section | 38 |
| 3.10 | Ansys model sketch | 39 |
| 3.11 | Results of force direction variation, overview | 40 |
| 3.12 | Reaction force for varying actuation force direction | 41 |
| 3.13 | Results of cross-section variation, overview | 43 |
| 3.14 | Reaction force for varying cross-sectional width | 44 |
| 3.15 | Structural stiffness for varying cross-sectional width | 44 |
| 3.16 | Comparison between surrounding and interosseous soft material | 45 |
| 3.17 | Structural stiffness for varying lever arm | 45 |
| 4.1 | Concept sketch variant 1 | 52 |
| 4.2 | Concept sketch variant 2 | 53 |
| 4.3 | Prototype with flexible palm and 3 DoF thumb base joint | 56 |
| 4.4 | Paint-transfer patterns | 58 |
| 4.5 | Prototype kinematics and actuation scheme | 61 |
| 5.1 | Hall sensors suggestion | 64 |
| B.1 | Total Opposition Test on kinematic model, 15° twist | 77 |
| B.2 | Total Opposition Test on kinematic model, 30° twist | 78 |
| B.3 | Total Opposition Test on kinematic model, 45° twist | 78 |
| B.4 | Automatic rotation in biaxial joints | 79 |
| B.5 | GRASP taxonomy on kinematic model, 15° twist | 80 |
| B.6 | GRASP taxonomy on kinematic model, 30° twist | 81 |
| B.7 | GRASP taxonomy on kinematic model, 45° twist | 81 |
| B.8 | Total Opposition Test on prototype | 82 |
| B.9 | GRASP taxonomy on prototype | 83 |
| D.1 | Mechanical drawing tendon spindle | 87 |

List of Tables

| | | |
|-----|---|----|
| 3.1 | Link lengths | 23 |
| 3.2 | Overview kinematic model features | 24 |
| 3.3 | Joint angle limits | 25 |
| 3.4 | TOT kinematic model | 26 |
| 3.5 | GRASP taxonomy kinematic model | 27 |
| 3.6 | Soft material specifications | 29 |
| 3.7 | Hertzian contact parameters | 30 |
| 4.1 | List of requirements | 50 |
| 4.2 | Morphological box | 50 |
| 4.3 | Evaluation matrix | 54 |
| 4.4 | TOT prototype | 57 |
| 4.5 | GRASP taxonomy prototype | 58 |
| C.1 | Ansys simulation settings | 86 |

List of Abbreviations

| | |
|------------|--------------------------------|
| CAD | computer-aided design |
| CMC | carpo-metacarpal joint |
| DIP | distal interphalangeal joint |
| DoF | degree of freedom |
| DP | distal phalanx |
| FEM | finite element method |
| HMC | hamato-metacarpal joint |
| IP | interphalangeal joint |
| MC | metacarpal bone |
| MCP | metacarpo-phalangeal joint |
| MP | medial phalanx |
| PP | proximal phalanx |
| PIP | proximal interphalangeal joint |
| RoM | range of motion |
| TMC | trapezio-metacarpal joint |
| TOT | Total Opposition Test |

1 Introduction

The hands are a central part of humans' agency in the world around them and fulfil a wide variety of functions. Not only are they used to move and manipulate objects in all kinds of ways, they also crucially provide context to the visual perception by interaction with the surroundings [1] and are essential for social interactions [2]. The various functions can be characterised as fine motor skills, rough use, sensory input, or combinations of these categories, as visualised in fig. 1.1. Due to this versatile use, they have developed to become a very elaborate universal tool over the course of evolution. Such a universal tool can also be useful in several robotic applications where the tasks and conditions are not as clearly defined as they usually are for an industrial gripper and may come with varying sets of requirements [3]. Countless robotic hands have been constructed and achieve remarkable performance in many aspects, but they undeniably fall short of the extraordinary dexterity of human hands [4]. While the development of sophisticated control systems and the use of artificial intelligence are certainly indispensable to improve the dexterity of robotic hands, those efforts would go to waste if the underlying mechanical system cannot adequately recreate the necessary motions [5].

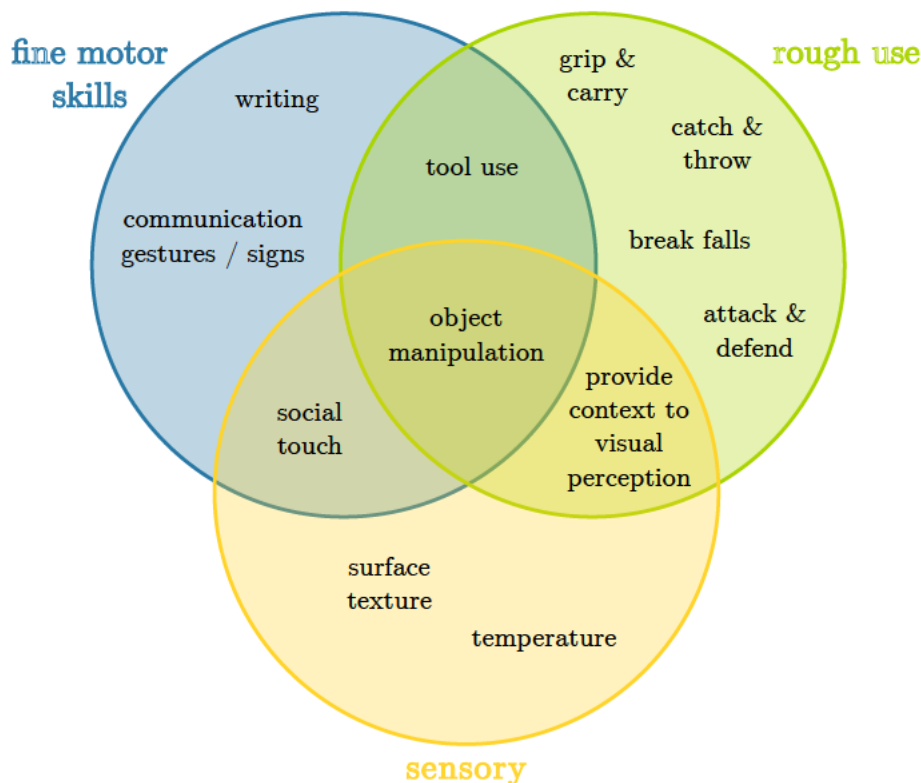


Figure 1.1 Hands fulfil many different functions for humans, that can be roughly grouped into fine motor skills, rough use, and sensory functions, though many tasks involve more than one of these attributes, and no category is completely independent of the others.

1.1 Motivation and Context

The most obvious application for robotic hands are prosthetics and assistance systems like the EDAN robot by the German Aerospace Centre [6] for people with medical conditions that prevent them from using their hands, e. g. tetraplegia, motor neuron diseases or simply old age. In the field of biomedical engineering, patient care robots are an upcoming application, cf. [7], as are humanoid service robots in other contexts, like service industries or domestic assistants, for which human-like manipulation of common objects has been stated as one of the basic requirements [8]. The universality of the hand is also useful in situations where the conditions are unknown, e. g. search-and-rescue missions and deep sea or planetary exploration [9].

In these fields, anthropomorphism of the robot, i. e. making it as similar as possible to the human counterpart not just in aesthetics but also in functionality, can provide several advantages over a purely technical system. Most importantly, in the case of prosthetics and teleoperated systems, it makes the robotic hand more intuitive to use, increasing the acceptance by the prosthetic user and the success rate for the teleoperator in situations where mistakes are expensive and potentially irreparable. Discrepancies between the biological and the robotic hand lead to problems in mapping the motions from one system to the other, which complicates control [10]. An aspect related specifically to the patient care sector is the fact that human touch has been shown to positively affect therapy success [11]. So conversely, a nursing or companion robot feeling very unhuman might affect the patients negatively. While this is only an assumption for now, it should be avoided by argument of the prudence principle. Regarding the aesthetic part, human-likeness has been shown to increase likeability and user acceptance [12]. Additionally, a human's intuitive feeling of whether or not a robotic hand looks "good" actually allows inferences about its functionality. As Grebenstein [13, p. 97] has pointed out, humans, even without any expertise in robotics or hand kinematics, have a solid intuitive understanding of how a hand should behave, stemming from a lifetime of experience in using their own hands. Thus, although the aesthetics of a robotic hand are by no means a sufficient criterion for its functionality, they can serve as an indicator for which parts may need revision.

However, the goal should not be to copy every aspect of the biological hand, but to identify the functionally relevant aspects and implement them by technological means, see section 2.1. Arguably the most important digit for dexterity is the thumb, as has been elaborated upon by various authors, e. g. [2, 13]. Prosthetic as well as other robotic hands can produce powerful grips but are lacking in dexterity, in part because the mechanical thumbs fall short of replicating the full functionality of the biological counterpart [10]. Another notable difference between biological systems and classical robotics is the interplay between rigid and soft structures in biology, whereas engineers traditionally prefer fully rigid systems for the sake of accuracy and controllability. Soft robotics is a comparatively new branch, with noticeable growth in the 21st century, that leverages compliant materials and thus opens up new opportunities, but also presents new challenges, see section 2.3 [3, 14]. In the context of hands, the palm holds the most potential for improvement by soft materials, since it is often a rigid platform in robotic hands, whereas in the biological hand, it flexes and adapts its shape in grasping.

1.2 Contribution

The aim of this work is to devise a mechanical concept and prototype for an anthropomorphic hand that is set apart from existing robotic hands by two features: First, a thumb that kinematically behaves like the human thumb, and second, a stable but flexible palm that allows formation of the palmar arch. While these two may sound like separate aspects, they are interdependent: The best thumb is useless if the rest of the hand does not behave accordingly, and a movable palm is irrelevant if the thumb does not reach proper opposition.

This thesis contains an investigation on the thumb kinematics, specifically regarding the thumb base joint, by the use of two common benchmarks for robotic hands. As an extension to those benchmarks, a new quantitative criterion for the thumb-finger opposition is proposed and tested for usability. Further, finite element method (FEM) simulations are used to examine first the material behaviour of a soft material with a stiffness similar to human cartilage, and then the structural behaviour of an idealised cross-sectional model of a palm. The findings of those analyses are used to devise a prototype for the mechanical design of an anthropomorphic palm including the thumb base joint, with the manufacturing focussed on 3D-printing. In the design, some constraints regarding the integration with other parts of the overarching project, e. g. the wrist and fingers, are taken into consideration, as are certain aspects of the actuation system. However, the actuation system is not designed in detail here, neither are the control or sensor systems dealt with in this work.

An outline of the thesis structure is given in fig. 1.2, with the corresponding chapters indicated: chapter 2 provides background information relevant to the thematic focus, chapter 3 presents the analyses on thumb kinematics and soft palm behaviour, and chapter 4 explains the prototype design. The final chapter 5 will give a conclusion on the present results and prospects for potential future work.

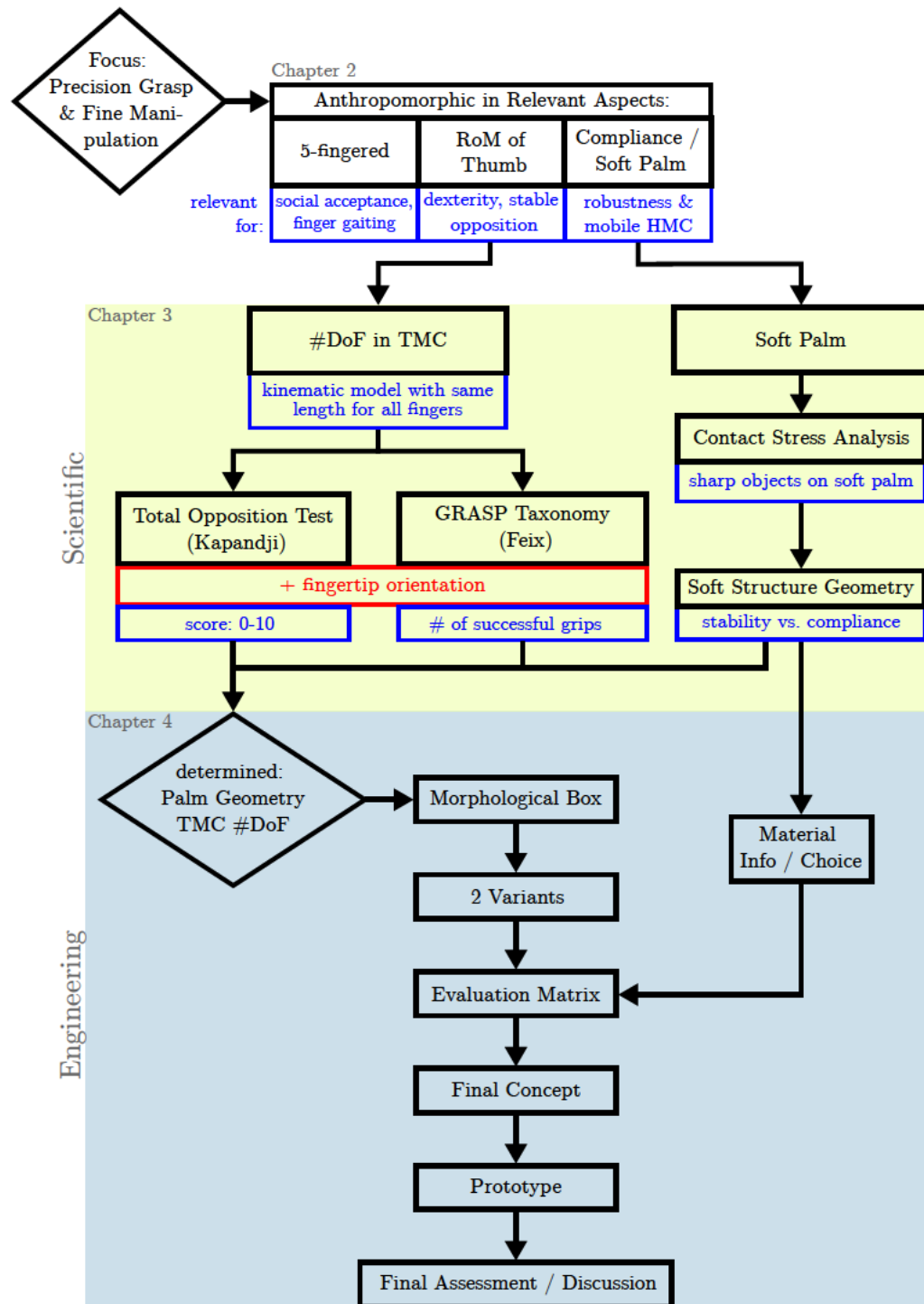


Figure 1.2 Synopsis of the thesis structure, starting with the thematic focus. Two research questions are to be investigated in the scientific part of the project by use of FEM simulations and two benchmark tests for hand kinematics with an added criterion for the fingertip orientation, taking into account certain externally given conditions. These insights will be used to inform the engineering part, where a prototype will be developed and evaluated. For acronyms not yet defined in the preceding text, see List of Abbreviations.

2 Background and Related Work

As a foundation for the studies on thumb kinematics and soft palm behaviour, the relevant theoretical background needs to be explained. Likewise, a summary of the current state of robotic hand technology is necessary to provide context for the subsequent prototype development. Since this work aims to replicate hand functionality as observed in humans, but not to copy the biological hand in its entirety, the fundamental approach of biomimetics will be shortly clarified before going into pertinent aspects of human hand anatomy. Afterwards, the role of compliance and robustness in robotics will be illustrated, and an overview on existing robotic hands will be given.

2.1 The Biomimetic Principle

Biomimetics is a relatively new branch at the interface between natural science and engineering, which aims to drive technological innovation by analysing and abstracting biological systems, as defined in the guideline VDI 6220. The approach is based on the paradigm that any extant biological trait has been optimised for its specific function over millions of years of competitive evolution, and can therefore be considered a viable solution worth looking at for inspiration in technological problem solving. It must be kept in mind, however, that it is only one of many possible solutions to the given problem and not necessarily the best one, because it has been subject to very specific constraints, initial conditions, etc. Researchers should consider that different constraints may apply in the technological setting and that limitations may be imposed by the currently available technology. Therefore, the goal is not to copy every detail from the biological system, but rather to identify the functionally relevant aspects, and use those to work out a technological implementation, often called “abstraction”. Ideally, any flaws that may be present in the biological system due to the evolutionary constraints should also be identified and not transferred in the abstraction process.

2.2 The Human Hand

In keeping with the biomimetic approach just described, the following paragraphs will provide information on the parts of the human hand that are functionally relevant for its prehensile abilities. Particular focus will be put on the thumb, the little finger, and its role in palm flexion.

Firstly, the anatomical nomenclature used in this thesis would merit clarification. For this work, the term “fingers” generally includes the thumb, so that a hand of human configuration would be described as “five-fingered”. If an explicit distinction is necessary, the term “long fingers” will be used as an umbrella term for the index, middle, ring, and little finger, as common in hand literature. As recommended by Napier [2], the fingers will not be numbered but addressed by their common name. The terms for individual bones and

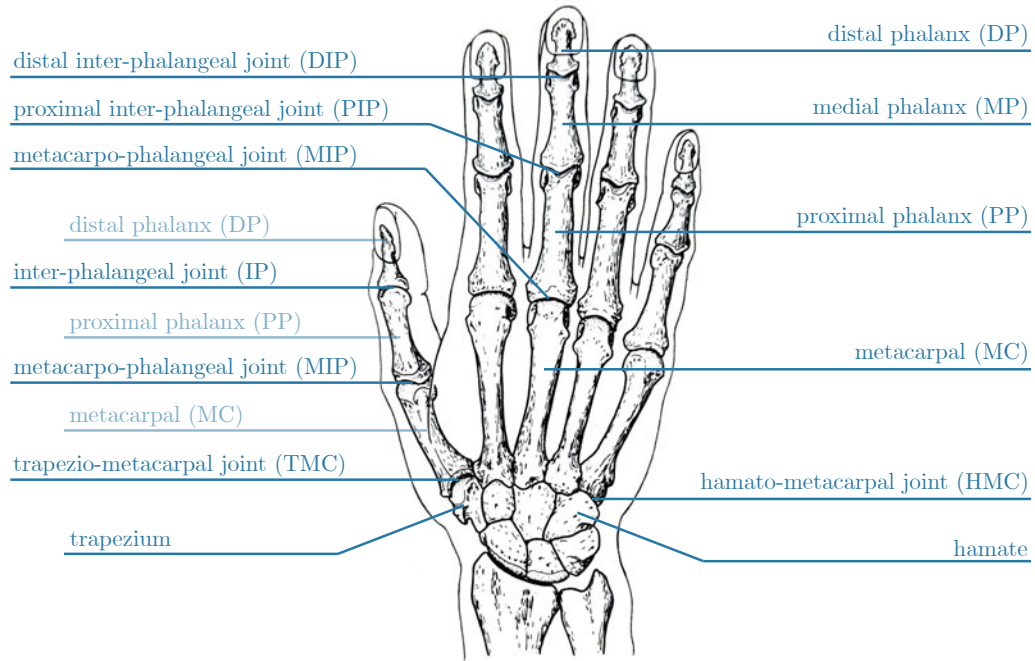


Figure 2.1 Human hand in dorsal view with nomenclature of bones and joints annotated, drawing adapted from [2]. For the sake of clarity, the positions are shown on the middle finger only, but apply analogously to the other long fingers. Similarly, the thumb follows the same naming scheme but has no medial phalanx, thus the redundant terms are repeated in grayed-out labelling.

joints are visualised in fig. 2.1. The bones of the fingers are called phalanges (*sg.* phalanx) and are differentiated by their proximity as distal phalanx (DP), proximal phalanx (PP), and, in case of a third one, medial phalanx (MP). The joint between two phalanges is called an interphalangeal joint (IP), of which the thumb only has one, whereas the long fingers have two, again differentiated by proximity as distal interphalangeal joint (DIP) and proximal interphalangeal joint (PIP). The bones in the palm are called metacarpal bones (MCs), and they articulate with the fingers by a metacarpo-phalangeal joint (MCP). On their proximal end, they articulate with the carpal bones, clustered in the wrist, by carpo-metacarpal joints (CMCs). Of these, only the trapezio-metacarpal joint (TMC), between the thumb and the trapezium bone, and the hamato-metacarpal joint (HMC), between the little finger and the hamate bone, are relevant in this work. [2]

The human hand has certain morphological features that have co-evolved with humans' abilities in tool making and other interactions with the environment and distinguish it from that of other apes and monkeys. Those features include the comparatively long and strong thumb, a mobile metacarpal of the little finger, and the corresponding hypothenar pad as an antagonist to the thenar pad of the thumb. [10, 15]

The Thumb and TMC

The thumb plays a key role in the way humans use their hands, with the loss of function estimated at 30-40% if the thumb is lost. It is visibly different from the long fingers, articulating at the base of the palm and being shorter with one phalanx less. However, when compared to other primate hands, it is remarkably long in relation to the other

fingers, which was evolutionarily useful for strong precision grasps and powerful use of stone tools. The ability to fully oppose the long fingers with the thumb is not unique and can be observed in some other primates, but it is exceptionally developed in humans. In order to provide stable opposition in multi-fingered grasps, the thumb needs to be significantly stronger than each long finger individually. The thumbs of other primates exhibit less rotation and lower grip strength, which led to different strategies for handling objects, e. g. grasping between the thumb and the side of the index finger. [2, 10, 15, 16]

Researchers generally agree that the thumb as a whole has 5 degrees of freedom (DoF) but are not quite unanimous on their exact distribution across the three joints [10, 13]. The IP is consistently described as a 1-DoF joint, but opinions differ on whether the MCP also has 1 and the TMC 3 DoF, or whether both are 2-DoF joints. Regardless of the exact configuration, the resulting movements are flexion / extension, which moves the thumb towards and away from the little finger, adduction / abduction, which moves it in and out of plane with the palm, and pronation / supination, which rotates the fingertip into and out of opposition with the long fingers [1, 2]. This axial rotation is coupled to the other two motions and is actuated by the respective muscles being attached to the dorsal side of the bones and wrapping around the outside to pull into the palm [13, 17]. A photo showcasing the reorientation capabilities of the thumb can be found in [13, p. 69].

The morphology of the TMC has been established to be a saddle joint, which Napier [2] describes to be almost as mobile as a ball-and-socket joint. He also says that it is the only CMC with a saddle joint, which is dissented by [15], see below. Kapandji [1, p. 258 ff.] goes to great lengths to describe the intricate details of the saddle surfaces and the overall joint structure. He touches on two common explanation attempts for which exact aspect of the joint structure enables the pronation movement, namely the “scoliotic” curvature of the saddle surfaces and the laxity in the joint capsule, both of which he finds insufficient for explaining the rotational component. Instead, he states that the TMC can be adequately represented by a biaxial joint, also called universal joint or Cardan joint, and proposes an inherent rotation as an accessory movement of that joint type due to the interplay of the two axes.

Kapandji discusses four ligaments responsible for actuation the TMC, paired into two antagonistic couples, and defines the anatomically neutral position as shown in fig. 2.2 a, where all actuators are in their most relaxed state. The joint axes lie oblique to the three classical anatomical planes, see fig. 2.2 b, and thus the rotations around them are not easily measured by angles in those planes. For that reason, Kapandji introduced the Total Opposition Test (TOT), which uses the hand itself as a reference system without the need for any external measuring devices, see section 3.1.1. Nevertheless, he gives descriptions for the extreme positions on each axis: In maximal adduction, the thumb’s MC reaches the plane of the palm and keeps a 60° angle to the index MC. In abduction, the thumb is described to be almost perpendicular to the palm. In extreme flexion, the tip of the thumb touches the base of the little finger and full extension brings it almost back into the plane of the palm. [1]

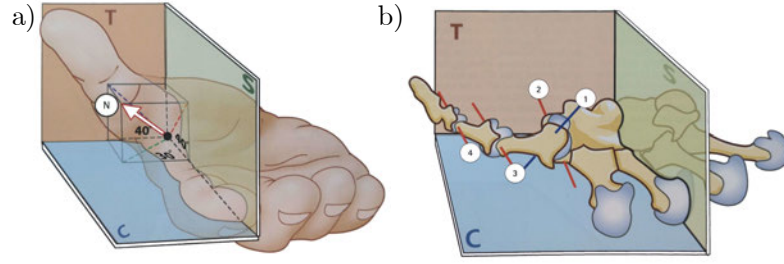


Figure 2.2 Illustrations regarding the anatomy of the thumb in relation to the anatomical planes (coronal, sagittal, transverse), adapted from [1]. a) Anatomically neutral position of the thumb, where all muscles involved in thumb motion are in their most relaxed state. b) Joint axes of the thumb, red for flexion / extension, blue for adduction / abduction.

The Palm and HMC

Any contemplation of the opposition and manipulation abilities in the human hand is incomplete without including the folding of the palm to reorient the ring and little finger towards the thumb [10]. Very similar to the thumb, the little finger’s MC articulates on a saddle-shaped CMC, which enables the distal head of the bone to be displaced in palmar direction and thus arches the palm [15]. The deformable palm has been shown to exhibit a spring-like behaviour when landing on the hands in catching a fall, with the combined stiffness of the wrist and palm determined at $k = 26.7 \text{ kN m}^{-1}$ [18]. Palm flexion can be observed in almost all hand postures where the little finger is not explicitly retracted to flatten the palm, from making a fist to holding a ball between the fingertips. It adapts the hand’s shape to the grasped object and adjust the workspace of the ring and little finger, so that they can both face the object and move around to manipulate it without colliding [1]. This reconfiguration has been shown to be relevant by the fact that surgical joint fusion of the HMC negatively affects palm mobility and leads to collision of the ring and little finger in flexion [15].

The palm features two large soft pads, called “thenar eminence” on the thumb’s side and “hypothenar eminence” on the side of the little finger. Together, they function like a vice to stabilise objects in what is called the “squeeze form” of the power grip, which allows tools like a hammer to be held in line with the forearm, increasing swing length and power of impact. The hypothenar eminence cushions the impact and stabilises the grip in both the dominant and non-dominant hand. This function was important enough for the evolutionary success to become a distinctive trait of the species, distinguishing the human palm from that of a chimpanzee, our closest living relative. As an antagonist to the thenar pad, it needs to be strong enough to oppose the grip force of the thumb and to take heavy impacts in tool use. This is reflected in the bone morphology: The MCs of the little and ring finger are noticeably shorter than those of the index and middle finger. In comparison with other species, the little finger MC is significantly more robust in terms of diameter-to-length ratio, whereas it is the most slender one in non-human primates. The articulating surface of the HMC is oriented with an inward twist and is larger than for the ring finger for better pressure distribution. [15, 19, 20]

Between the grip stabilisation, workspace adjustment, and collision robustness, the flexible palm is highly relevant for everything from power grasping to precise object manipulation and interaction with unknown environments.

2.3 Compliance and Robustness in Robotics

In classical robotics, manipulators like grippers or hands are built from rigid parts, which can usually perform one specific task very efficiently, but struggle to adapt to changing external conditions [14]. They are sensitive to disarticulation and require complex control strategies to avoid collisions with the environment [3]. However, in many robot applications, apart from very well-controlled industrial work stations, collisions with the environment cannot be considered an exception, but should be seen as a standard occurrence and thus taken into account when designing a hand¹. In some cases, collisions might even be desirable, e. g. in reinforcement learning [16]. Robustness by compliance can help a robotic system support such collisions without fatal damage. Additionally, compliance allows a robotic hand or gripper to passively adapt to the shape of an object to provide a more stable grasp [21].

So far, compliance has often been implemented in the software as “active compliance” [21], e. g. by impedance or stiffness control. This maintains well-defined model behaviour for control systems, but disadvantages are the reaction time [22] and the simple fact that anything relying on active control is sensitive to electronic failure or software bugs. An alternative, relatively new approach to the problem is to use soft materials in the construction of the robot to achieve structural compliance, which allows instantaneous, passive reaction to unexpected perturbations. Currently, soft robots still fall victim to limitations in modelling and control algorithms, since conventional controllers are based on the assumption that the robot’s movements can be described by the classical 6 DoF, which is true for rigid-link robots but not for soft structures. Additionally, soft structures are in danger of deforming under their self-weight if not constructed carefully, which further conflicts with current control approaches. However, once new, adequate approaches to the modelling of such systems have been found, they hold the potential for simplifying control schemes by shifting the paradigm from a timid, collision-avoidance approach to more daring strategies that accept or even utilise environment contact. In the case of hands and grippers, stable grips could be achieved without the need for complex grasp planning by leveraging the “morphological computation”, i. e. the contextual adaptation of behaviour due to the physical properties and compliant interactions. This can, for example, be seen in fully soft hands like the one presented in [23] conforming automatically to differently shaped objects when actuated with the same closing command. Additionally, soft robots are generally considered safer for human-robot-interaction, in both industrial and domestic contexts. They are also preferable for prosthetics and rehabilitation devices, since they are better able to conform to the soft tissues of the body and more suitable for replicating the complex motions of biological joints. [3, 14, 24]

The trade-off that comes with soft structures and passive compliance, especially in grasping-related applications, is the danger of insufficient structural support for lifting, holding, and manipulating objects. Hybrid soft-rigid-systems can overcome this problem by combining the stability and accuracy of rigid skeletons with the robustness and flexibility of soft materials [25, 26]. This combination also enables the introduction of structural anisotropy if the embedded skeleton allows motion in one direction but stabilises the structure in another direction.

¹ *internal communication*

While more and more works on hybrid and fully soft robotic systems are being published, Negrello et al. [9] have pointed out that no consensus or common benchmark for the robustness in robotic hands has been established yet. Instead, it is often only reported in the form of anecdotal demonstrations.

2.4 State of the Art in Robotic Hands

Research on robotic hands covers a wide variety of models, from 3-fingered, underactuated versions focused on low complexity to 5-fingered versions with 20+ DoF aiming for maximum dexterity. All of those generally perform well in power grasps [21, 27], but seem to struggle with precision grasps [23]. The kinematic model of the thumb is one of the main sources of differences, since its biomechanics are highly complex and modelling them has been an on-going challenge [10]. The TMC is almost always implemented as a biaxial joint [28], which is also used by Kapandji [1] as an analogy for describing the biological joint, cf. section 2.2. Konnaris et al. [29] constructed it as a ball-and-socket joint, but then restricted the motion to two axes. The number of models taking the palm flexion into account in any way is very limited. Of those, three have an oblique joint in an otherwise flat and rigid palm in the area where the MCs of the ring and little finger would be [13, 29, 30]. Another approach is to fold the rigid palm along an approximately longitudinal hinge, which has been implemented twice [31, 32]. Apart from those discrete articulations, there are two fully soft hands with explicitly actuated palms [23, 33].

Reviews on robotic hand systems in research, specifically with regard to their kinematics and thumb implementation, have been given elsewhere in much more detail than could be done in this short chapter [3, 10, 13, 34]. In order to make a meaningful contribution to those, the overview given here will focus on 5-fingered hands that are in commercial use, with special attention to their thumb and palm configurations, making no claim to be complete. A visual summary is given in fig. 2.3, short descriptions of each hand will be given in the following.

The Awiwi / David Hand was developed by Grebenstein [13] with the aim of replicating human performance as closely as possible. Due to constructional constraints, the thumb has 4 DoF and compensates for the missing 5th DoF by meticulously tuned twist and inclination angles in the MCP and IP. In its original version, the Awiwi hand had an actuated palm joint for reorientation of the ring and little finger, contributing to the hand's impressive performance in the dexterity evaluation. In its adoption to the David robot, the palm DoF was left out to reduce the system complexity. This hand is tendon-driven and served as the main reference for this thesis due to direct contact within the institute. Therefore, it is included in this selection even though it is a research platform and not in commercial use.

The Shadow Dexterous Hand is a tendon-driven system provided by the Shadow Robot Company (London, UK). It is one of only two hands to feature a 5 DoF thumb, with both the TMC and the MCP having two rotation axes. The palm is mostly rigid, but has a separated part below the little finger, which hinges on an oblique axis. It can be teleoperated by a sensor glove also provided by the company. [35]

Phoenix is a general purpose robot by Sanctuary AI (Vancouver, Canada) intended for working in industrial and domestic contexts. A demonstration video showcasing its in-hand manipulation abilities reveals 3 DoF at the base of the thumb and 1 DoF each for the MCP and IP, making it the second hand with a 5 DoF thumb. Actuation of the fingers is driven by a hydraulic system. The palm is rigid without any joints. [36, 37]

Robonaut 2 is the second generation of a system developed by NASA and General Motors Company (Detroit, Michigan, USA) to support astronauts in extra-vehicular activities. Like the first Robonaut version, the hand is tendon-driven. Its thumb is described to have four phalanges with four 1 DoF joints, meaning that there is a considerable distance between the two axes that would constitute the TMC. A fixed twist between the second and third joint is introduced to account for the 5 DoF of a human thumb. The palm is entirely rigid and used to accommodate electronic parts. [38]

Figure 02 is a general purpose robot by Figure AI, Inc. (Sunnyvale, California, USA), similar to the Phoenix system. It has been tested in a production line at a BMW factory. The hand comes with a 4 DoF thumb that consists, like the one in the Robonaut hand, of four phalanges with the first two axes clearly separated into two joints. The long fingers terminate at the MCPs with no actuation of the rigid palm. The actuation system is not clearly specified, but seems to be a direct-drive system with motors placed directly in the hand and fingers, since the demonstration videos show a clear gap at the wrist with no tendons or hydraulic lines running through it. [39]

iCub is an open source humanoid robotic testbed with child-like size and appearance, available from the Istituto Italiano di Tecnologia. The hand is tendon-driven, its thumb has 4 DoF, with the TMC axes being two of only four joints that are not coupled to any other of the overall 19 joints. The palm is rigid and serves as housing for electronics and tendon routing. [40, 41]

Nadine is an extremely life-like social robot developed in the MIRAlab at the University of Geneva, that has been applied in long-term projects as a customer service agent in an insurance company, as a companion in a retirement home, and as an interactive exhibition in a museum. The design was kept very close to the human hand, being the only one of the hands presented here to replicate the bone-and-soft-tissue combination of the biological system. The thumb is connected to the palm by a ball-and-socket joint in at least one version, but it is only actuated on two axes, making for a 4 DoF thumb. Due to the hybrid soft-rigid construction, the palm is in principle flexible but is not included in the tendon-driven actuation. Thus, passive palm flexion would likely occur in interaction, but cannot be actively employed to adapt the hands shape or reorient the fingers. [8, 26, 42–44]

Tesla Gen-3 is the new version of the hand for the general purpose robot Optimus by Tesla, Inc. (Austin, Texas, USA). A demonstration of it was shown at Tesla’s “We, Robot” event in October 2024, of which non-professional footage was shared on social media [45],

where it received attention for its remarkably quick and fluid motions. No official specifications have been published yet, but the footage suggests a 4 DoF thumb and a mostly rigid palm that includes an oblique joint to turn the little finger inwards.

Another category of robotic hands where well-functioning kinematics are indispensable is the prosthetics sector. Remarkably advanced models are the CX hand by Taska Prosthetics (Christchurch, Canterbury, New Zealand), the bebionic hand by Ottobock (Duderstadt, Germany), and the Ability hand by PSYONIC (San Diego, California, USA). However, prosthetic hands are subject to very different constraints and challenges, e. g. even higher demands on the weight and extremely limited neural input available for mapping onto the system control [10]. Therefore, they will not be covered in more detail for this work.

Overall, fully rigid structures and classical control regimes are still very dominant in these anthropomorphic hands. Soft parts can mostly be found as skin-like coverings or pads on dedicated contact surfaces. Consequently, there is a lot of open potential to include the morphological computation described by Zahedi and Ay [46] in future hands.




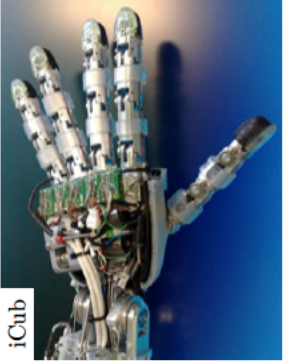




| <div>palm flexion</div> <div>thumb</div> | | yes | | no | |
|--|--|--|--|---|--|
| <div>4 DoF</div> | | <div>Tesla Gen-3</div>  | | <div>Nadine</div>  | |
| | | <div>Awiwi / David</div>  | | <div>iCub</div>  <div>Figure 02</div>  | |
| <div>5 DoF</div> | | <div>Shadow Hand</div>   | | <div>Phoenix</div>  | |

Figure 2.3 Overview of 5-fingered robotic hands in commercial use, sorted by their thumb and palm implementations. Image sources: Tesla Gen-3 [45], Nadine [42], Robonaut 2 [38], Awiwi / David [13], iCub [47], Figure 02 [39], Shadow Hand [48], Sanctuary AI [36].

3 Thumb Kinematics and Palm Compliance

This chapter presents the two parametric studies that were conducted in order to have a sound basis for design choices in the prototype design. One study concerns the thumb kinematics, investigating whether a 2-DoF TMC provides sufficient range of motion (RoM) to replicate the functionality of the human thumb. The other study characterises the behaviour of the soft material by use of FEM simulations, first in simple contact pairings with a rigid material and then in an idealised palm configuration under an approximated actuation load.

In the following sections, each study will be addressed in turn: The underlying hypothesis will be motivated and formulated, the corresponding methods described, and the respective results presented. Afterwards, an integrated discussion on the findings of both studies will be given.

3.1 Analysis of Thumb Kinematics

An extensive study on thumb kinematics has been conducted by Grebenstein [13], yielding valuable insights on robotic thumb design. However, that study was based on the prerequisite that only 4 DoF would be allowed for the entire thumb due to actuation constraints. With the MCP and IP each being a 1-DoF hinge joint, that leaves 2 DoF for the TMC. Grebenstein acknowledged that the human thumb does have 5 DoF and compensated for the missing 5th DoF by meticulously tuning twist and inclination in the MCP and IP axes. This approach introduced contradictory requirements for power grasps and lateral precision grasps [13, p. 103 ff.]. The very parameter that varies between the two is the thumb pronation by the active 5th DoF, so fixing it to match one inevitably impedes the other. Grebenstein decided to tune towards the power grasp, arguing that it is more common in robotic applications. While that is true, it begs the question whether it is more common because it is more important in use or because it is easier to implement, cf. [49].

With that in mind, the present study focuses more on precision grasps. The restriction to a 4-DoF thumb was not given for this project, which leaves the option of a 3-DoF TMC. The additional DoF would come with increased control complexity, and current robotic hands with 2-DoF TMC already achieve a lot of important functionalities. Therefore, in order to decide whether the additional DoF brings a worthwhile increase in performance, two common dexterity benchmarks, namely the TOT and the GRASP taxonomy, were used to show systematically which functions can be achieved with a 2-DoF TMC and which ones are lost by the simplification. As will be explained below, the two metrics will be extended by a new criterion for the fingertip orientation, offering a more objective, quantitative way to assess the thumb-finger opposition. For this, the angle between certain

vectors placed in the fingertips will be evaluated. Specifically, the hypothesis for this study part is:

H: Two degrees of freedom in the trapezio-metacarpal joint are not sufficient to achieve the functional range of motion of the human thumb, as measured by the Total Opposition Test and the GRASP taxonomy, if opposition angles are taken into account.

The TOT and the GRASP taxonomy are routinely used in robotic hand literature to assess human-like dexterity, e. g. [8, 13, 50]. The following sections will explain those two benchmarks along with the reasoning for the newly introduced opposition criterion, and the kinematic model developed to test the kinematics hypothesis will be presented before providing the results of the kinematic metrics.

3.1.1 Evaluation Metrics

The two tests named in the hypothesis focus on different aspects of hand kinematics. The TOT is a quick testing routine to measure thumb mobility after hand surgery and has been widely adopted in robotic literature, where it is usually called “Kapandji test”. The GRASP taxonomy is a set of grasp primitives extracted from extensive footage of human hand usage. Naturally, both contain the orientation of the fingertips as an intrinsic attribute, but neither includes a clear criterion on how to evaluate it.

Total Opposition Test

The TOT was developed by Kapandji [51] to assess the thumb’s range of motion by using the hand itself as a reference system, since Kapandji found the more classical methods of measuring angles in fixed planes unsatisfactory. With the new measurement system, he intended to address two issues: Firstly, he argued that the gradual pronation of the thumb’s fingertip, i. e. its reorientation to meet the other fingers pulp-to-pulp, is not reflected in the classical angular measurements. Secondly, in his clinical routine, he found the determination of angles by external instruments impractical and lacking in precision. Thus, he described 11 positions to be reached successively, using the hand itself as the reference system. The positions are labelled stages 0 – 10, over the course of which the thumb proceeds gradually from a non-oppositional, flat posture of full adduction to a position of maximal abduction and pronation [1, p.306]. Each stage is characterised by the thumb touching a certain part of the respective long finger, as shown in fig. 3.1, starting at the side of the index finger’s PP and ending at the little finger’s MCP. Kapandji acknowledges that the positions can also be reached without any actual opposition motion by having the thumb crawl across the palm rather than following what he calls the “long path of opposition”, but he says in that case “the test is useless” [1]. He offers the example of a cylindrical object like a rolled-up sheet of paper being placed between the thumb and the long fingers: only if that is possible, the test is valid [1, 51].

It is important to note that this procedure is not a pure measurement of opposition, as pointed out in [52]. Neither is it a grasping test in any way, meaning that success in reaching tip-to-tip opposition is not an indicator for how well that hand can grasp or handle various objects. The TOT is a quick and easy assessment of the thumb mobility expected

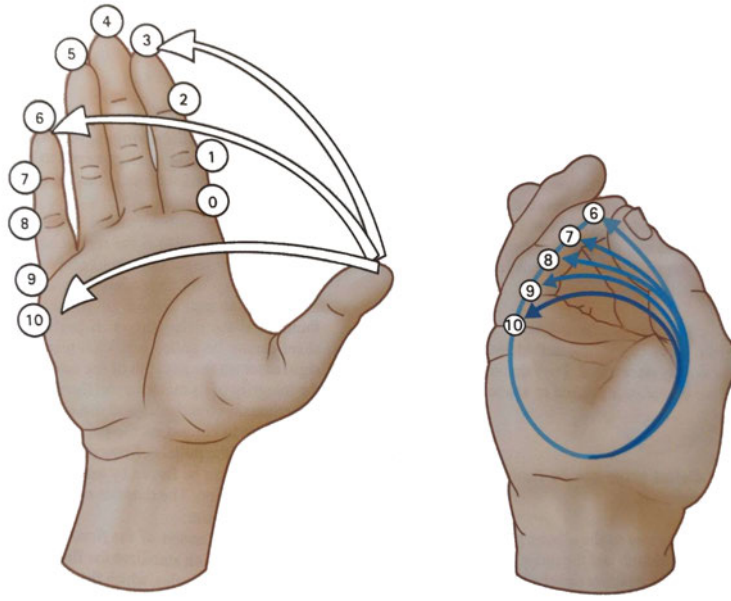


Figure 3.1 Positions used in the Total Opposition Test established by Kapandji to measure the thumb mobility in human hands [1, p.307].

from a clinically unremarkable hand, practical to use without measurement devices and intuitive to perform on a human hand. Not quite so intuitive is the transfer to robotic hands, since the initial parameter space is much more open than what the healthy human hand starts with, allowing unnatural positions not considered in the test. The test was developed on and for biological hands, which means that any deviation from that kinematic configuration, like a soft continuum structure for the thumb or the omission of phalanges, makes the test obsolete.

If the TOT is not a grasping test and depends so heavily on the anthropomorphic kinematic configuration, that begs the question why it should be used at all for robotic hands. The main benefit of evaluating how closely the behaviour of a robotic hand matches that of a human hand would be in teleoperation scenarios like the Surface Avatar project by the European Space Agency. In such contexts, the mapping from control to execution becomes increasingly complicated the more the robot’s behaviour deviates from the human motions [10]. The intention of applying this test to robotic hands should not be solely to show *whether* the thumb can get in contact with the fingers, but to show *how well* it can approach the underlying human performance. That would be facilitated by a quantitative criterion for the degree of success in each posture instead of a binary “yes / no” decision. This idea will be elaborated below by utilising the fingertip orientation as a proxy for observing Kapandji’s requirement of the “long path of opposition”, since that seems to be a challenge in current implementations of the TOT. Additionally, the strict sequence that Kapandji assigned to the stages is often given a more relaxed interpretation in the assessment of robotic hands, e. g. [23, 50, 53]. For the sake of clearer communication, the results could in those cases be reported as the number of successful postures rather than the “Kapandji score” of the highest stage, where a score of 7, for example, implies that all previous stages were also successful. To demonstrate the difference, the results of this study will be reported in both styles in parallel.

GRASP Taxonomy

The GRASP taxonomy is a classification of 33 static one-handed grasps that was synthesised from other taxonomies with the goal of creating one systematic, exhaustive categorisation of human grasping types. It was named after the GRASP project of the European Commission and is not an acronym. The taxonomy was validated against extensive video material of human hand usage. [49]

The grasps are arranged in a matrix with columns for power, precision, and intermediate grasps and rows for thumb position (adducted vs. abducted). Further categorisation criteria were the opposition type, divided into palm, pad, and side, and the “virtual finger”, in which fingers are grouped if they work as a functional unit, often to oppose the thumb. For each grasp, Feix et al. defined a certain object, the specifications of those can be found on the corresponding website [54] under “Dataset”. Many cells contain multiple grasps with similar properties, which are mainly distinguished by the object shape. According to the authors of the taxonomy, those groups can be merged into one grasp representative for the respective cell, which was done for this study. Also, as mentioned above, the present work prioritises precision over power grasping, therefore only grasps from the precision and intermediate columns were used. The “Adduction Grip” was excluded since it does not involve the thumb, so were the “Tripod Variation” and the “Writing Tripod” because they are merely more specialised versions of the “Tripod” grasp. This left 6 grasps to be examined in this study, which are shown in fig. 3.2 in a simplified version of the matrix set up by Feix et al. The specifications of the objects used for these grasps are listed in appendix B.1. For ease of reading, this subset will still be referred to as the GRASP taxonomy hereinafter.







| VF | Intermediate | | Precision | | | |
|----------|--|---|---|--|--|---|
| | 2 | 3 | 2 | 2-3 | 2-4 | 2-5 |
| Abducted | | | Palmar Pinch  | Prismatic 2 Finger  | Quadpod  | Precision Sphere  |
| Adducted | Lateral  | Lateral Tripod  | | | | |

Figure 3.2 Reduced set of the GRASP taxonomy [49] used in this study. VF: virtual finger.

Fingertip Orientation

As mentioned above, biological hands can only exist in a restricted parameter space, while roboticists deal with a much more open parameter space when designing a robotic hand from scratch, with freedom to also implement unnatural configurations. Both of the metrics for human-like hand behaviour described here were developed based on observation of human hands, where reorientation of the fingertips into proper opposition happens automatically when actuating the posture, so it would not have been necessary for the authors to define exact orientations. The issue becomes obvious in cases like [32, 33, 50, 53, 55], where the authors intend to actuate the TOT postures on their robotic hands, but the fingers only come into lateral contact. Since the test definition includes no clear criterion on the fingertip orientation, the postures are deemed successful. Against this background, an additional criterion would be helpful for judging whether the designed hand reaches the required positions with adequate fingertip orientation.

Taniguchi et al. [56] present a method for measuring the angle between the longitudinal axes of the thumb and ring finger DP in opposition as a way to quantify thumb pronation. They visually marked the axes by drawing black lines on the nail surfaces and then measured the angle between them in photographs taken in bird's eye view of the ring fingernail. The root idea of evaluating the orientation of certain axes of the finger is concordant with the procedure suggested below. However, they restricted palm flexion in order to eliminate the rotation of the ring finger, whereas the present work explicitly aims to include the HMC motion and fingertip reorientation. Therefore, Taniguchi et al.'s approach might in principle be useful for generating baseline data of opposition angles in human hands if the methodology was adjusted to include the palm flexion, but their specific results will not be used as a reference here, since they differ in essential boundary conditions. Additionally, the use of the longitudinal axis restricts the result to one very specific posture in a way that is neither necessary nor advantageous for the target information, as will be explained below.

Instead, this work proposes an evaluation of the angle between vectors placed at the fingertips, as depicted in fig. 3.3, based on the local coordinate systems from the computer-aided design (CAD) model. Each axis of those coordinate systems has a vector representing it in the hand's global coordinate system, visualised as red lines in fig. 3.3, which can then be used to find the opposition angle α_{opp} between the two fingers by way of the scalar product, see eq. (1).

$$\alpha_{opp} = \arccos \left(\frac{\vec{v}_{thumb} \cdot \vec{v}_{finger}}{|\vec{v}_{thumb}| \cdot |\vec{v}_{finger}|} \right) \quad (1)$$

Defining which vectors should be paired and what an ideal contact would look like calls for division of the TOT stages into two groups: In stages 0 – 2, the pulp of the thumb lays flat on the side of the index finger, which puts the thumb's x-axis parallel to the y-axis of the respective phalanx of the index finger. Stages 3 – 10 put the fingers in frontal contact, though it is inconsequential whether they touch tip-to-tip, pulp-to-pulp, or somewhere in between. However, the rolling motion between those two extremes hinges around the y-axis of both fingers, which means that those should ideally be parallel. Since real contact will deviate from the ideal definition, a tolerance criterion is needed for which angles are to be accepted as successful contact, visualised as cones around the axis in fig. 3.3.

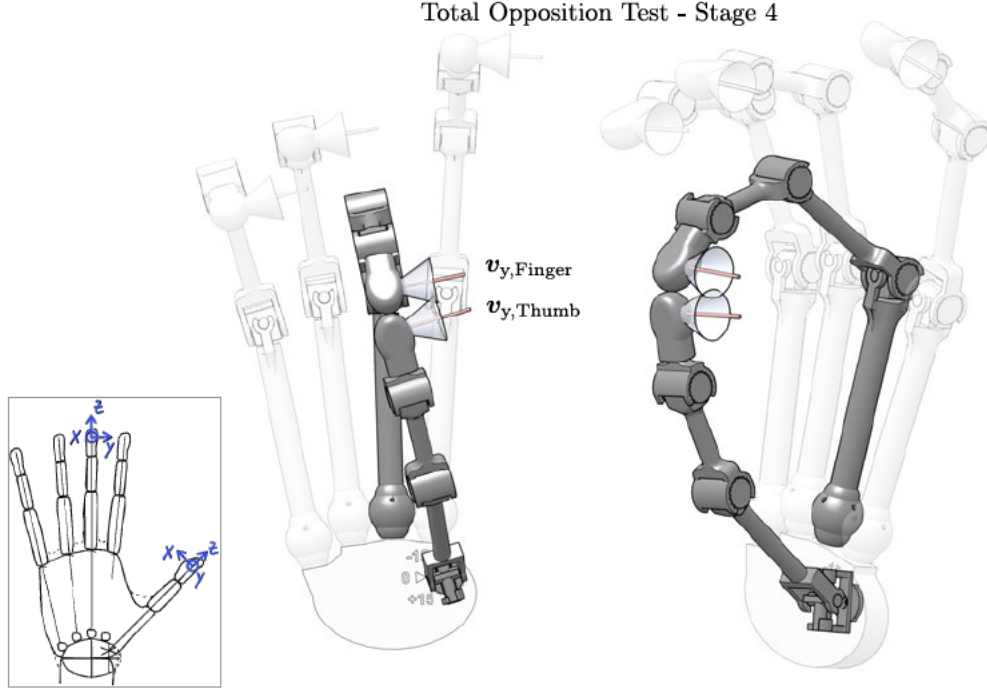


Figure 3.3 Visualisation of the vectors used for evaluation of the opposition angle, the insert shows the underlying coordinate systems in the fingertips. In perfect opposition, the vectors of the y-axes (red lines) would be parallel, the tolerance limit of angles accepted as successful contact are visualised as cones around the vectors.

Assuming ideal force transmission in case of ideal contact, any deviation would introduce a lateral force component, increasing the total force required to reach sufficient normal force and putting lateral load on the joints. Depending on the information available about the robotic hand, the angle can be determined, for instance, based on friction cones, the available actuator force, or lateral joint stiffness; though the aesthetic aspect, as argued in chapter 1, should also be kept in mind. For the early developmental stage of the system in this project, a more general approach was chosen, in which the normal component shall always be at least 90 % of the total fingertip force, which amounts to an angle of ca. 25° . This purely trigonometric approach is subject to some simplification, but will serve the purpose of testing the method to see whether it is expedient as a quantitative criterion for opposition quality.

By the same reasoning, the contact angle evaluation can also be applied to the GRASP taxonomy, though the combination of vectors becomes a bit more complicated to define. Unlike the TOT, the taxonomy grasps do not always consist of a single finger opposing the thumb, but often involve several of the long fingers. These are grouped to a “virtual finger”, as described by Feix et al. [49], which can mathematically be represented by taking the vector sum of their respective fingertip vectors. The resulting vector is inserted for \vec{v}_{finger} in eq. (1). Exceptions apply to the “Tripod” and “Lateral Tripod” grasps, where an angle of approximately 120° between the middle finger’s y-vector and the x-vectors of thumb and index finger would be expected for a stable tripod. The tolerance criterion would then be applied to that expected angle, leading to a range of $120 \pm 25^\circ$.

3.1.2 Kinematic Model

The human hand is an impressive product of evolution, with complicated interactions of subsystems, motion couplings, etc., though not every part is relevant for a kinematic study. In trying to understand such complex structures, models broken down to the fundamental properties can be immensely helpful. As emphasised by Grebenstein [13], the physical interaction with the moving parts is essential for gaining a deep understanding for the system's behaviour. The key is to find a level of abstraction where aspects not directly pertinent to the study focus are removed without oversimplifying or leaving out aspects that affect relevant behaviour.

To this end, Kapandji devised a paper model, which is provided in his book [1]. It represents all finger joints as simple hinges, the TMC as a combination of two orthogonal hinges, and also provides for the palmar offset of the TMC. Grebenstein [13] used that model as a starting point, developed it further, and was able to demonstrate many insightful findings, especially on the effects of twist and inclination of the hinge joints. While this paper model is already useful in many ways, Grebenstein concluded that 3D-printing could be used to extend the concept.

A 3D-printed kinematic model offers several advantages, the most obvious being that the structures are not reduced or projected into a 2D version. This allows better representation of the complex TMC, and its parameters can be varied more easily. The 3D construction also holds the possibility of limiting the RoM of each joint to physiological values described by Kapandji [1]. Additionally, the visual interpretation of fingertip contact is more intuitive if the shape actually resembles that of biological fingers rather than pieces of cardboard meeting with hard edges and flat sides. A minor disadvantage, however, is the higher entry threshold, since 3D-printing equipment and CAD skills are required.

For the purpose of answering the hypothesis presented in section 3.1, such a 3D-printed kinematic model of the human hand was devised, built and applied in this thesis. Several iterations led to the final version shown in fig. 3.4a. A detailed description on constructional features and design choices is given in appendix A. Notable features are the flexible palm and a 2-DoF TMC on a fixture that can be rotated around its third axis in steps of 15° . The first TMC axis intersects the palmar plane far distal to the MCPs (fig. 3.4b), the second axis is orthogonal to the first. For the three variations examined in the evaluation metrics, the TMC was rotated by 15° , 30° , and 45° , respectively (fig. 3.4c-f). Of these, the 30° version is considered the baseline, as it matches Kapandji's description that the thumb meets the little finger base when flexed from neutral position. The other two variations serve to demonstrate the effects of either direction on the performance in the evaluation metrics. The exact rotation angle can be used to compare variations of the same model, but when comparing different hand models to each other, the description of the axis orientation relative to the long fingers should be used, e. g. meeting the little finger. This is the functionally relevant aspect and the corresponding angular value will differ according to the hand morphology: In a more slender hand, this constellation might be reached with 25° TMC rotation, while it might take 40° for a wider hand.

Figure 3.5 shows a kinematic scheme of the joint configuration, the link lengths are given in tab. 3.1. For the sake of modularity, all long fingers were modelled with the same length, which is not physiologically accurate, but will serve the purpose for a first approach and can be iterated upon in future versions of the model. Guided by the RoM

angles described in [1], the joints include end stops to limit them accordingly. A tabular overview of these features and whether they match their biological counterpart or were adjusted for constructional reasons is given in tab. 3.2.

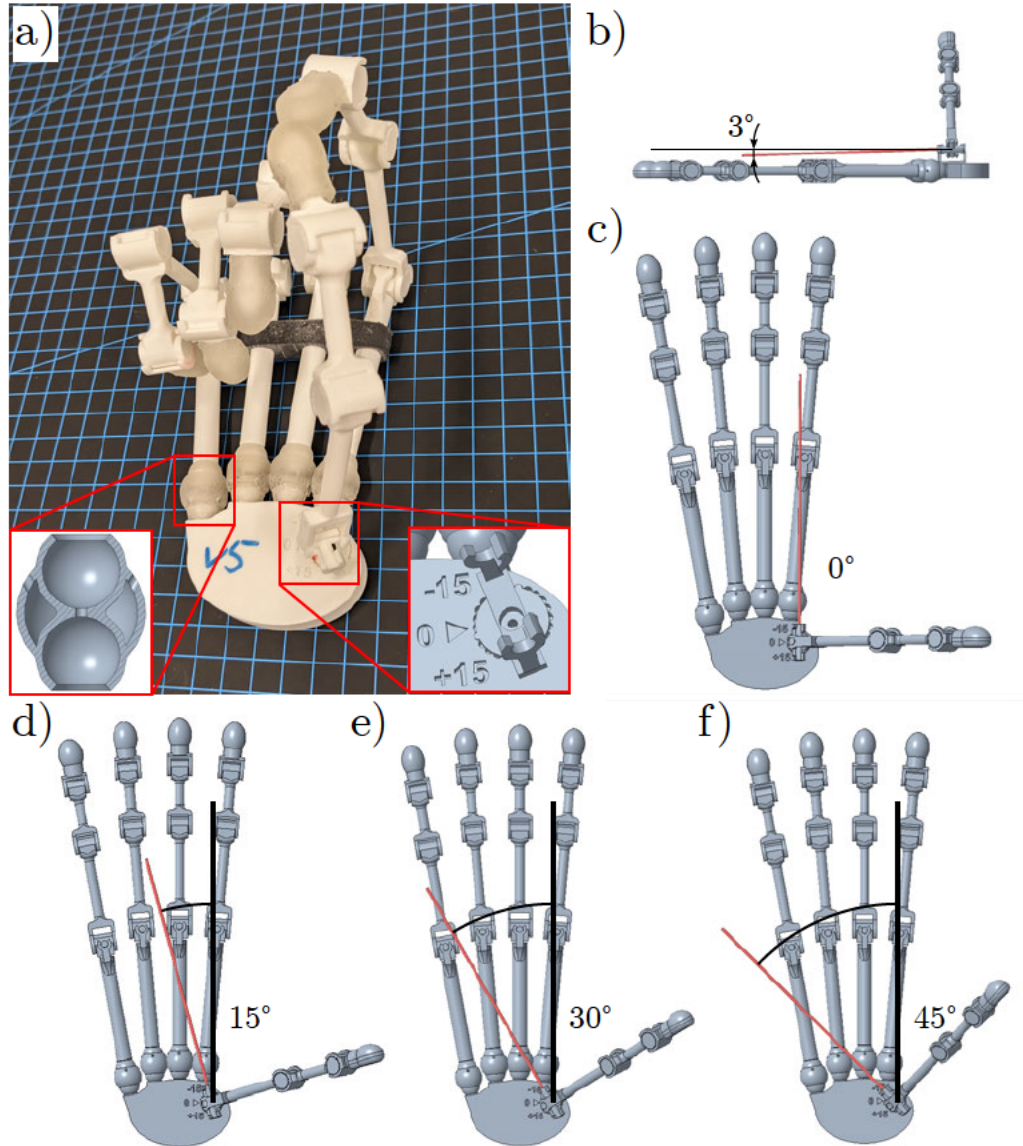


Figure 3.4 Final version of the kinematic model of a human hand, devised to investigate and demonstrate the effects of changing parameters in the TMC on the finger-thumb-opposability and dexterity. a) Photograph of the printed model, with inserts showing a cross-section of the soft joint (left) and a close-up of the adjustable TMC fixture (right). Background grid: 1 cm. b) Inclination of the first TMC axis shown on the CAD model. c) Geometric neutral for the TMC rotation. d-f) Three TMC rotation variants compared in the kinematic metrics.

3.1 Analysis of Thumb Kinematics

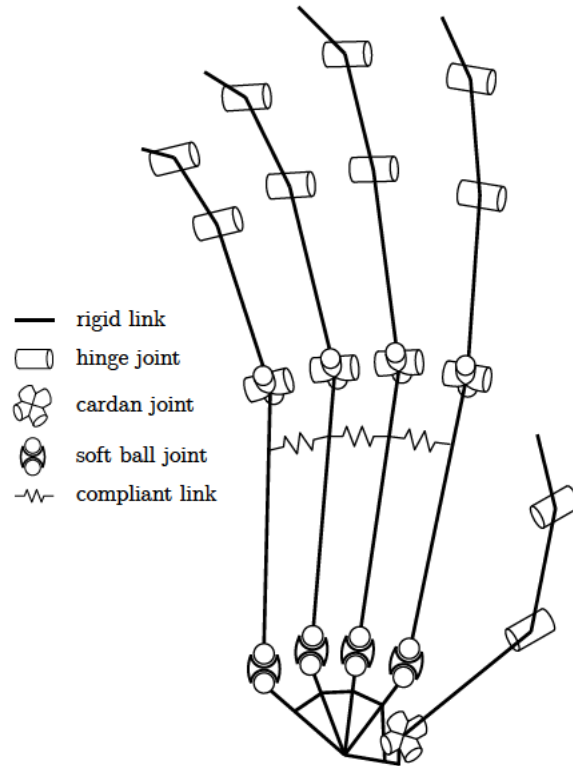


Figure 3.5 Scheme of the kinematic model. All hinge joints are parallel to the corresponding axis in the Cardan joint of the same finger.

Table 3.1 Link lengths used in the kinematic model, for detailed explanation see appendix A.

| link | length [mm] | |
|------------------|--------------|-------|
| | long fingers | thumb |
| distal phalanx | 25 | 30 |
| medial phalanx | 35 | - |
| proximal phalanx | 60 | 40 |
| metacarpal bone | 80 | 60 |

Table 3.2 Overview of relevant features of the 3D-printed kinematic model and whether they match the respective biological counterpart. For detailed explanations, see appendix A.

| | Feature | Implementation | Matches biology? | Note |
|--------------|-------------------------|--|------------------|--|
| thumb | # DoF | 4 | × | main investigation point |
| | TMC joint type | Cardan | (✓) | approximates saddle joint acc. to [1] |
| | TMC palmar displacement | 10 mm | ? | based on [13] |
| | TMC lateral positioning | TMC below index finger | ✓ | personal observation, option for future investigation |
| | | towards little finger ($30^\circ \pm 15^\circ$) | ✓ | var. for investigation |
| | TMC abduction axis | intersect palmar plane not at MCPs (3°) | ? | based on [13] |
| | TMC flexion axis | orthogonal to abduction axis | × | can be approximated as orthogonal acc. to [1] |
| palm | MCP & IP axes | parallel to TMC flexion TMC axis | ✓ | acc. to [1]; tuned to compensate 5 th thumb DoF in [13] |
| | flexion | HMC motion & soft band | ✓ | allows continuous arch |
| | carpus | elliptical platform, ratio 3:2 major to minor axis | × | approximation of the 8 carpal bones |
| long fingers | CMCs | soft capsule | × | for motion in HMC & convenient assembly |
| | MCP joint type | Cardan | ✓ | |
| | PIP & DIP joint type | hinge | ✓ | |
| | PIP & DIP inclination | parallel to MCP flexion | × | s. [13], could be considered in future versions |
| | finger lengths | same for all | × | for modularity |
| | link lengths | approx. based on biological ratios for middle finger | ✓ | see appendix A |
| general | hinge joint limits | end stops | (✓) | guided by descriptions in [1] |

Digital Twin

The 3D-printed kinematic model is useful for physical interaction, but does not provide exact vectors for evaluation of the opposition angles. For that, a digital model was needed that can perform the same movements as the physical one. The kinematic configuration described above was modelled as a motion skeleton in Creo Parametric (version 7.0.6.0, PTC Inc., Boston, Massachusetts, USA), with most of the joints set as pin joints, the TMC as a combination of two pin joints, and the HMC as a gimbal joint with 3 rotational DoF. The above-mentioned RoM limits were added as minimum and maximum angles in the joint definitions, the exact values are listed in tab. 3.3. Since no values were available for the HMC and only small excursions were expected, that joint was left unrestricted.

In the “Mechanism” options, a servo motor was placed on each joint and associated with a unique parameter. These parameters were accessed from a Python script to change the joint angles via a “PyCreoBridge”. The Jupyter notebook containing the script is provided as supplementary material with the digital version of this thesis, see appendix E. In the same script, the 3D-transforms of the fingers involved in the current grasp or posture were read from Creo. Those provide the information necessary to perform the calculation of the opposition angle as explained in section 3.1.1.

For the TOT, the postures were first simulated for the baseline variant with 30° twist in the TMC. For the other two variants, the joint angles of the long fingers were kept the same, and only the thumb position was adapted to reach the required posture, so as to ensure strict comparability. For the GRASP taxonomy, objects modelled after the specifications in [54] were placed by coordinate systems relative to one finger involved in the respective grasp. Again, the postures were simulated for the 30° twist variant, and then only the thumb position was adjusted in the other two variants.

Table 3.3 Joint angle limits prescribed for the kinematic model, positive values are for flexion, negative values represent hyperextension. The limits are generally guided by physiological values, but none were found for the HMC.

| | | joint | min [°] | max [°] |
|-------------|--|---------------|---------|---------|
| long finger | | DIP | -30 | 90 |
| | | PIP | 0 | 120 |
| | | MCP flexion | -40 | 90 |
| | | MCP abduction | -15 | 15 |
| thumb | | IP | -40 | 90 |
| | | MCP | 0 | 90 |
| | | TMC flexion | -30 | 90 |
| | | TMC abduction | -45 | 55 |

3.1.3 Evaluation Results

The opposition angles for all TOT stages and all three TMC variations are listed in tab. 3.4. Pictures of the respective postures can be found in appendix B.1, figs. B.1 to B.3. In strict Kapandji scores, all three models would be left with a score of 0. In the alternative version of scoring, the baseline variant with 30° twist reached 7 of 11 postures within the tolerance limits. The other two both performed 4 postures successfully, but not the same ones.

The 15° variant was best suited for opposition of the index and middle finger, while the 30° variant was successful in all stages after the middle finger. None of the models reached the lateral contact in stages 1 and 2 within the tolerance, but the 45° variant was closest to it. Notably, in the 15° variant, the thumb was unable to reach the opposing long finger at all within the prescribed joint angle limits in all but one of the stages for ring and little finger, and just barely made contact in stage 7, which cannot be called stable opposition. For the sake of argument, the limits were relaxed to see which angles would be necessary to reach the positions. The resulting values are also listed in tab. 3.4, separated by “/”. This did help in reaching opposition of the ring finger, but only produced increasingly absurd positions for all later stages, cf. fig. B.1, appendix B.1.

Table 3.4 Opposition angles from TOT with the kinematic model, three variations of fixed twist in TMC. Entries of “-” indicate that the required position on the finger could not be reached at all within the prescribed joint angles. Values achieved with relaxed joint limits are given separated by “/”. Success of each stage is given individually, but since all stages must be passed in correct sequence, any successful stages after one or more failed stages are practically obsolete and thus given in parentheses.

| stage | +15° | | +30° | | +45° | |
|-------|----------------------|---------------|----------------------|---------------|----------------------|---------------|
| | opposition angle [°] | success (y/n) | opposition angle [°] | success (y/n) | opposition angle [°] | success (y/n) |
| 0 | 15.9 | y | 21.3 | y | 14.0 | y |
| 1 | 60.5 | n | 33.8 | n | 26.0 | n |
| 2 | 62.0 | n | 43.4 | n | 31.7 | n |
| 3 | 21.3 | (y) | 38.8 | n | 51.8 | n |
| 4 | 5.6 | (y) | 30.1 | n | 45.6 | n |
| 5 | - / 10.8 | n / (y) | 19.8 | (y) | 39.2 | n |
| 6 | - / 27.0 | n / n | 9.5 | (y) | 18.6 | (y) |
| 7 | (20.9) / 28.5 | (y) / n | 8.0 | (y) | 16.5 | (y) |
| 8 | - / 38.8 | n / n | 12.9 | (y) | 18.1 | (y) |
| 9 | - / 60.2 | n / n | 17.8 | (y) | 37.5 | n |
| 10 | - / 74.6 | n / n | 19.1 | (y) | 38.7 | n |

3.1 Analysis of Thumb Kinematics

The opposition angles evaluated from the GRASP taxonomy, performed with all three TMC variations, are listed in tab. 3.5. The corresponding pictures can be found in appendix B.1, figs. B.5 to B.7. The 15° variant achieved the best results with 5 of 6 grasps successful, whereas the 30° variant only reached 2 grasps within the tolerance limit. The 45° variant succeeded in the one grasp where the 15° variant failed, but in none of the others.

Table 3.5 Opposition angles from the GRASP taxonomy with the kinematic model, three variations of fixed twist in TMC. For the “lateral tripod” grasp, three angles are given, one for each finger pairing: thumb-index (TI), thumb-middle (TM), index-middle (IM). In contrast to the parallelism criterion of the other grasps, these three angles are expected to be at $120^\circ \pm 25^\circ$.

| grasp | $+15^\circ$ | | $+30^\circ$ | | $+45^\circ$ | |
|--------------------|----------------------------|---------------|----------------------------|---------------|----------------------------|---------------|
| | opposition angle $[\circ]$ | success (y/n) | opposition angle $[\circ]$ | success (y/n) | opposition angle $[\circ]$ | success (y/n) |
| lateral | 43.7 | n | 28.6 | n | 18.6 | y |
| lateral tripod | 110.5 (TI) | y | 110.0 (TI) | y | 107.3 (TI) | n |
| | 129.6 (TM) | | 139.8 (TM) | | 146.9 (TM) | |
| | 101.9 (IM) | | 101.9 (IM) | | 101.9 (IM) | |
| palmar pinch | 24.7 | y | 31.4 | n | 38.9 | n |
| prismatic 2 finger | 18.6 | y | 37.0 | n | 52.4 | n |
| quadpod | 16.0 | y | 33.0 | n | 50.1 | n |
| precision sphere | 9.7 | y | 24.7 | y | 40.9 | n |

3.2 Linking Kinematics to Structure: The Case for a Compliant Palm

The two kinematic metrics presented above are entirely based on human hands, which means that their very core idea assumes that the hand they are applied to exhibits the kinematic configuration of a human hand. Therefore, any robotic hand that is to be evaluated by either of those tests should be as close as possible to the biological hand in its kinematics. If that is not the case, the resulting postures are only remote resemblances of the ones defined in the metrics, and the conclusions drawn from them about the anthropomorphism of the respective hand hold danger of overinterpretation of the data.

The thumb mobility and opposability, which has been dealt with in the previous sections and receives copious attention in the literature, is probably the most striking feature of human hand kinematics. No less important for the kinematic configuration is the compliant palm. Its relevance in the biological hand has been described in section 2.2, but it lacks representation in robotic hands, cf. section 2.4. The rise of soft materials in robotics now provides an opportunity to include flexion of the palm, not just by folding it along a discrete hinge or making an entirely soft hand, but by implementing the bone-and-soft-tissue configuration found in the biological hand. The following sections will give further insight on this idea.

3.3 Soft Palm – Material and Structural Analysis

The issue of the soft articulated palm was approached from a very general perspective at first, gradually narrowing down to simulations closer to the structure in the robotic hand. Since this type of robotic palm has little precedence, the options for the research focus were very open with only few *a priori* restrictions. The main anchor was the soft material available at the institute, which were two kinds of UV-curing resins for stereolithography 3D-printing available from Formlabs, Inc. (Somerville, Massachusetts, USA): “Elastic 50A Resin”, a silicone-like elastomer, and “Silicone 40A”, a pure silicone material. The main material properties are listed in tab. 3.6, the data sheets are provided as supplementary material with the digital version of this thesis, see appendix E. The elastic resin used here was the first version of the product. Formlabs has since released a new version called “Elastic 50A Resin V2” with marginally different material properties from the ones listed here.

Two research questions regarding the material and structural behaviour of a soft palm were investigated. The first step was to examine how the pure soft material interacts with rigid material, which could be anything from environment structures to tools or grasped objects. The specific question was formulated as follows:

Q: In unidirectional pressure contact, how do rigid body geometry and soft material thickness affect the stress in the soft body?

Secondly, an idealised cross-section through the MCs was modelled with connecting soft material, where an actuation force was applied to the bone of the little finger to induce the palm flexion. Different parameters were varied successively to answer the question:

Q: How do the cross-sectional geometry of the soft material and the application of the actuator force influence the displacement of the little finger metacarpal bone and the generated grip force?

For each of these research questions, the simulation methods and results will be presented consecutively in the following sections.

Table 3.6 Material properties of the two soft resins available for this work, both products by Formlabs, Inc.

| | Elastic 50A | Silicone 40A |
|-------------------------|-------------|--------------|
| Shore hardness | 50A | 40A |
| tensile strength [MPa] | 3.23 | 5 |
| elongation at break [%] | 160 | 230 |

3.3.1 Material Contact Stress Behaviour

Since the robotic hand’s main function will be to interact with the environment, it will routinely be in contact with other objects. With the goal of this project being to incorporate soft components into the hand, contact between rigid objects and those soft components becomes a relevant scenario for which the material behaviour should be investigated.

This contact situation can become increasingly complex, but a simple, straightforward approach to characterising a material’s interaction behaviour is the Hertzian contact stress analysis, where object primitives, i. e. spheres, cylinders, and plates, interact under uni-directional pressure. The calculation assumes small deformations in the elastic range, as they would occur in classical engineering materials like steel or other metals. Soft materials like silicone, however, allow much more elastic deformation to a point where the stress distribution in the material would not be accurately represented anymore by the Hertzian equation, s. below. Instead, FEM simulations can be used to represent a soft body deforming against a rigid object. Thus, the analytical calculation of Hertzian pressure was used as a starting point for investigating the behaviour of silicone-like materials, with the low-force range serving as a plausibility check for subsequent FEM simulations of the same object primitives.

Analytical Approximation

As an analytical baseline, a parametric study of Hertzian contact between a rigid body of circular cross-section and a soft body of various geometry was conducted. The corresponding FEM analysis would later be done as a 2D simulation with constant thickness, which corresponds to two cylinders meeting in parallel orientation. The contact area would start out as a line and then gradually broaden into a rectangle as the two cylinders deform and flatten slightly. The maximum compressive stress in the centre of that contact area can be found by eq. (2).

$$p_0 = \sqrt{\frac{F \cdot E}{2\pi \cdot r \cdot l \cdot (1 - \mu^2)}} \quad (2)$$

with:

$$r = \frac{r_1 \cdot r_2}{r_1 + r_2}$$

$$E = \frac{2 \cdot E_1 \cdot E_2}{E_1 + E_2}$$

where F is the force in N, $E_{1,2}$ is the Young's modulus of cylinder 1 and 2 respectively in N m^{-2} , $r_{1,2}$ is the radius of cylinder 1 and 2 respectively in mm, l is the length in contact in mm, and μ is the Poisson's ratio for both bodies.

The variables of interest were the material stiffness of the soft body, the body geometry, and the contact force. Their value ranges are listed in tab. 3.7. The stiffness of the soft material to be used in later application was expected to lie somewhere in the range of 1 - 10 MPa, so the value was varied around that. The stiffness of the rigid body was chosen at 10^9 MPa, much higher than that of the soft body in all variations, so as to make deformations of the rigid body negligible. The flat soft body is represented by a very large radius, chosen at 10^9 mm.

Table 3.7 Values or ranges used for the parametric study on Hertzian contact between soft and rigid body.

| parameter | unit | value (range) |
|--------------------|------|------------------------------|
| F | N | 10^x with $x = 0 \dots 6$ |
| E_{soft} | MPa | 10^x with $x = -2 \dots 4$ |
| E_{rigid} | MPa | 10^9 |
| r_{soft} | mm | $[-200, 100, 10^9]$ |
| r_{rigid} | mm | $[1, 100]$ |
| l | mm | 10 |
| μ | - | 0.5 |

The calculated stresses for all six geometry pairings and all combinations of contact force and soft body stiffness are plotted in fig. 3.6. Of the two materials available, the lower tensile strength is plotted as a reference plane in red. The Matlab script for obtaining those values is provided as supplementary material with the digital version of this thesis,

see appendix E. While this rough inspection does not yield precise quantitative insights, it does give an overview on how sensitive the stresses are to each parameter, and thus which parameter might be particularly relevant for closer examination.

Overall, a considerable portion of the graph falls below the reference plane, meaning that there is a realistic range of force and stiffness combinations in which the material can be expected to support the stress. Changes in force or stiffness have roughly the same effect on the plotted stress. It should be kept in mind, however, that for combinations of low stiffness and high force, i. e. the right-hand corner of the graph, the analytical solution cannot be assumed to be accurate since the assumption of small deformation will be violated, see above.

For the pairings with the large rigid body, the stresses are noticeably lower than with the small one, i. e. a larger part of the graph is below the tensile strength plane. In these three pairings, the soft body geometry takes a discernible effect on the resulting stress: Though not easily visible on the log scale, the peak stress reduces by half, from ca. 2060 MPa for the convex soft body to ca. 1030 MPa for the concave one. In the three pairings with the smaller rigid body, the stress peak is considerably higher and barely affected by the soft body geometry, dropping only by 0.75 % from 14 640 MPa for the convex soft body to ca. 14 530 MPa for the concave one. Thus, it seems that contact bodies with a small radius are a significant stress factor and would merit closer inspection. In the application context, this would correspond to gripping or colliding with thin wires or sharp objects like needles and shards.

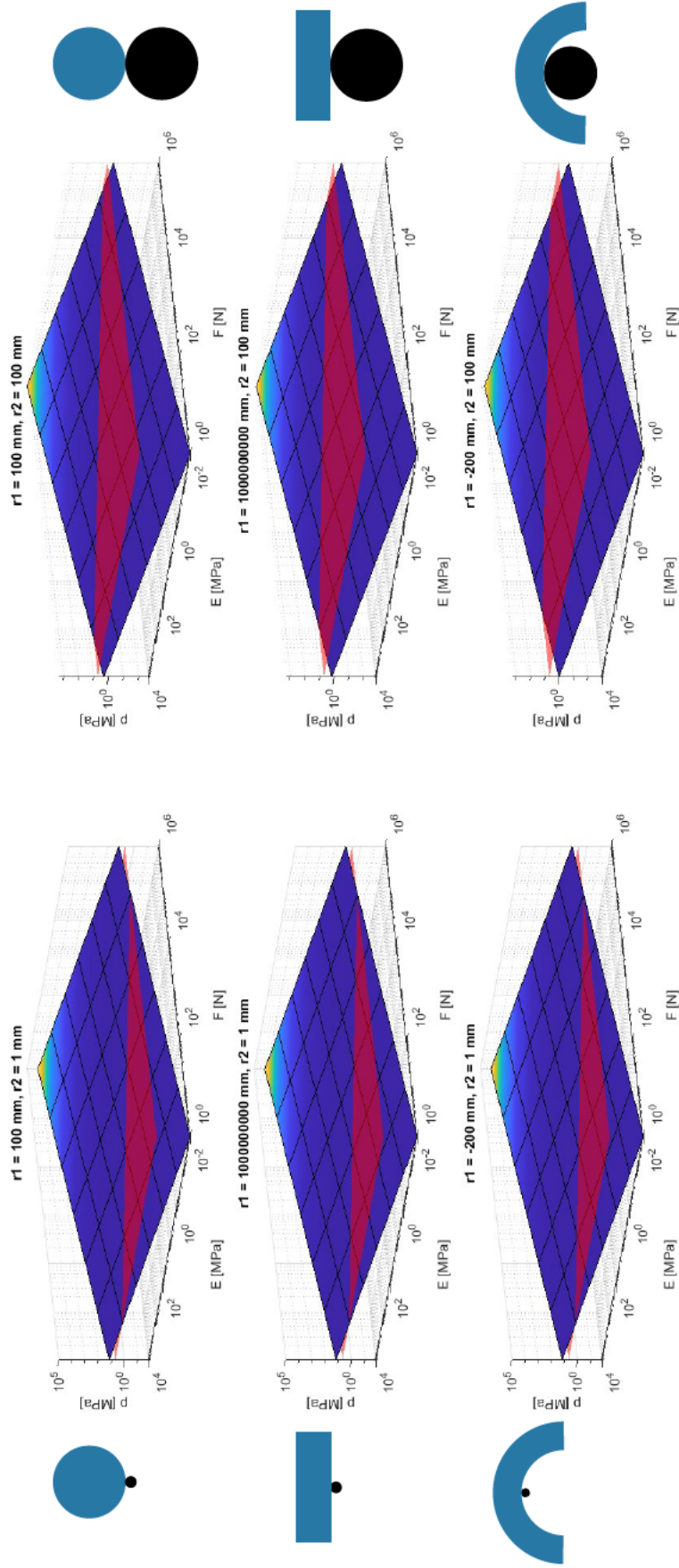


Figure 3.6 Hertzian contact stresses calculated for a range of forces and Young's moduli for the soft body in different combinations of body geometries, all axes log-scaled. The respective shape combination is indicated by icons next to each plot, soft body represented in red, rigid body in grey, icons not to scale.

Methods

As already mentioned, the soft material deforms more than allowed for in the Hertzian contact stress calculation. At the point where the assumptions of the analytical approach are left, numerical simulation, i. e. FEM, can take over. By default, FEM structural analysis also assumes linear Hookean behaviour with small deformations. To deal with cases where structures are expected to exhibit significant deformation, FEM software generally offers an option to solve for large deformations, without having to leave the classical mechanics modelling and employ more complex, non-linear modelling approaches.

Following this simpler approach of large deformation modelling in classical mechanics simulation, pressure contact between a soft and rigid body with the properties given above was simulated in Ansys Workbench (Ansys, Inc., Canonsburg, Pennsylvania, USA). First, as a verification that the chosen modelling approach is viable, the contact pairings from the analytical approximation were recreated. From that starting point, building on the conclusion from the analytical approximation, the effect of the rigid body's size on the stress in the soft material was examined more closely. The soft body was kept flat from this point on, since the analytical comparison had indicated that the soft body geometry does not have a noteworthy effect on the stress when the rigid body is small and the flat shape is the easiest one to construct and constrain in the FEM simulations. More specifically, the soft body was brought into pressure contact with convex rigid bodies of radius 10 mm, 1 mm and 0.5 mm. With regard to the application context, where usage of the soft material as a skin for the robotic hand would be conceivable, it was also investigated how the height of the soft body, from 10 mm down to 0.25 mm, affects the resulting stress at a constant force of 5 N, compared for rigid body radii of 1 mm and 0.5 mm. This height in simulation corresponds to the skin thickness in physical application. Extending this idea, the contact was also modelled with a rigid-bodied bone embedded in the soft material, pushing against a contact body of radius 0.5 mm. In this model, the diameter of the bone was increased so that the thickness of the "skin" layer covering it decreased. Lastly, the smallest rigid body ($r = 0.5$ mm) was constructed as a salient on a larger flat plate to simulate an object with sharp protrusions or an irregular surface and compare it to the same-sized isolated rigid body. A schematic overview on which parameters were varied in the simulations is given in fig. 3.7.

Material Properties Characterisation of rubber-like materials is often provided by several stress-strain value pairs rather than giving a single value for the Young's modulus because their stiffness behaviour is not linear [57]. Nevertheless, a scalar value was needed for the FEM approach chosen here, so the value pairs provided in the data sheets were used to calculate a mean value for each of the two available materials named in section 3.3. Those amounted to ca. 1.48 MPa for the Elastic 50A resin and ca. 1.57 MPa for the Silicone 40A resin, the detailed values can be found in the corresponding Matlab script provided as supplementary material with the digital version of this thesis, see appendix E. This being a parametric study, where values need to be realistic for the general type of material but not necessarily accurate to one specific material, 1.5 MPa was chosen as a representative value for the Young's modulus of the simulated soft material. This value approximately matches the modulus of human cartilage [14].

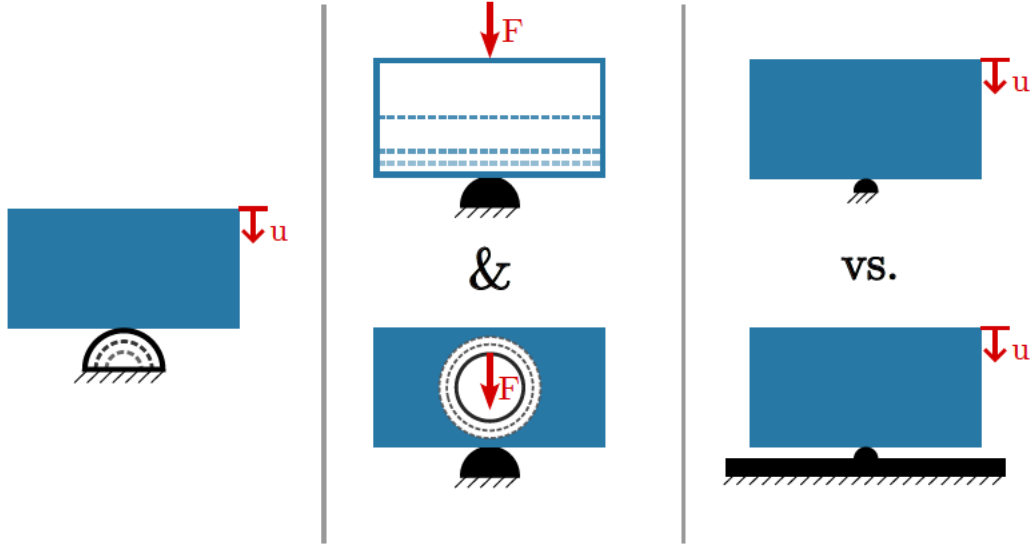


Figure 3.7 Schematic overview of the parameters changed (dashed lines) in the FEM simulations to examine the soft material (blue) behaviour in contact with a rigid body (black). Left: rigid body radius. Centre: skin thickness, both stand-alone and over an embedded bone. Right: comparison between isolated rigid body and salient on a larger surface.

Simulation Settings A tabular summary of the settings described here in detail can be found in tab. C.1, appendix C. The simulations were conducted as “Static Structural” 2D analyses with a constant thickness of 10 mm. The soft body was modelled as a 20×10 mm rectangle, for contact with the rigid body of $r = 10$ mm, the soft body width was increased to 100 mm to ensure that the full stress distribution was resolved without boundary-induced artefacts. The rigid body was modelled as a semi-circle of varying radius. Since the tangential contact between the arc and the soft body’s straight edge led to problem with contact simulation, a small flat line was introduced at the top of the semi-circle, no more than 10 % of the radius in length.

In the “Engineering Data” options, two materials were created as copies of the default “Structural Steel”, were named “rigid” and “soft”, and assigned to the respective bodies in Ansys Mechanical. For the rigid material, the Young’s modulus was changed to 10^9 MPa, cf. tab. 3.7, density and strength parameters were left unchanged since differing values were neither given nor necessary. For the soft material, the Young’s modulus was set to 1.5 MPa, as reasoned above, and the ultimate tensile strength to 5 MPa. For lack of better information, the tensile and compressive yield strength were both set just below the ultimate tensile strength at 4.9 MPa. The Poisson’s ratio was set to 0.49 for both materials because the analytical approximation was calculated with $\mu = 0.5$, but that value is not accepted in the Ansys settings.

The automatic mesh size was kept for most of the model, but a local edge sizing with an element size of 0.2 mm was applied to the lower edge of the soft body to ensure sufficient mesh resolution for the deformation. The contact was set up as frictionless, with the bottom edge of the soft body chosen as “contact body”, and the arc and small flat line of the rigid body chosen as “target body”. This contact type models sliding without resistance, where separation of the contact bodies is possible. It requires the model to be well constrained and automatically adds weak springs to stabilise the simulation. A helpful explanation of the different contact types in Ansys is given in [58].

The simulation was spread over 10 steps of 0.1 s each. Except for the skin thickness comparison under constant force, the pressure was applied as a remote displacement to a remote point on the top edge of the soft body, with the behaviour set to “rigid”. The remote displacement allows restriction of rotation of the nodes around the z-axis, which is not possible for regular displacement in a 2D simulation. The displacement was ramped linearly across the time steps and was increased iteratively until the simulation failed. The rigid body was kept in place by a fixed support, i. e. no displacement in x- and y-direction, and the resulting reaction force was used as an output variable for comparing different simulations. The stress plots were examined for stress peaks or areas reaching above the maximum material strength of 5 MPa, see above. All stress values reported here are the Equivalent von Mises stress.

Results

None of the simulations reached critical stress values before failure due to exceeding the modelling assumptions, giving the error message: “The solver engine was unable to converge on a solution for the nonlinear problem as constrained.” Failure always occurred just below or just above 1 MPa.

The object size strongly affected the stress, as the increase in stress over reaction force was considerably higher for smaller rigid bodies, see fig. 3.8 a. All three simulations reached their stress maximum at ca. 1 MPa, but the force required to cause this stress did not decrease proportionately with the object radius. At a tenth of the initial radius of 10 mm, the tolerated force remained well above 10 % at one sixth. A further halving of the radius resulted in a 50 % reduction in force.

A strong non-linear effect was also observed with the height of the soft body, as shown in fig. 3.8 b. Under constant load, the stress stayed stable when the soft body was more than 2 mm high, but increased potentially for heights < 2 mm. The deviation in stress from the embedded-bone model to the pure soft material with the same contact radius was barely discernible, with differences in the order of 10^{-2} MPa.

Regarding the salient vs. isolated contact comparison, the former took more than five times the force before reaching the same maximum stress of ca. 1 MPa at 28 % more displacement, see fig. 3.8 c. The stress increased steeply until the soft body made contact with the larger surface, reaching about half of the maximum stress at that point, and afterwards went on approximately linearly but at a much more shallow slope. The stress distribution, shown in fig. 3.8 d, is much less localised than in the isolated contact, but there is still a distinct stress peak directly at the contact site with the salient body.

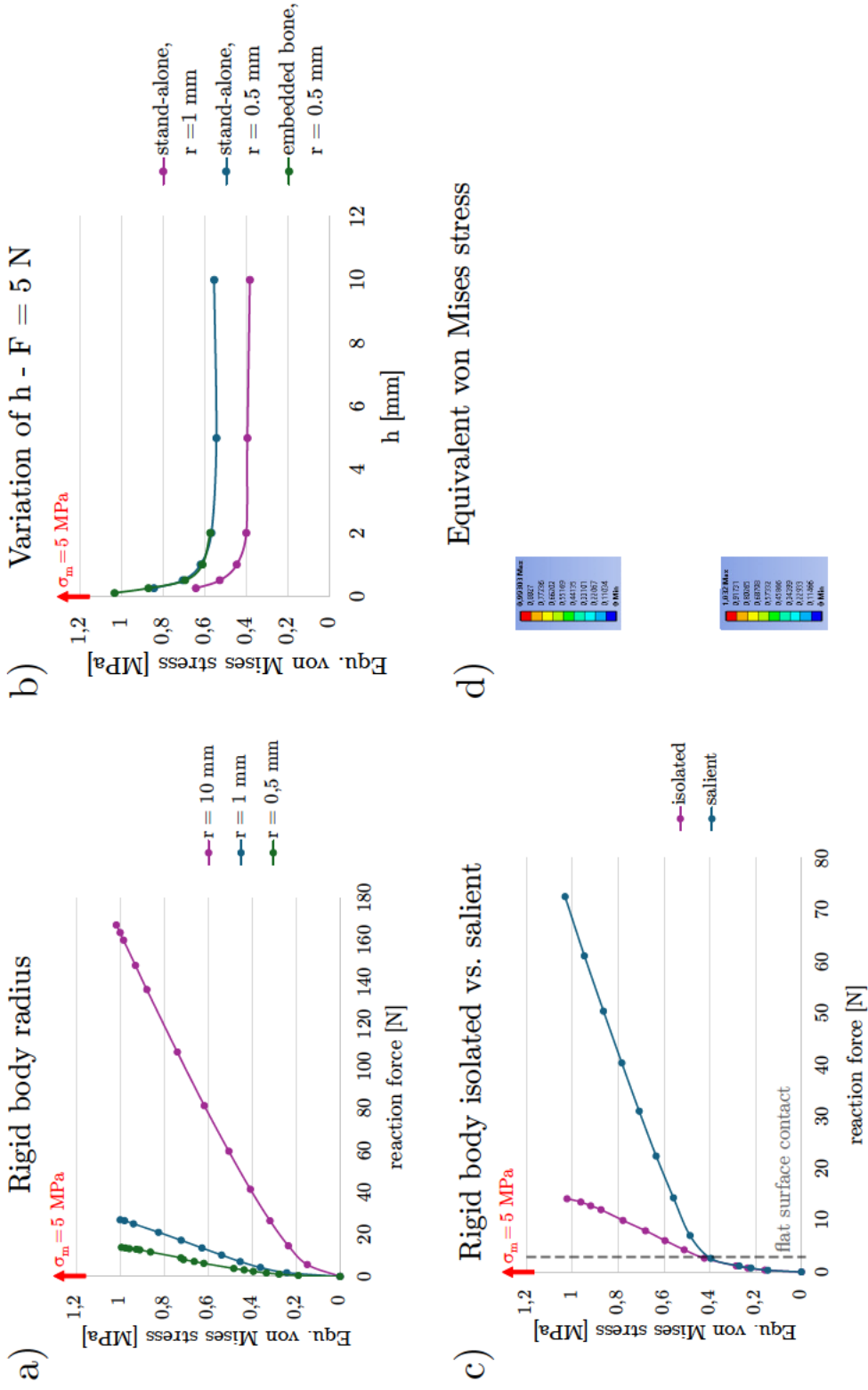


Figure 3.8 Results of parametric study on soft material behaviour in pressure contact. a) Stress over force for different rigid body sizes. b) Stress over soft body height for different rigid body sizes and a constant force of 5 N, with either just the soft material or an embedded bone. c) Stress over force comparison between the default isolated rigid body and a same-sized structure as part of a larger, flat rigid body. d) The same, shown as contour plots of the stress distribution at maximum load, colour scale values in MPa.

3.3.2 Structural Behaviour

Anthropomorphic continuous-elastic palm flexion is intended to be the distinctive feature of the hand developed here. The core approach is the combination of a rigid skeletal structure for stability with a flexible matrix for compliance. The amount of flexion achieved by a given actuator force is influenced by several parameters, i. a. the force direction, the soft material's cross-sectional geometry, and the lever arm of the actuation force, which were varied successively to answer the second research question presented in section 3.3.

Methods

In approximation of the skeleton in the human palm, a simplified cross-section through the MCs was assumed as sketched in fig. 3.9 a, with 5 bones surrounded by soft tissue. As part of the idealisation, the bones were assumed as cylinders, parallel to each other and equally spaced. In keeping with the overall system concept, the palm flexion will be tendon-driven. The simplest tendon placement would be to attach it on the palmar side of the little finger and pull towards the middle finger. The actuator force F_a was assumed at 100 N from previous experience on similar systems. To reduce the simulation costs, the symmetric model was cut in half at the centre, through the bone of the middle finger (fig. 3.9 b). As mentioned above, three factors for modulating the palm flexion (fig. 3.9 c) were examined:

1. the direction of F_a , given by its angle from the horizontal: 0° , 5° , 10° , 15° , 30° , 45°
2. the cross-sectional geometry of the soft material, specifically two aspects of it:
 - a) the material width b in the interosseous spaces: 8 - 12 mm
 - b) whether the soft material surrounds the bones or only connects between them
3. the lever arm of F_a , i. e. the distance of the tendon insertion point from the horizontal mid line of the palm cross-section: 3.9 - 6.9 mm

Whenever a new cross-sectional geometry was modelled, that model was checked for deformation under gravity before recording the data on palm flexion and grip force. Physiological values for the typical excursion of the little finger MC in palm flexion were not available. Based on the motion tracking done by Grebenstein [13] and personal observation, the target displacement was set to be equal to the bone's diameter. Fingertip forces of other robotic hands or grippers at the institute were known to be around 30 N, e. g. [13], so that value was chosen as the minimum contact force to be reached here.

Model construction Figure 3.10 shows the model sketch from Ansys Spaceclaim. The bone diameter and approximate distance between the bones were taken from the kinematic model. Following up on the material behaviour results, the surrounding soft material was constructed so that there was a layer of at least 2 mm surrounding the bones in all places. Since local indentation stress was not the focus of this study part, the external rigid object, serving as the contact body for evaluating the resulting grip force, was constructed with a radius of 5 mm. It was placed slightly above the palm and moved towards the middle finger in four steps of 2.5 mm each, so as to record the generated reaction force in various

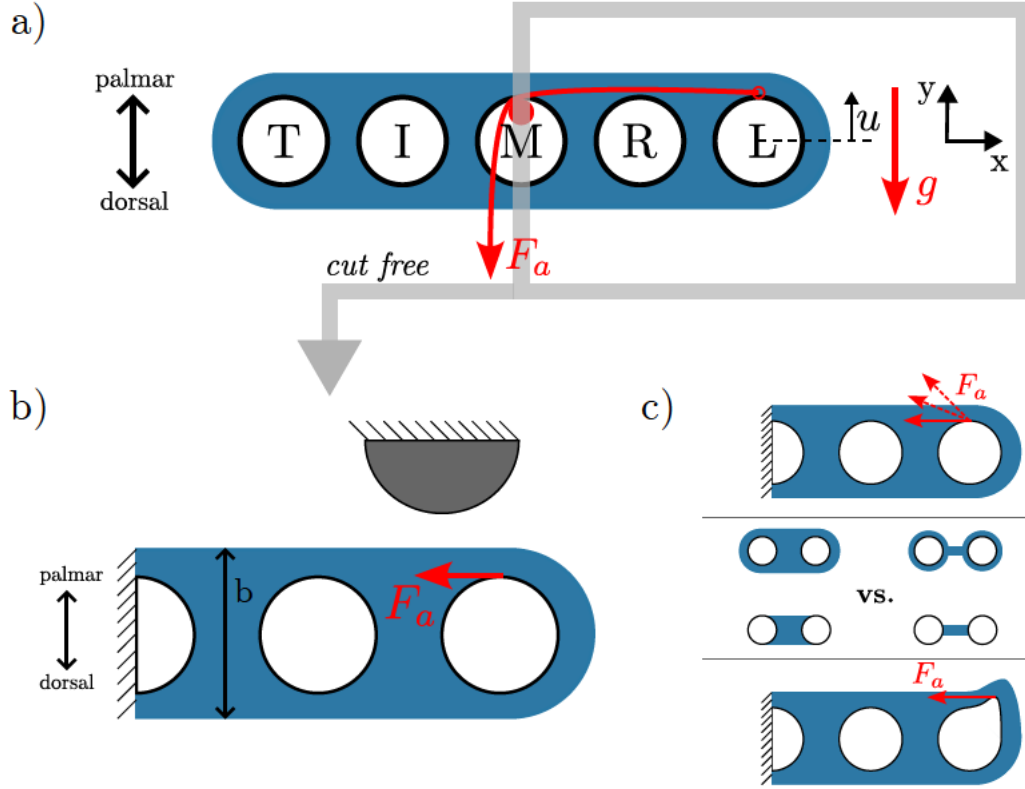


Figure 3.9 Idealised model sketches of palm cross-section with rigid bones (black lines) in a flexible matrix (blue), not to scale. Fingers labelled by their first letter, $F_a = 100$ N. a) Simplified arrangement as parallel, equally spaced cylinders, with an actuator tendon (red) attached on the palmar surface of the little finger and pulled towards the middle finger. The structure should be compliant enough for the little finger to be displaced upwards under the actuation force F_a , but stable enough to support itself under gravity load. b) Structure cut free at the axis of symmetry through the middle finger, a fixed rigid contact body is used to evaluate the generated grip force. c) Parameters to be changed to modulate the resulting deformation: force direction, cross-sectional thickness, lever arm.

stages of palm flexion. By the final step, i. e. $x = 10$ mm, the contact body was sufficiently far away to allow the little finger to reach the target displacement of 8 mm.

Simulation Settings Analogous to the previous finite element method simulations, 2D “Static Structural” analyses were performed, though now with a constant thickness of 80 mm, since that was the bone length for the MCs in the kinematic model. The material properties were largely transferred from the ones given above, but the densities were adjusted to 1.23 g cm^{-3} as an average value for silicone [59] in the soft material and 2.70 g cm^{-3} for aluminium [60] in the rigid material. In this study part, the density was relevant for the deformation under gravity. Aluminium was chosen because it is currently the most likely material to be used when the entire hand-arm-system is manufactured beyond the prototype stage.

Based on a preliminary convergence analysis, the general element size was set to 0.7 mm. Local edge sizing of 0.2 mm was applied to all edges except for the left-hand edges of middle finger and soft body. A nonlinear adaptive region was introduced in the soft body to further

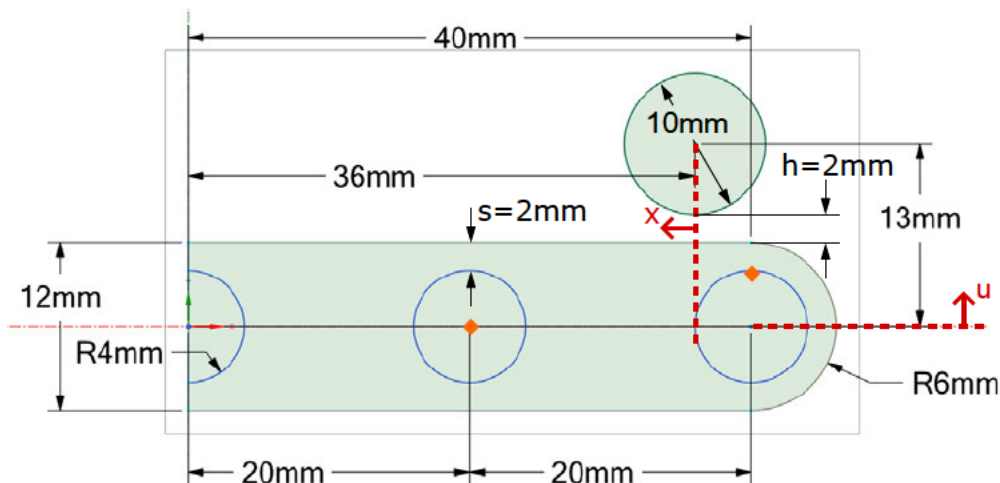


Figure 3.10 Model sketch taken from Ansys Spaceclaim, with additional annotations for the target deformation direction u and contact object positioning x . Orange diamonds indicate the remote point locations.

refine the mesh where necessary. The contact between the soft body and the contact object was set to frictionless. The edges between the bones and the soft matrix were defined as shared edges in Spaceclaim, so that there would be true coincidence between the nodes for both bodies on either side of the edge.

The simulation was again executed over 10 steps of 0.1 s. The behaviour of the ring finger was constrained by a rigid-behaviour remote point fixed to the bone center. A second remote point was placed on the little finger, 0.1 mm below the uppermost point of the bone. This remote point was used to apply $F_a = 100$ N as a remote force in negative x-direction. The left-hand vertical edges of the middle finger bone and the soft body were constrained by a fixed support, as was the entire face of the contact object. When checking for deformation under gravity, the remote force suppressed and “Standard Earth Gravity” applied instead. The stress distribution in the soft body, the total displacement of the little finger bone and the force reaction in the fixed support of the contact object were read out as result variables. Again, all stress values reported are the Equivalent von Mises stress. For the tabular summary of the settings, see tab. C.1 (appendix C).

Results

An overview of the results for varying force direction is given in fig. 3.11. Higher angles for F_a consistently produced a stronger force reaction F_r , while the direction of F_r was barely affected by the direction of F_a , but rather by the amount of palm flexion. Additionally, the contour plots show that the compressive stress concentration between the bones became visibly less pronounced with increasing F_a angle. Value and angle from the vertical of F_r are plotted in fig. 3.12. Within each stage of flexion, the angle variation was negligible with no more than 3° . The baseline model with a horizontal F_a stayed below the target grip force of 30 N for the first three stages of flexion, but even a small pitch in F_a of 5° brought the resulting F_r up to the target force in the first flexion stage.

The effects of varying the cross-sectional width are visualised in fig. 3.13. The two most slim models were prone to buckling and thus slipping out underneath the contact object.

Overview force direction variation

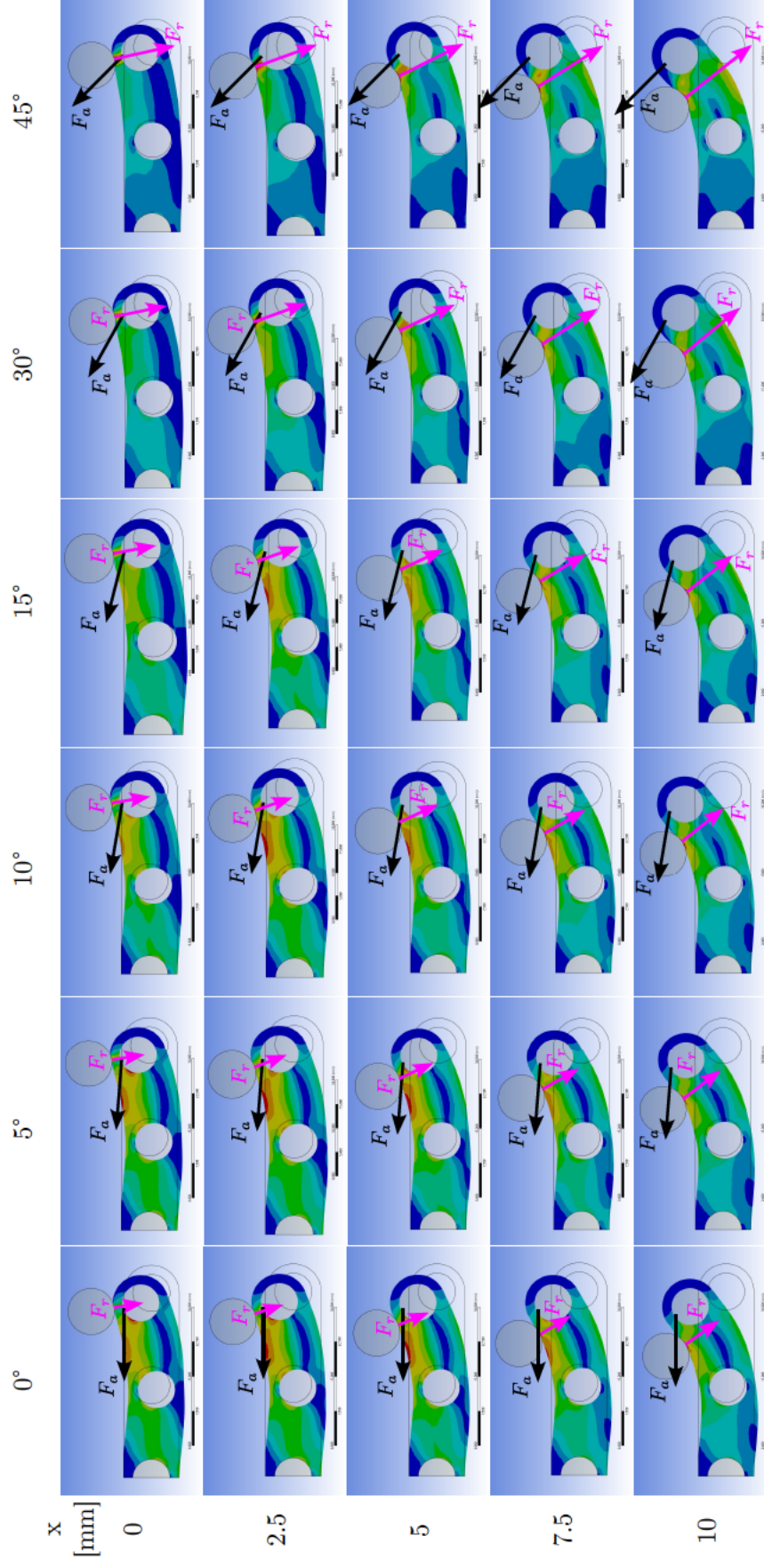


Figure 3.11 Overview of the stress contour plots for varying force angles in different stages of flexion, modulated by contact object position x . Actuation force (black arrows) and reaction force (magenta arrows) annotated, arrow lengths scaled to force value, $F_a = 100\text{ N}$ for all models, colour scales not uniform.

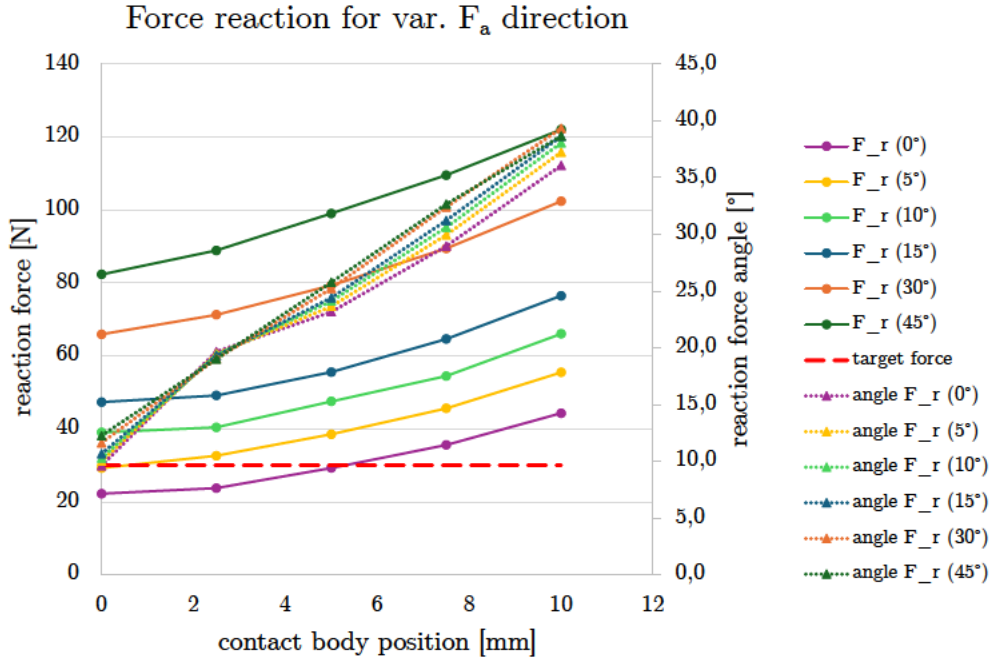


Figure 3.12 Value and angle of the reaction force plotted over contact body position (representative for the amount of palm flexion) for varying actuation force angles, target grip force plotted for reference.

The resulting extreme deformation led to simulation abort, the respective models are framed in red in the overview. They are depicted at the last successful simulation step before buckling, with the corresponding F_a annotated. Again, value and angle from the vertical of F_r are plotted in fig. 3.14. The reduction in material width did not lead to higher reaction forces, though the variation in angle is much higher. It did, however, bring on a noticeable reduction in structural stiffness, as shown in fig. 3.15. The difference becomes clear in the initial part of the flexion motion, before the displacement of the little finger is restricted by the fixed contact body. Hence, the data resolution was increased by simulating finer force steps below 20 N. The displacement per force increased to multiple times the baseline value for the smaller cross-sections (fig. 3.15 a), up to 470 % for a width of 8 mm and $F_a = 8$ N. Figure 3.15 b shows that the differences between the cross-sections were most pronounced before F_a reached 12 N, afterwards all models were in full contact with the rigid object. For that early section, the structural stiffness k is plotted over the material width in fig. 3.15 c. The biggest proportionate decrease was achieved at 8 mm width and $F_a = 8$ N, where the stiffness was reduced down to one fifth of that in the baseline model with 12 mm width at the same force. The deformation under gravity ranged from 0.41 mm in the 12 mm-wide model to 0.91 mm in the 8 mm model.

The model where the bones are connected but not surrounded by soft material only solved successfully for very small actuation forces and then quickly started giving the convergence error that was already observed in the previous study part on material behaviour. For a material width of 8 mm and $F_a = 1$ N, there was no striking difference in the qualitative stress distribution or maximum stress (fig. 3.16). The geometry of the surrounding material led to small stress peaks in the curves of the outline, but at this

stage, no appreciable load could be observed on the soft material “bridges” covering the bones.

Lastly, the increase in lever arm also led to a reduction in structural stiffness, though less pronounced than it was observed for the cross-sectional width. From the baseline model with the remote point at 3.9 mm from the midline to the maximum distance of 6.9 mm, the stiffness was consistently reduced down to 57 % across the early simulation steps until F_a reached 12 N (fig. 3.17 a). The stiffness reduction was not linear across the increase in lever arm, with the determination coefficient for a linear trendline at $R = 0.972$ and for a potential trendline at $R = 1$ (fig. 3.17 b). The first step away from the bone surface yielded the largest decrease in stiffness by ca. 20 %, each further step brought less reduction, ca. 15 % and 10 % respectively.

Overview cross-section variation - surrounding material

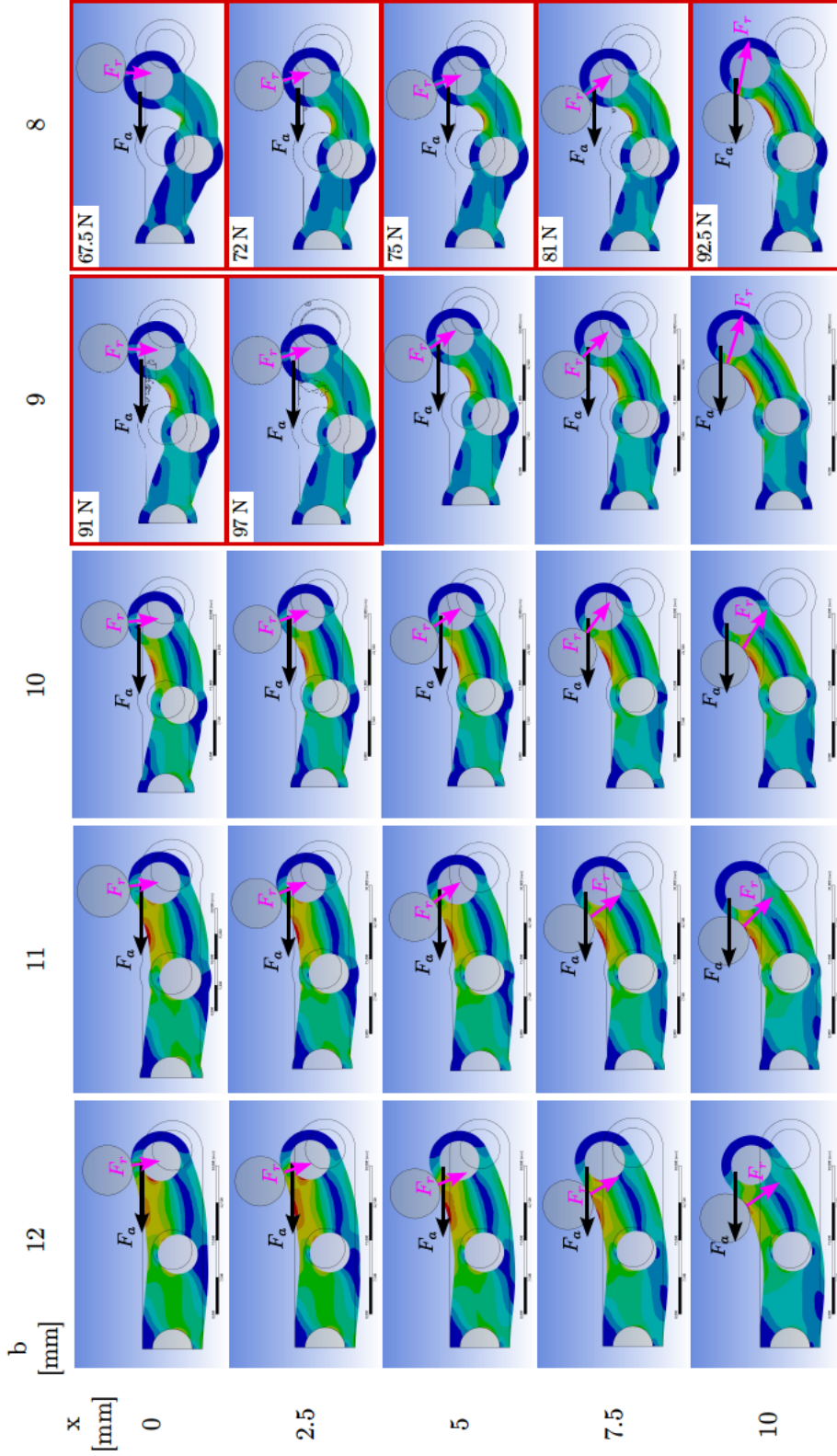


Figure 3.13 Overview of the stress contour plots for varying cross-sectional width in different stages of flexion, modulated by contact object position x . Actuation force (black arrows) and reaction force (magenta arrows) annotated, arrow lengths scaled to force value, colour scales not uniform. Models framed in red are depicted at the simulation step immediately before buckling, with the corresponding F_a annotated.

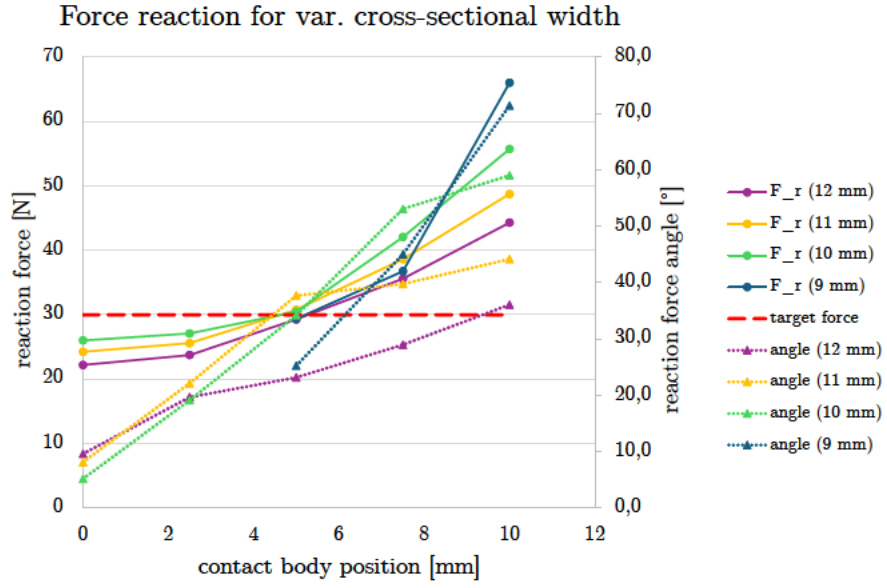


Figure 3.14 Value and angle of the reaction force plotted over contact body position (representative for the amount of palm flexion) for varying cross-sectional width, target grip force plotted for reference. Data from models that buckled before reaching $F_a = 100$ N is not included.

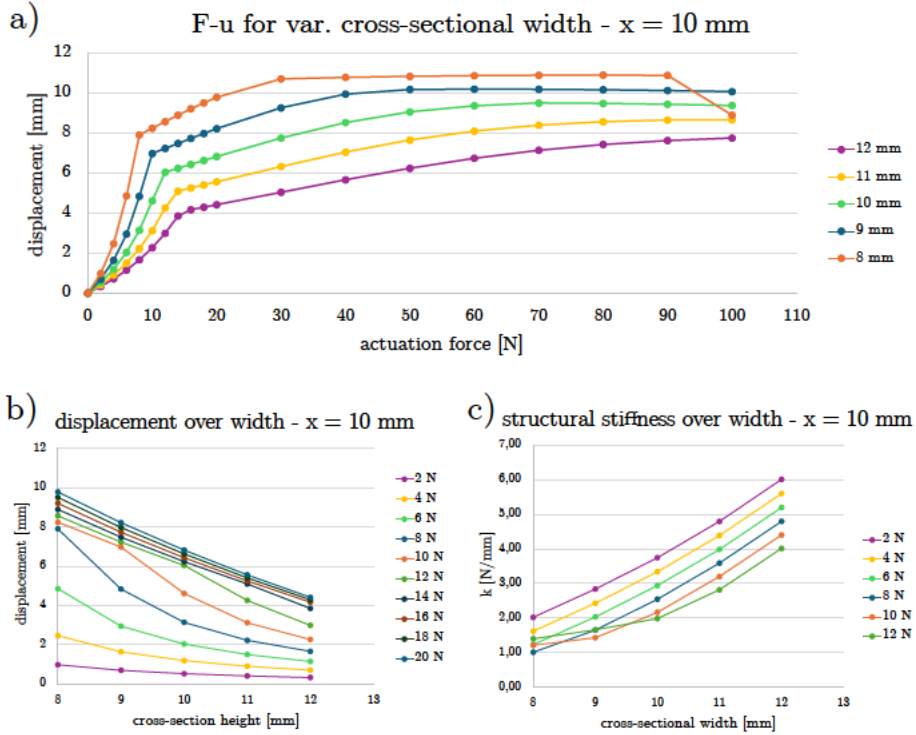


Figure 3.15 Force-displacement data for varying cross-sectional width, all plots for maximum flexion (contact body position $x = 10$ mm. a) Little finger displacement u over actuation force, with additional data points for the early part of the simulation, before the motion is restricted by the contact body. b) Displacement over cross-sectional width, plotted for the early simulation steps. c) Structural stiffness k over width, plotted for the early simulation steps.

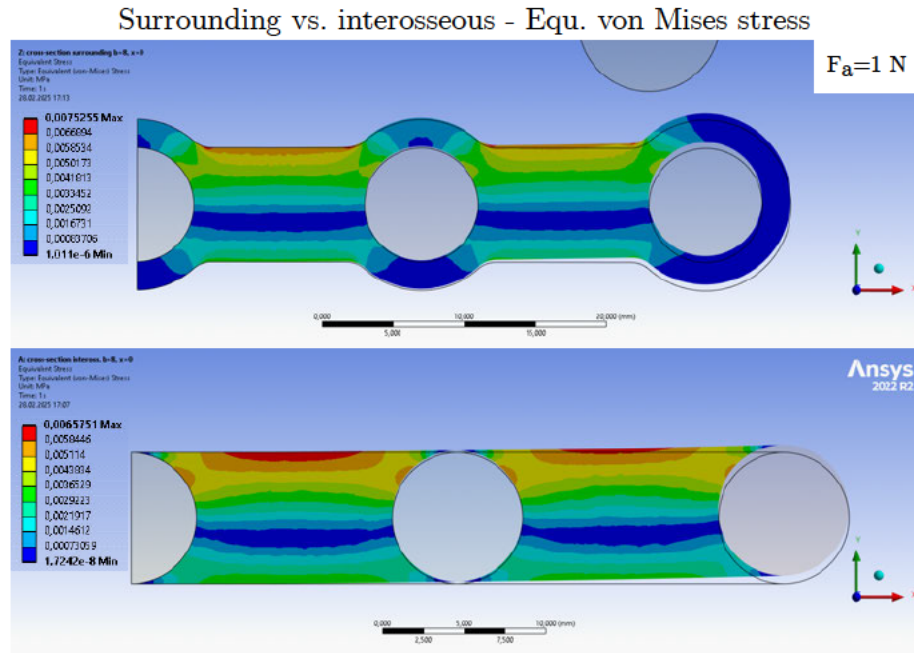


Figure 3.16 Equivalent von Mises stress distribution compared between surrounding and interosseous soft material, for 1 N horizontal actuation force. Colour scale values in MPa.

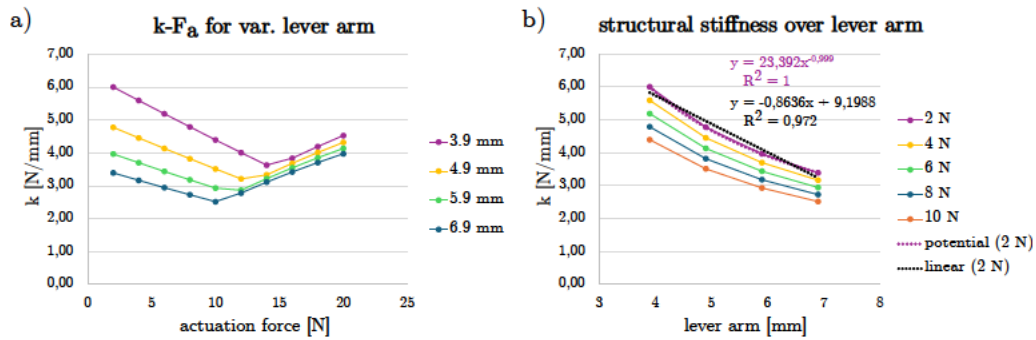


Figure 3.17 Structural stiffness k for varying lever arm, i. e. distance of the remote point from the model's horizontal midline. a) k over F_a for the early simulation steps, before displacement was restricted by the contact body. b) Stiffness reduction did not scale linearly with the increase in lever arm.

3.4 Integrated Discussion

As already claimed in the introduction, the two aspects examined in this work, the thumb kinematics and the palm flexion, are not independent of each other: In the kinematic metrics, each TMC variant was well-suited for different parts of the postures and grasps, but none reached full score, which indicates that including the 3rd DoF can offer improved kinematic performance. However, since the models used to obtain these findings all featured a flexible palm and used that feature to achieve the reported results, that conclusion is only valid if the resulting robotic hand is also able to actuate palm flexion. Stiff-palmed hands would certainly come out with different results in the metrics and thus, the conclusions may differ as well.

The results of kinematic metrics underline the point made in section 3.1.1: A hand’s performance in the TOT is not necessarily an indicator for its precision grasping abilities. This was shown most clearly by the 15° TMC twist variant, which had the poorest performance of the three in the TOT, but the best one in the GRASP taxonomy. An explanation for this could be that the dexterity in precision grasping seems to depend in large parts on the tripod of the three radial fingers. This fact is exploited in some prosthetics hands, as shown in [61], where ring and little finger are purely cosmetic. This finding for the static grasping ability, in turn, cannot be directly transferred to manipulation abilities, where just the tripod will likely not be sufficient for more complex tasks.

The metrics results are also in accord with what Grebenstein [13] described about the lateral grasp and large object grasps putting conflicting requirements on the thumb in the case of a 2 DoF TMC. In the GRASP taxonomy, the 15° twist variant was successful in all but the lateral grasp, while the 45° twist variant was well within the tolerance for the lateral grasp but did not meet the criterion for any other grasp. Grebenstein’s solution to this problem was balancing the twist and inclination in the MCP and IP. The approach followed here of actuating the rotation around the third axis is an alternative to that. The analysis initiated in this work could be extended to acquire much more detailed results by combining the two approaches and including the twist and inclination parameters.

Another aspect demonstrated especially by the 15° twist variant is a limitation in Kapandji’s hypothesis of automatic rotation in the TMC as an accessory movement of the biaxial joint, cf. section 2.2. The rotation he describes does happen, but it is not sufficient to reproduce the fingertip reorientation for tip-to-tip opposition. It is a rotation only around the adduction / abduction axis, meaning that the pulp of the thumb’s fingertip always faces that axis, which Kapandji also makes clear in his illustrations. However, to properly oppose all long fingers, it needs to be able to face away from that axis, if only slightly so, cf. fig. B.4, appendix B.1.

Regarding the expedience of the newly introduced vector evaluation as a fingertip orientation criterion, the bottom-line differs for the two metrics. Generally, it provides a means of classifying on a continuous scale how well or poorly a hand performs in the test rather than just a discrete yes-or-no criterion. If, for example, two hands both achieve the “prismatic 2 finger” grasp within the tolerance criterion, but one does so with an opposition angle of 6° and the other with 23°, the former could be considered more desirable. In the same way, if two hands both fail at stage 5 of the TOT, with opposition angles of 26° and 43° respectively, the angular evaluation would automatically put into context which model is further away from the goal.

In actual application, the contact angle evaluation was quite useful for the TOT, but less so for the GRASP taxonomy, at least in the current stage of model development. In a purely kinematic model, like the motion skeleton in Creo, with no control system or physics simulation, actuation of in-hand postures by setting each joint angle may be tedious but is feasible. With the addition of objects to be grasped, the outcome also depends on how the object was positioned in the CAD model. In this case, the objects were placed by rather simple translations and rotations from the coordinate system of one finger involved in the grasp. In reality, the relative positioning to the fingers can be much more complex, which greatly influences how the fingers are positioned to contact the object and thus how the contact angle calculation comes out. This problem might be mitigated by using more sophisticated physics simulation environments, e. g. MuJoCo, which would require a slightly more sophisticated control regime than used in the present modelling. Additionally, sensor gloves, like those used in motion capture applications, could be used for open-loop control, so that the grasping might be implemented more organically and yield more realistic results.

Apart from that, the unnatural finger placement in some grasps and postures can also partly be ascribed to the fact that all fingers were chosen to be the same length. Especially in the little finger, where the length difference is most prominent, this led to noticeably different behaviour in the TOT and the “Precision Sphere” grasp than what was expected from observation of human hands. Moreover, the kinematic model was scaled to roughly $1.5\times$ the size of a human hand, but the grasping objects were kept at the size specifications prescribed for the original taxonomy. This means that, in relation, the model is grasping very small objects, therefore some of the unnatural postures might be explained by the hand being oversized and needing to adjust. As a result of all these factors combined, the “Lateral Tripod” grasp was the most difficult to simulate. The postures shown in figs. B.5 to B.7 (appendix B.1) hardly look like the reference pose shown in the original GRASP taxonomy in [49], but trying different joint angles and object positioning yielded no better results.

Then again, the parallelism of the vectors chosen for evaluation might be too much of a simplification, especially with the summation of the long fingers’ vectors to represent the virtual finger. This would be an interesting aspect for further scrutiny, possibly taking into account force-closure workspaces or other weighting methods. Another limitation of the current evaluation is that it only considers the orientation of the fingers to each other, but not towards the object center and / or surface, which are relevant as well. For reliable baseline data, a thorough evaluation of the respective vectors in human grasping behaviour, e. g. by use of sensor gloves, would be helpful.

With regard to the material behaviour, some valuable insights can be inferred despite all simulations stopping long before the stress reached values anywhere close to the material strength. The non-linear increase in stress per force with decreasing contact object radius indicates that an adaptation of the grip force to the object size, known or expected, can be reasonable. The handling of objects even sharper than the present simulation allowed is conceivable in several potential fields of application for a robotic hand, such as scalpel blades in medical fields, glass shards in search-and-rescue, or sharp-edged rocks in space exploration. Similarly, if the soft material is to be used as an outer covering of the hand, that “skin” can be recommended to be at least 2 mm thick based on the results obtained here, since the stress per force was stable until that point but went up steeply when the material was thinner. This should be considered regardless of whether the soft material is

directly covering rigid parts or is spanning free space. However, if the edge is a feature on a larger flat object, e. g. a structured surface, the contact stress is less likely to become a problem.

The parametric study part on the force direction has shown that even a small pitch in the actuation force is enough to put more of it into effect for the palm flexion and less for compression of the material. Depending on constructional constraints, the actuating tendon could be routed towards the wrist instead of the middle finger, which would require new simulations, but could yield better effects, since it might allow larger angles. Decreasing the cross-sectional width was a very effective measure for lowering the structural stiffness of the palm model, and especially facilitated the initiation of the palm flexion motion. However, it came with a distinct danger of buckling when it was decreased too far. These insights will be helpful when designing the palm geometry for the prototype, since it is a parameter that is easy to implement and adjust. Deformation under gravity was low at less than 1 mm for all models, but the exact tolerance limit depends on the control regime later on, so no detailed judgement can be given at this point. The soft material geometry surrounding the bones seemed to have no apparent advantage for the qualitative stress distribution over the purely interosseous connection, but may still be preferred due to other constructional advantages. The early calculation abortions in the interosseous model were likely caused by the thinning corners towards the bones. In future research, this aspect of investigation could be expanded to examine more variations of this type of geometry. One option would be to gear the geometry more closely to the interosseous muscles in the biological hand. Lastly, the variation of the lever arm has shown that setting the tendon insertion point slightly further out from the general bone circumference can be helpful in actuating the palm flexion, but extreme distances would likely not be worth the constructional effort.

The FEM modelling approach chosen here was useful to get a first impression of the material and structural behaviour, but it leaves potential for more sophisticated simulations. The convergence error used as a stop criterion in the material behaviour models and also observed in some of the structural behaviour models was most likely due to excessive element distortion. This would explain why the error always occurred closely around stresses of 1 MPa, which is far below the material strength but would, by way of the Young's modulus, always correspond to a certain amount of deformation. A possible approach to deal with this would be remeshing, which increases modelling costs but also yields more realistic results.

A further step to make the simulation more representative of the real structure would be to use non-linear hyperelastic modelling approaches like Neo-Hookean, Yeoh, Mooney-Rivlin, Ogden, or similar models [62]. These models reproduce the behaviour of rubber-like materials better than the classical Hookean modelling approach. The discrepancy was conceded deliberately for this work to keep simulation costs low, but would merit further consideration in future studies.

4 Prototype Design and Evaluation

The findings obtained in the previous chapter were used to design a prototype, uniting the concepts of a soft palm and a joint providing 3 DoF in the TMC. The design choices were based on a morphological box, from which two concepts were devised and sketched. These were compared in an evaluation matrix and the better one was implemented by means of 3D-printing. The resulting prototype's performance was assessed by the same two metrics presented above for the kinematic model. Additionally, the increase in contact area of the palm was visualised by a simple demonstration of paint transfer. The following sections will provide more details on each of these steps.

4.1 Design Process and Criteria

In the design process, certain requirements needed to be considered, e. g. regarding the interface to the wrist or providing space for the finger actuation. The wrist dimensions were given as a prerequisite, whereas the fingers were implemented as dummies, since they will be developed in further research. The list of requirements is provided in tab. 4.1. Additional general design goals were for the prototype to be lightweight and modular where possible.

To construct a concept for the prototype, relevant design features were collected in a morphological box, shown in tab. 4.2, along with various options for how those features could be expressed. Some of those expressions have been used in existing robotic hands, others are unique to this project. Two design concepts were devised from different combinations of feature expressions chosen from the morphological box, which are sketched in figs. 4.1 and 4.2. They were subsequently graded in an evaluation matrix with both plain and weighted scores in order to choose one concept for implementation, see tab. 4.3. Each variant will be briefly described in the following.

Table 4.1 List of requirements to be considered in the prototype design, classified as either mandatory (m) or optional (o).

| critereon | specification | type |
|-------------------------------|---|------|
| DoF in TMC | 3 (<i>add/abd, ext/flex, twist</i>) | m |
| | or continuum | o |
| RoM TMC | 1. Total Opposition Test [1] | m |
| | 2. GRASP taxonomy (columns intermediate & precision) [49] | m |
| wrist connection | elliptical base platform, 90×50 mm | m |
| actuation | flex shafts ($d = 2.8$ mm) & tendon spindles (17×7 mm) | m |
| | 4 per long finger | o |
| number of actuators for thumb | 5 | o |
| HMC | same joint type as TMC | m |
| | with restricted RoM | o |

Table 4.2 Morphological box for various expressions of features to be included in the palm design concept. For each feature, one or a combination of several expressions is chosen, resulting in an ensemble to form one possible version of the system. This was repeated to obtain a second version. Expressions highlighted in blue were used in variant 1, yellow in variant 2, and green in both variants. The designs developed on this basis were sketched and compared in the evaluation matrix to choose one for implementation.

| Feature | Expression | | | |
|----------------------------|---------------------------------|--------------------------------------|-------------------------------|------------------------------|
| | 1 | 2 | 3 | 4 |
| 3 DoF joint | saddle joint | ball & socket joint | continuum / soft structure | soft capsule with air torus |
| actuation | tendons | pneumatic / hydraulic | direct drive | shape memory alloy / polymer |
| robustness approach | dislocation | structural compliance | active compliance | |
| palm type | fully rigid | bones connected by soft tissue | bones embedded in soft tissue | fully soft |
| palm flexion | hinge joint on little & ring MC | rolling contact surfaces between MCs | continuum soft tissue | |

Variant 1 In this concept, the soft material serves simultaneously as “connective tissue” between the MCs and as a skin covering the entire palm. It is fixed to the wrist base by button-like structures, of which a cross-section is shown in fig. 4.1 (top right insert), creating a firm, but reversible connection. Following up the FEM results presented in section 3.3.2, the palm cross-section is sketched as full-material between the MCs, prioritising stability and avoiding danger of buckling. However, the structure’s stiffness can still be adjusted by incorporating material cut-outs between the fingers. Furthermore, this variant features a joint that combines the principles of a ball-and-socket joint and a saddle joint. If a classical ball joint is to stay intact without any external load, the socket needs to cover more than half of the ball, which puts severe restrictions on the RoM. A saddle joint can be constructed as two complementary curved surfaces rotated by 90° to each other. In this combined version, the two sockets snap onto the ball with a grip of two small “cups”, positioned diametrically, on two orthogonal axes and can then glide freely around the ball surface (fig. 4.1, bottom right insert). The snapping mechanism allows for dislocation without structural damage under overload. By leaving or cutting out more material between the snap-on cups, the RoM can be adjusted or limited as necessary. This type of joint connects the MCs of thumb and little finger to the elliptical wrist base. The same joint is also used for the MCPs of the long fingers, but modified to restrict the twist. The MCs of index, middle, and ring finger are embedded in the soft material with no rigid attachment to the wrist base. Each finger is to be actuated by 4 tendons, which wind onto spindles positioned in the MCs. These spindles are in turn driven by flexible shafts, which can transmit torsional moment while being bent along their axis. This arrangement allows for torque to be transmitted from motors in the forearm through the wrist into the fingers without coupling the finger flexion to the wrist motion, which is the case in other hands in use at the institute and has been described to cause problems. The tendon spindles in each finger are positioned in two pairs, one being adjacent in lateral direction, the other in dorsopalmar direction, which allows for the distal flexible shafts to pass the proximal spindles without complicated routing.

Variant 2 The second concept focuses on the soft material providing a flexible connection between the MCs without encasing the entire palm, which makes the actuation components more accessible and leaves options for a separate glove. The thickness of the band of soft material in the sketch is not necessarily to scale and can be chosen to achieve the desired stiffness, while the principle of thinner sections passing through the MCs would stay the same (fig. 4.2, A-A view). In this design, the top of the MCs needs to be removable, so that the soft band can be placed and then fixed by screwing the top back on (fig. 4.2, B view), which increases component count and assembly complexity. This variant also makes use of the soft material to form a joint capsule for the TMC and HMC. It attaches to the rigid structures by the same button mechanism used in variant 1, so that this joint can also dislocate under overload. Movement in all directions is enabled by a thin-walled, air-filled torus between the two button heads. The MCs of index, middle, and ring finger are fixed very similarly, but with a solid cylinder instead of the air torus making for a stiff connection. The finger actuation concept is the same as in variant 1. The tendon spindles are positioned analogously, the routing of the flexible shafts is only slightly different due to the bones now all being attached to the wrist base.

The comparison in the evaluation matrix reveals that the two variants achieved very similar scores, both plain and weighted, each having different benefits. In the end, variant 1

came out with a slightly higher rating and was therefore chosen for implementation in the prototype.

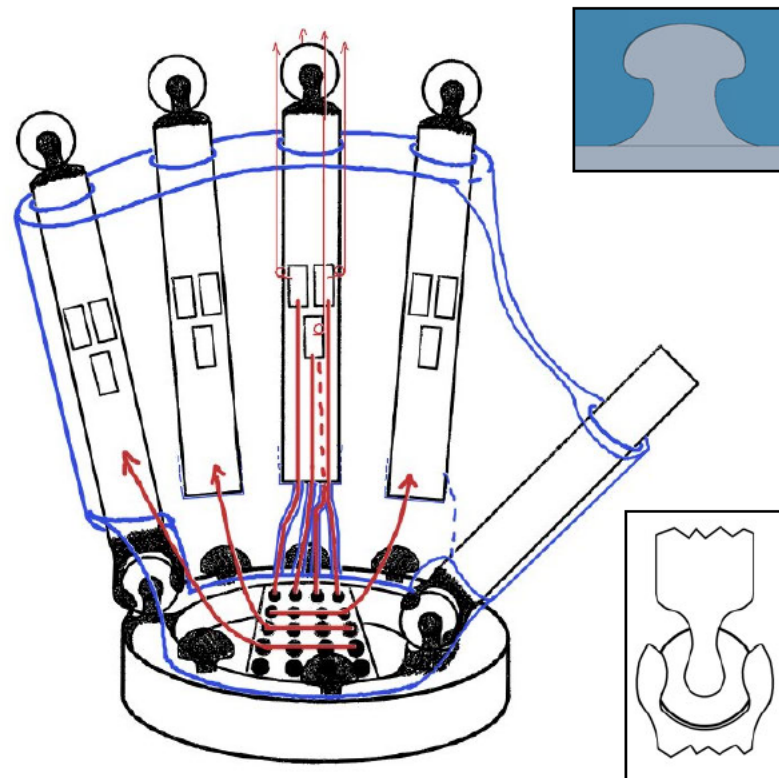


Figure 4.1 Concept sketch of variant 1, where the soft material (blue lines) envelops the entire palm, thus embedding the bones and serving as a protective skin. It attaches to the base by mushroom-shaped button heads reaching (insert top right, soft material blue, rigid material grey). The TMC and HMC feature a dislocatable joint that combines properties of saddle and ball joints (insert bottom right). The routing of flexible shafts and tendons is sketched in red exemplarily for the middle finger. For the sake of clarity, only the respective row of flexible shafts is indicated for the other fingers.

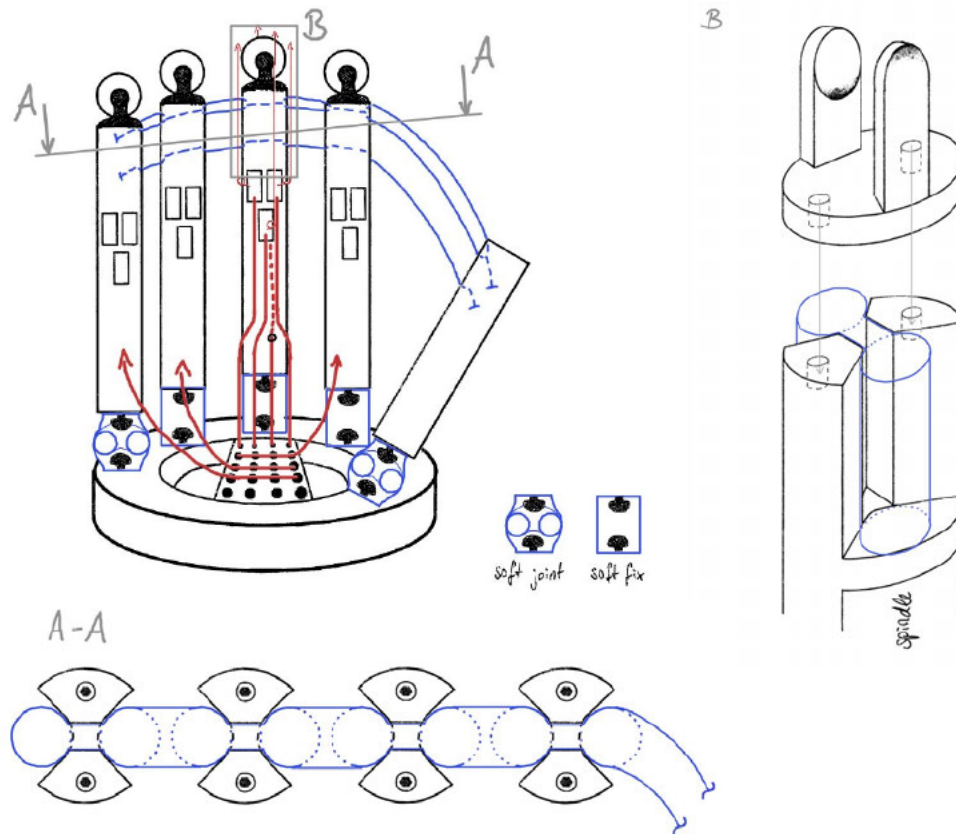


Figure 4.2 Concept sketch of variant 2, where the soft material only connects *between* the bones, leaving the actuation components accessible for maintenance. The finger base joints consist of soft capsules. **A-A view:** The soft band consists of thin sections that fit into cut-outs in the bones and thicker sections in the interosseous spaces that modulate the structure's stiffness. **B view:** To place the soft band, the bone needs to be disassembled at the top and then screwed back together.

Table 4.3 Evaluation matrix for the two variants devised from the morphological box. Scores are given from 0-5.

| criteria | weight (%) | variant 1 | | variant 2 | |
|---|---------------|-----------|-------------------|-----------|-------------------|
| | | score | weighted score | score | weighted score |
| low mass / material consumption | 15 | 3 | 0.45 | 5 | 0.75 |
| low component count | 15 | 5 | 0.75 | 3 | 0.45 |
| protection / skin function | 10 | 5 | 0.5 | 0 | 0 |
| accessibility for maintenance | 10 | 3 | 0.3 | 5 | 0.5 |
| axial stability | 20 | 3 | 0.6 | 4 | 0.8 |
| integrability of thumb into flex structure | 10 | 3 | 0.3 | 4 | 0.4 |
| flexshaft routing space | 20 | 4 | 0.8 | 3 | 0.6 |
| Σ | 100 | 26 | 3.7 | 24 | 3.5 |

4.2 Prototype Description

Starting from the sketch shown in fig. 4.1, some minor adjustments were made to incorporate all aspects. The resulting prototype is shown in fig. 4.3, notable points will be explained here. A short video demonstrating the actuation chain of the flexible shafts and tendon spindles is provided as supplementary material with the digital version of this thesis, see appendix E.

While the sketch shows the soft structure leaving openings around the TMC and HMC, it is closed all around in the final prototype. A first version was printed with an almost solidly filled palm, where only cavities for the MCs and the flexible shafts were cut out. Since that turned out to be much too stiff and heavy, two changes were made: Firstly, the palm was hollowed out except for two internal bands to embed the MCs, which considerably reduced the part's mass. In accordance with the FEM findings, a skin thickness of at least 2 mm was kept in all places that will potentially interact with the environment. Secondly, notches were added in the bands between the bones, as the FEM simulation indicated that this is an effective method to reduce the structural stiffness. The notches increase in size from index to little finger. Again, a 2 mm-thick skin was left covering the notches, thus maintaining a smooth palm surface.

The thumb's resting position, visible in fig. 4.3 c, as dictated by the soft structure's shape is owed to the fact that the corresponding construction plane was defined by the index finger's longitudinal axis and the TMC centre point. The originally circular cross-section of the MCs was extended by tendon guides on two sides, as can be seen in fig. 4.3 d, in the distal part of the bones. The geometry of the bone positioning was guided by the elliptical shape of the wrist base and is indicated in fig. 4.3 e. Due to manufacturing constraints, the size was increased by a factor of 1.5 from the link lengths used in the kinematic model.

The flexible shafts used here are products provided by the company BIAX Flexible Power (Schmid & Wezel GmbH, 74889 Sinsheim, Germany). The tendon spindles are a custom design and were manufactured by the institutes workshop, the mechanical drawing is provided in fig. D.1, appendix D. The tendon for the palm flexion is routed beneath the skin, running from a fixed insertion point in the tendon guide extension of the middle finger to the proximal palmar tendon spindle in the little finger. Two of the three thumb tendons are also routed internally, running from insertion points on the palmar and dorsal sides on the wrist to the two proximal spindles in the MC. The third tendon inserts in the tendon guide extension of the thumb bone and is actuated on the proximal palmar spindle of the middle finger. It was left to run externally across the palm in the current version to demonstrate the basic idea, but will be routed in a less exposed fashion when the actuation is developed in detail in future work.

4.3 Evaluation

The prototype's performance was evaluated by the same tests used for the kinematics investigation, i. e. the TOT and GRASP taxonomy. The opposition angles are presented in tabs. 4.4 and 4.5, pictures of the postures and grasps can be found in appendix B.2.

For the TOT, the opposition angles extracted from the CAD model were within the specified tolerance for all 11 stages, yielding a full score of 10. The postures were also

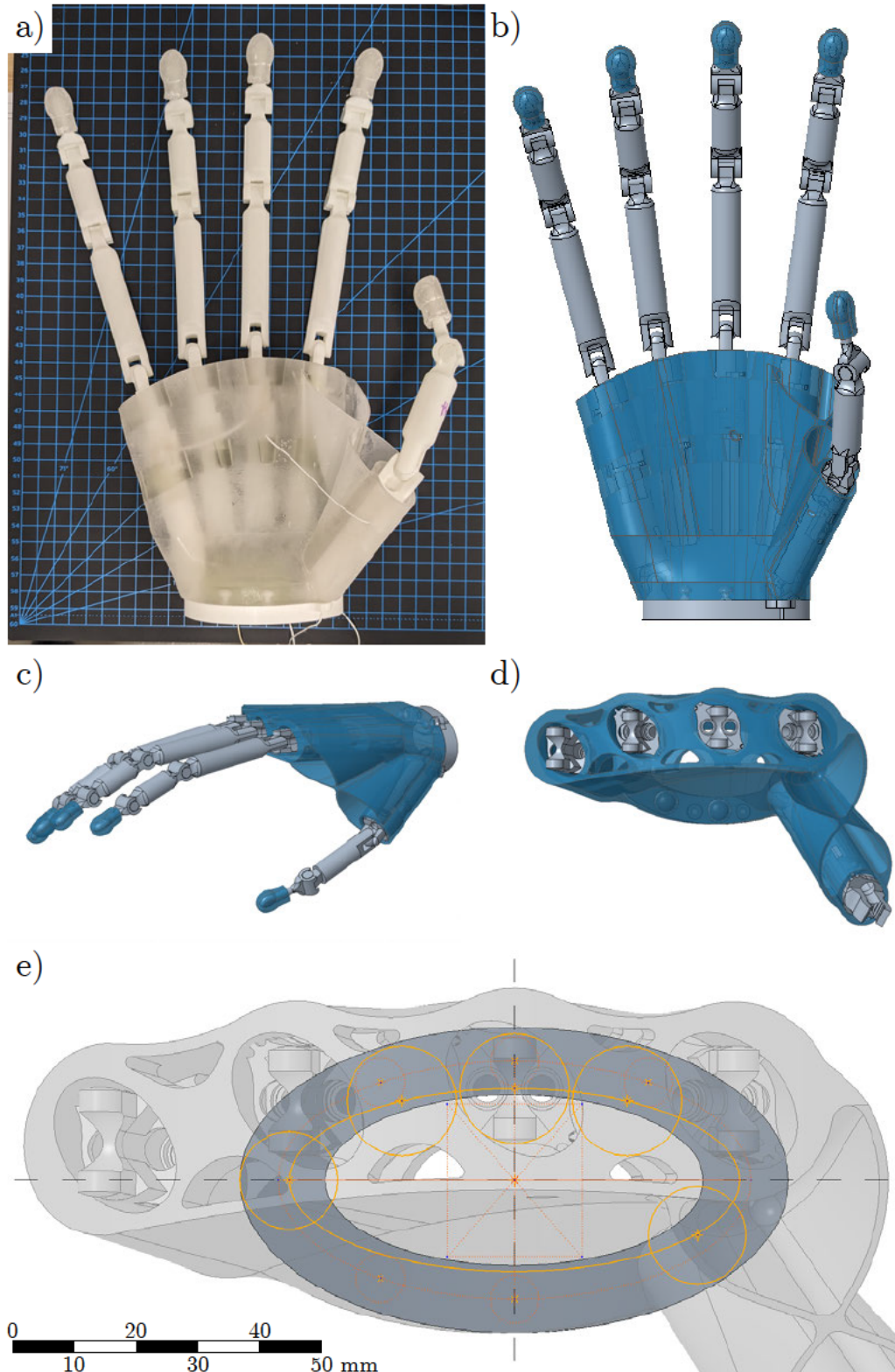


Figure 4.3 Prototype of an anthropomorphic hand with a flexible palm and a 3 DoF thumb base joint. a) Photograph of the 3D-printed hand in palmar view, background grid size 1 cm. b) The same view in the corresponding CAD model. c) CAD model approximating the resting posture in the biological hand, laterodistal view. d) Distal view of the palm without the finger phalanges, showing the shape of the MCs and the cut-outs in the soft material. e) Projected positions of the proximal MC ends sketched against the base platform, scale only valid for this subfigure.

4.3 Evaluation

recreated on the physical model. Since it has no functioning actuation or control system yet, it had to be manipulated by hand into the respective positions. For the most part, the result looks very similar to the CAD model, cf. fig. B.8, appendix B.2. However, visible differences between the printed model and the digital twin occurred for stages 4 - 6, where the printed model reached better opposition in stages 4 & 5, but was difficult to coordinate into the right position for stage 6.

For the GRASP taxonomy, 4 of 6 simulated grasps were reached successfully, while the lateral tripod and the quadpod exceeded the tolerance angle. Again, the grasps were also attempted with the physical model, see fig. B.9, appendix B.2. While the “lateral”, “palmar pinch”, and “precision sphere” grasps look fairly similar in comparison, the “lateral tripod”, “prismatic 2 finger”, and “quadpod” show obvious differences. Generally, the postures appear more natural in the printed model.

In addition to the quantitative tests, paint-transfer patterns as introduced in [31] were used to demonstrate the increased contact area achieved by the flexible palm. Figure 4.4 shows the results of the prototype when the palm is left flat - as it would be in a rigid-palmed model - compared to the same prototype when the flexibility of the palm is put to use to conform to the object shape, and a human hand for comparison. In the latter, an attempt was made to keep the fingers away from the object so as to only showcase the palm functionality. It was, however, nearly impossible to actuate the palm flexion without also flexing the little finger and thus bringing it into contact with the object. The comparison illustrates that the flexible palm achieves much more contact area than the flat one, and the resulting paint-transfer pattern is also much closer to the one seen in the human hand.

Table 4.4 Opposition angles from TOT with the 3D-printed prototype.

| stage | opposition angle [°] | success (y/n) |
|-------|----------------------|---------------|
| 0 | 13.4 | y |
| 1 | 20.2 | y |
| 2 | 15.3 | y |
| 3 | 20.3 | y |
| 4 | 23.3 | y |
| 5 | 21.3 | y |
| 6 | 19.0 | y |
| 7 | 21.1 | y |
| 8 | 14.8 | y |
| 9 | 16.2 | y |
| 10 | 24.9 | y |

Table 4.5 Opposition angles from the GRASP taxonomy with the prototype.

| grasp | opposition angle [°] | success (y/n) |
|--------------------|---------------------------------------|---------------|
| lateral | 6.2 | y |
| lateral tripod | 90.9 (TI) 164.8 (TM) 104.3 (IM) | n |
| palmar pinch | 21.2 | y |
| prismatic 2 finger | 24.5 | y |
| quadpod | 33.7 | n |
| precision sphere | 24.7 | y |

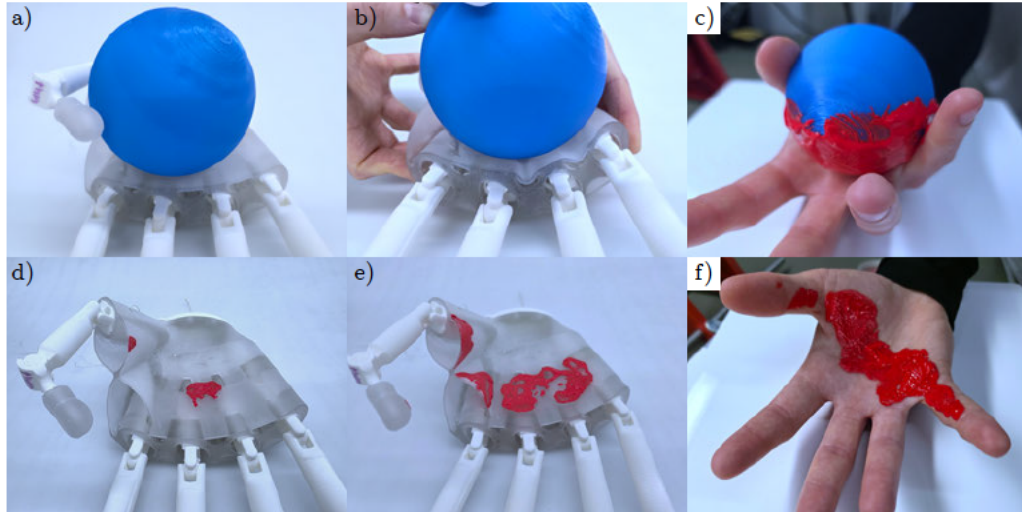


Figure 4.4 Paint-transfer patterns as a demonstration of the contact area when grasping a spherical object. a, d) Very little contact achieved by the hand model when the flexibility of the palm is not put to use, i. e. mimicking a rigid palm. b, e) The same model, but employing the flexible palm to adapt to the object shape. c, f) Human hand for comparison.

4.4 Discussion

Overall, the final model performed noticeably better in the two metrics than the kinematic model in most cases, indicating that the 3. DoF in the TMC does offer an advantage over the 2-DoF version. It is thus a viable alternative to fine-tuning twist and inclination in the thumb MCP and IP, which was the approach chosen in [13].

The difference is most obvious in the TOT, where the Kapandji score in the strict sense was 0 for all three variations of the 2-DoF joint, while the 3-DoF model reached a full score of 10. Even with the relaxed criterion, the highest score reached by a 2-DoF variation was 7. In the GRASP taxonomy, the prototype outperformed the 2-DoF variations of $+30^\circ$ and $+45^\circ$, but fell behind the $+15^\circ$ variation. One caveat to be pointed out here is that, for the sake of comparability, the joint angles for the long fingers were carried over exactly from the simulations on the kinematic model for both the TOT and the taxonomy grasps. In the latter, only very minor changes were made if necessary to maintain contact with the object. As the photos taken of the physical model show, in some cases much more natural grasps can be achieved if other finger positions are allowed, and the resulting opposition angles would likely be much closer to the goal. The same was true for some TOT positions, where the extracted angles turned out larger than expected from the physical interaction. However, the postures that could intuitively be produced on the physical model could often not be recreated in the CAD model with the current control approach of setting each joint angle manually. Some of it may be due to inaccuracies and play in the 3D-printed joints, and some grasp could be improved by shifting and fine-tuning the limit stops in the TMC. Ultimately, though, it comes down to the point already discussed in section 3.4: The evaluation of the hand in both metrics, but specifically the taxonomy grasps, would greatly benefit from a more sophisticated control regime and simulation environment.

To the best of the author’s knowledge, this is the first anthropomorphic hand featuring an active flexible palm with embedded bones. As Pozzi et al. [34] have compiled in their extensive review, several robotic hands with continuous soft structures for the palm without the stabilising effect of the internal skeleton have been developed, and three papers have been published about articulated palms [30–32], where the otherwise flat palm is folded along discrete lines by hinge joints. Yang et al. [55] do indeed present a prosthetic hand with impressively human-like bones, but their palm remains passive and thus fixed in a flat configuration. The prototype developed here successfully combines the benefits of an internal skeleton and a continuously flexible matrix. The flexion of the palm is brought about by moving the outermost part of the skeleton, letting the flexible matrix transfer the motion proportionately to the other bones, which induces a smooth curvature of the palm. This offers a natural appearance and allows for effective shape adaptation in grasping. The paint-transfer patterns were merely used as a qualitative demonstration here, but could be further processed to yield an actual quantification of the contact area, as demonstrated by [31]. If this was done consistently for several hand models, it could become a useful metric for systematic comparison of soft-palmed robotic hands.

Apart from the performance metrics, some constructional aspects of the prototype merit discussion. The most obvious one is the size of the model. It is currently about twice as big as a regular human hand, the long-term goal is to get it roughly life-sized. To some extent, the size might be reducible by the use of different manufacturing techniques, e. g.

powder-based instead of filament-based 3D-printing. The most prominent constraint was, however, the accommodation of the four tendon spindles in each MC, so the packaging of those should be the starting point when trying to reduce the size. Coupling of the PIP and DIP in the long fingers and a passive extension mechanism could decrease the number of necessary tendon spindles altogether. Additionally, the space between the bones in the palm could likely also be reduced, though the effect of that on the structural stiffness should be taken into consideration.

Detailed engineering of the actuation system was not the goal of this project, but some insights were gained nonetheless: The tendon routing for the palm flexion as it is in the current version is a valid start, but can be further fine-tuned. A different fixation to the middle finger MC or adaptations to the bone shape could help implementing a larger force attack angle, which the FEM simulation indicated as a way to facilitate the initiation of the flexion motion. Should the simple tendon drive prove insufficient for generating the necessary force, mechanisms like a pulley tackle or capstan drive could be options to amplify the tendon force. An alternative to the current routing would be to terminate the palm flexor tendon at the wrist instead of the middle finger, see fig. 4.5. This would be closer to the biological tendon and could be compared to the current choice in simulation and physical testing to decide which version is more effective.

The tendon triangle for thumb actuation is not quite functional yet, but the optimisation of that would be enough to fill a study all on its own. The return properties of the flexible material can be put to use more efficiently and could be coordinated with the tendons. Currently, the tendon inserting at the palmar side of the wrist would mainly pull the thumb in the same position as the resting shape of the soft material dictates, which renders the tendon obsolete. The tendon on the dorsal aspect of the thumb does not sufficiently adduct it towards the index finger. It could instead be routed towards the index MC, see fig. 4.5, coupling supination to adduction if it terminates on the outside of the thumb MC. Furthermore, the external routing of the flexor tendon across the palm is clearly suboptimal. A different construction approach to the thumb's resting position might be helpful, e. g. with the soft structure's default shape in a flat hand position. This might give a better baseline for properly placing the tendons.

Lastly, the axial stability of the palm might be a concern: The proximal ends of the index, middle and ring finger bones are not stabilised against anything, which makes for easy routing of the flexible shafts but also impedes force transmission. This is especially relevant for the middle finger, since it is to serve as a platform for both the palm flexion and thumb actuation to act upon. Preliminary tests of the tendon actuation as suggested above have shown that the palm tends to fold down on itself when tightening the thumb's palmar tendon. Providing at least the middle finger MC with a rigid connection to the wrist base might prevent that and also make the palm flexion more effective. However, the flexible shafts themselves will contribute to stabilising the bones once the system is fully assembled, seeing how they would be fixed in the tendon spindle on one side and in the forearm-based motor on the other side. The entirety of 20 flexible shafts running through the wrist might provide more stiffness than anticipated, so this aspect remains to be seen and iterated upon once a full version of the hand exists.

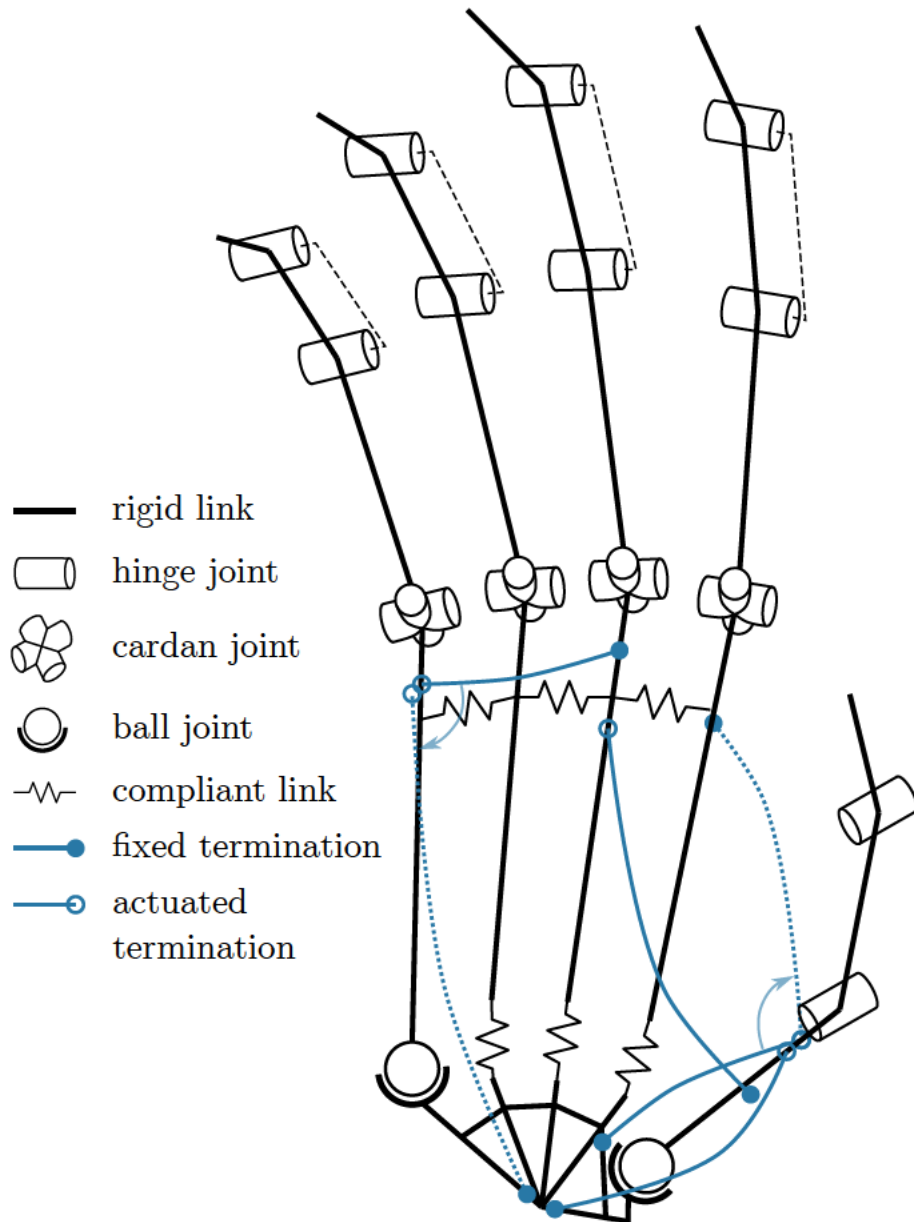


Figure 4.5 Kinematics and actuation scheme of the prototype, with suggestions for improvement over the current version. Dashed black lines indicate coupled joints, solid blue lines the current tendon routing, and dotted blue lines alternative options for the tendons.

5 Conclusion and Future Work

In summary, this work provides valuable insights for designing a palm for an anthropomorphic hand. It was shown that a fully human-like kinematic behaviour cannot be achieved if the TMC is simplified to a biaxial joint without compensation for the missing DoF. A quantitative evaluation of fingertip orientation was tested and found useful for TOT, but needs revision for object grasping as in the GRASP taxonomy. Regarding the use of soft materials, qualitative statements about minimal skin thickness and adjusting grip force to object size were obtained and options to modify the structural stiffness of the palm were explored. Notching the soft material between the bones was found to be highly effective in reducing the bending resistance, to the point where very thin cross-sections were prone to buckling. Removing the tendon insertion point further from the bone centre also lowered the structural stiffness, but the effect weakened with increasing distance. Angling the actuation force outwards facilitated the initiation of the palm flexion motion and reduced the compressive stress in the soft matrix. Based on those findings, a hybrid soft-rigid prototype was built with 3D-printed parts, which integrates a 3-DoF joint for the TMC and a compliant palm with embedded bones, providing longitudinal stability but axial flexibility. It performed noticeably better than the 2-DoF TMC model in the TOT but had no clear advantage in the GRASP taxonomy, which might partially be due to the way the test was implemented here. Suggestions for the tendon actuation were included in the design and offer opportunities for further development of the concept.

Future Work Proximate follow-up on this work should include size reduction, elaboration of the actuation system, and introduction of a control system. After all, as pointed out in the very beginning of this thesis, good kinematics are essential for a well-functioning hand, but are of no use without an appropriate control system. This relationship is demonstrated excellently by the human brain and the successive development of motor skills in babies and toddlers. On this note, a sensory system will also be necessary to provide environmental perception as well as proprioception as input to the control system. Specifically, to overcome some of the challenges of soft robotic structures, Hall sensors could be used in the TMC and HMC (fig. 5.1) for position sensing of the MCs, thus determining the shape of the deformable palm. The properties of the palm could be further investigated with more sophisticated FEM simulations. Ultimately, the degree of anthropomorphism can be increased. Palm compliance has been explored as a parameter of social acceptance in handshake scenarios for tele-presence robots by Arns, Laliberté, and Gosselin [63]. A similar study could be done with later stages of this hand to fine-tune the palm's properties. Finally, the bone-and-soft-tissue morphology is necessary, but not sufficient to convincingly imitate a human hand. Ueno et al. [12] have shown that the temperature is a crucial factor, but further parameters remain to be explored.

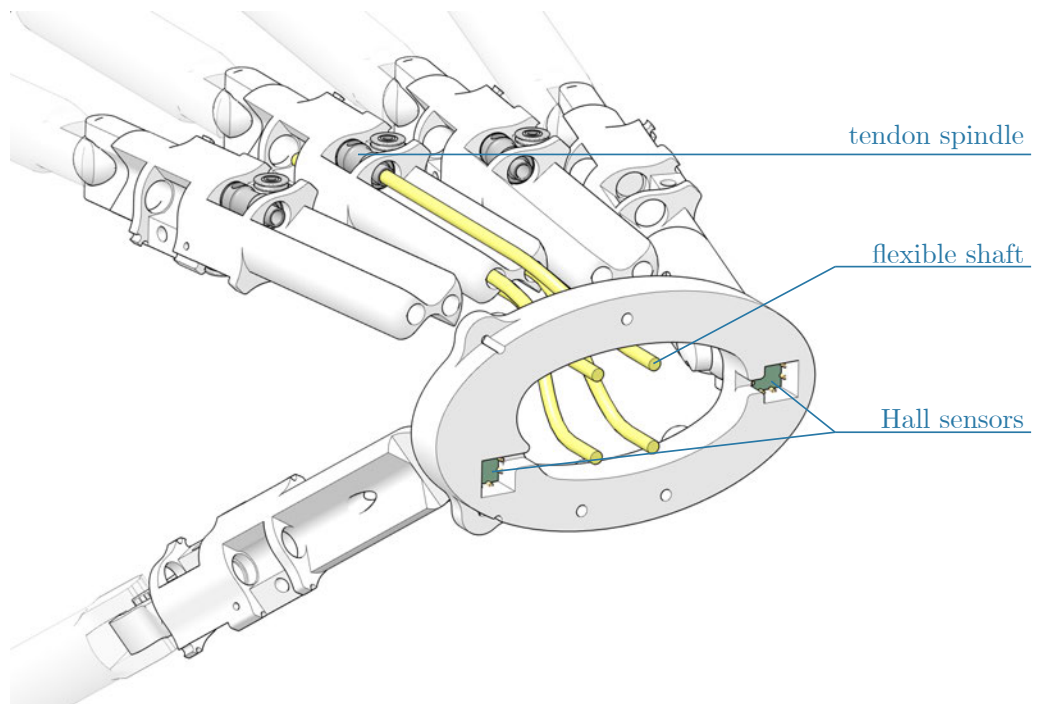


Figure 5.1 Suggested placement for Hall sensors in the TMC and HMC for position sensing of the bones and consequently, shape determination of the flexible palm.

Bibliography

- [1] A. I. Kapandji. *The Physiology of the Joints: The Upper Limb*. 7th ed. Handspring Publishing Limited, Apr. 2019.
- [2] J. R. Napier. *Hands*. Rev. ed. by Russell H. Tuttle. Princeton Science Library. Princeton (N.J.): Princeton university press, 1993.
- [3] C. Piazza et al. “A Century of Robotic Hands”. In: *Annual Review of Control, Robotics, and Autonomous Systems* 2. Volume 2, 2019 (May 2019), pp. 1–32. DOI: 10.1146/annurev-control-060117-105003.
- [4] J. Falco et al. “Grasping the Performance: Facilitating Replicable Performance Measures via Benchmarking and Standardized Methodologies”. In: *IEEE Robotics & Automation Magazine* 22.4 (Dec. 2015), pp. 125–136. DOI: 10.1109/MRA.2015.2460891.
- [5] A. G. Billard. “In Good Hands: A Case for Improving Robotic Dexterity”. In: *Science* 386.6727 (Dec. 2024), eadu2950. DOI: 10.1126/science.adu2950.
- [6] EDAN. URL: <https://www.dlr.de/de/rm/forschung/robotersysteme/mobile-plattformen/edan> (visited on 05/06/2025).
- [7] PROBO Robotics / Humanoid Robotics Österreich. URL: <https://www.probo-robotics.at> (visited on 12/06/2024).
- [8] L. Tian et al. “Towards Complex and Continuous Manipulation: A Gesture Based Anthropomorphic Robotic Hand Design”. In: *IEEE Robotics and Automation Letters* 6.3 (July 2021), pp. 5461–5468. DOI: 10.1109/LRA.2021.3076960.
- [9] F. Negrello et al. “Benchmarking Resilience of Artificial Hands”. In: *2019 International Conference on Robotics and Automation (ICRA)*. May 2019, pp. 8374–8380. DOI: 10.1109/ICRA.2019.8793793.
- [10] V. K. Nanayakkara et al. “The Role of Morphology of the Thumb in Anthropomorphic Grasping: A Review”. In: *Frontiers in Mechanical Engineering* 3 (June 2017). DOI: 10.3389/fmech.2017.00005.
- [11] J. Arcega et al. “The Human Touch: Is Modern Technology Decreasing the Value of Humanity in Patient Care?” In: *Critical Care Nursing Quarterly* 43.3 (July 2020), pp. 294–302. DOI: 10.1097/CNQ.0000000000000314.
- [12] A. Ueno et al. “Touching a Human or a Robot? Investigating Human-likeness of a Soft Warm Artificial Hand”. In: *2020 29th IEEE International Conference on Robot and Human Interactive Communication (RO-MAN)*. Aug. 2020, pp. 14–20. DOI: 10.1109/RO-MAN47096.2020.9223523.
- [13] M. Grebenstein. “Approaching Human Performance: The Functionality Driven Awiwi Robot Hand”. PhD thesis. ETH Zurich, 2012.
- [14] D. Rus and M. T. Tolley. “Design, Fabrication and Control of Soft Robots”. In: *Nature* 521.7553 (May 2015), pp. 467–475. DOI: 10.1038/nature14543.

- [15] M. W. Marzke, K. L. Wullstein, and S. F. Viegas. “Evolution of the Power (“Squeeze”) Grip and Its Morphological Correlates in Hominids”. In: *American Journal of Physical Anthropology* 89.3 (1992), pp. 283–298. DOI: 10.1002/ajpa.1330890303.
- [16] M. Grebenstein et al. “The Hand of the DLR Hand Arm System: Designed for Interaction”. In: *The International Journal of Robotics Research* 31.13 (Nov. 2012), pp. 1531–1555. DOI: 10.1177/0278364912459209.
- [17] D. A. Neumann and T. Bielefeld. “The Carpometacarpal Joint of the Thumb: Stability, Deformity, and Therapeutic Intervention”. In: *Journal of Orthopaedic & Sports Physical Therapy* 33.7 (July 2003), pp. 386–399. DOI: 10.2519/jospt.2003.33.7.386.
- [18] S. N. Robinovitch and J. Chiu. “Surface Stiffness Affects Impact Force during a Fall on the Outstretched Hand”. In: *Journal of Orthopaedic Research* 16.3 (1998), pp. 309–313. DOI: 10.1002/jor.1100160306.
- [19] R. S. Rohde, J. J. Crisco, and S. W. Wolfe. “The Advantage of Throwing the First Stone: How Understanding the Evolutionary Demands of Homo Sapiens Is Helping Us Understand Carpal Motion:” in: *American Academy of Orthopaedic Surgeon* 18.1 (Jan. 2010), pp. 51–58. DOI: 10.5435/00124635-201001000-00007.
- [20] T. L. Kivell et al. “Form, Function and Evolution of the Human Hand”. In: *American Journal of Biological Anthropology* 181.S76 (2023), pp. 6–57. DOI: 10.1002/ajpa.24667.
- [21] A. M. Dollar and R. D. Howe. “The Highly Adaptive SDM Hand: Design and Performance Evaluation”. In: *The International Journal of Robotics Research* 29.5 (Apr. 2010), pp. 585–597. DOI: 10.1177/0278364909360852.
- [22] A. M. Dollar. “Design Principles for Robust Grasping in Unstructured Environments”. PhD thesis. Cambridge, Massachusetts: Harvard University, Oct. 2006.
- [23] R. Deimel and O. Brock. “A Novel Type of Compliant and Underactuated Robotic Hand for Dexterous Grasping”. In: *The International Journal of Robotics Research* 35.1-3 (Jan. 2016), pp. 161–185. DOI: 10.1177/0278364915592961.
- [24] K. Ghazi-Zahedi et al. “Morphological Computation: The Good, the Bad, and the Ugly”. In: *2017 IEEE/RSJ International Conference on Intelligent Robots and Systems (IROS)*. Sept. 2017, pp. 464–469. DOI: 10.1109/IROS.2017.8202194.
- [25] S. D. Gollob et al. “A Multi-Material, Anthropomorphic Metacarpophalangeal Joint With Abduction and Adduction Actuated by Soft Artificial Muscles”. In: *IEEE Robotics and Automation Letters* 7.3 (July 2022), pp. 5882–5887. DOI: 10.1109/LRA.2022.3161714.
- [26] L. Tian et al. “Fast 3D Modeling of Prosthetic Robotic Hands Based on a Multi-Layer Deformable Design”. In: *International Journal of Bioprinting* 8.1 (Sept. 2021), p. 406. DOI: 10.18063/ijb.v8i1.406.
- [27] C. della Santina et al. “Toward Dexterous Manipulation With Augmented Adaptive Synergies: The Pisa/IIT SoftHand 2”. In: *IEEE Transactions on Robotics* 34.5 (Oct. 2018), pp. 1141–1156. DOI: 10.1109/TR0.2018.2830407.
- [28] E. Todorov and Z. Xu. “Design of a Highly Biomimetic Anthropomorphic Robotic Hand towards Artificial Limb Regeneration”. In: *2016 IEEE International Conference on Robotics and Automation (ICRA)*. Stockholm, Sweden: IEEE, May 2016, pp. 3485–3492. DOI: 10.1109/ICRA.2016.7487528.

- [29] C. Konnaris et al. “EthoHand: A Dexterous Robotic Hand with Ball-Joint Thumb Enables Complex in-Hand Object Manipulation”. In: *2016 6th IEEE International Conference on Biomedical Robotics and Biomechatronics (BioRob)*. June 2016, pp. 1154–1159. DOI: 10.1109/BIOROB.2016.7523787.
- [30] J.-M. Boisclair, T. Laliberté, and C. Gosselin. “On the Design of an Adaptable Underactuated Hand Using Rolling Contact Joints and an Articulated Palm”. In: *Journal of Mechanisms and Robotics* 15.5 (Oct. 2023), p. 051001. DOI: 10.1115/1.4055605.
- [31] P. Capsi-Morales et al. “Exploring the Role of Palm Concavity and Adaptability in Soft Synergistic Robotic Hands”. In: *IEEE Robotics and Automation Letters* 5.3 (July 2020), pp. 4703–4710. DOI: 10.1109/LRA.2020.3003257.
- [32] O. Shorthose et al. “Design of a 3D-Printed Soft Robotic Hand With Integrated Distributed Tactile Sensing”. In: *IEEE Robotics and Automation Letters* 7.2 (Apr. 2022), pp. 3945–3952. DOI: 10.1109/LRA.2022.3149037.
- [33] Y. Liu et al. “Dexterous All-Soft Hand (DASH) with Active Palm: Multi-Functional Soft Hand beyond Grasping”. In: *Smart Materials and Structures* 32.12 (Dec. 2023), p. 125012. DOI: 10.1088/1361-665X/ad07a3.
- [34] M. Pozzi et al. “Actuated Palms for Soft Robotic Hands: Review and Perspectives”. In: *IEEE/ASME Transactions on Mechatronics* 29.2 (Apr. 2024), pp. 902–912. DOI: 10.1109/TMECH.2023.3328944.
- [35] *Shadow Dexterous Hand Series - Research and Development Tool*. Sept. 2023. URL: <https://www.shadowrobot.com/dexterous-hand-series/> (visited on 09/11/2024).
- [36] *Technology*. URL: <https://www.sanctuary.ai/technology> (visited on 05/05/2025).
- [37] *Sanctuary AI Demonstrates In-Hand Manipulation Capabilities for Improved General Purpose Robot Dexterity*. URL: <https://www.sanctuary.ai/blog/sanctuary-ai-demonstrates-in-hand-manipulation-capabilities-for-improved-general-purpose-robot-dexterity> (visited on 05/05/2025).
- [38] L. B. Bridgwater et al. “The Robonaut 2 Hand - Designed to Do Work with Tools”. In: *2012 IEEE International Conference on Robotics and Automation*. May 2012, pp. 3425–3430. DOI: 10.1109/ICRA.2012.6224772.
- [39] *Figure*. URL: https://www.figure.ai/?trk=article-ssr-frontend-pulse%5C_little-text-block (visited on 05/05/2025).
- [40] *Product Catalog - iCub - IIT*. URL: <https://icub.iit.it/products/product-catalog> (visited on 05/05/2025).
- [41] A. Schmitz et al. “Design, Realization and Sensorization of the Dexterous iCub Hand”. In: *2010 10th IEEE-RAS International Conference on Humanoid Robots*. Dec. 2010, pp. 186–191. DOI: 10.1109/ICHR.2010.5686825.
- [42] *Nadine Social Robot – MIRALab*. URL: <https://www.miralab.ch/index.php/nadine-social-robot/> (visited on 05/05/2025).
- [43] *Nadine Intelligent Social Robot /.* URL: <https://nadineforgood.ch/> (visited on 05/05/2025).

- [44] L. Tian et al. “Design of a Flexible Articulated Robotic Hand for a Humanoid Robot”. In: *2019 IEEE-RAS 19th International Conference on Humanoid Robots (Humanoids)*. Oct. 2019, pp. 572–577. DOI: 10.1109/Humanoids43949.2019.9035025.
- [45] *Tesla Optimus Gen 3 Hand Revealed at RoboTaxi Event #shorts #roboticinnovation #robotics*. URL: <https://www.youtube.com/shorts/PkVqXKsosaAQ> (visited on 05/05/2025).
- [46] K. Zahedi and N. Ay. “Quantifying Morphological Computation”. In: *Entropy* 15.5 (May 2013), pp. 1887–1915. DOI: 10.3390/e15051887.
- [47] A. Schmitz et al. “Touch Sensors for Humanoid Hands”. In: *19th International Symposium in Robot and Human Interactive Communication*. Sept. 2010, pp. 691–697. DOI: 10.1109/ROMAN.2010.5598609.
- [48] *Shadow Hand*. URL: <https://robotsguide.com/robots/shadow> (visited on 05/05/2025).
- [49] T. Feix et al. “The GRASP Taxonomy of Human Grasp Types”. In: *IEEE Transactions on Human-Machine Systems* 46.1 (Feb. 2016), pp. 66–77. DOI: 10.1109/THMS.2015.2470657.
- [50] B. J. Tasi, M. Koller, and G. Cserey. “Design of the Anatomically Correct, Biomechatronic Hand”. In: *Computing Research Repository* (2019).
- [51] A. I. Kapandji. “Clinical Evaluation of the Thumb’s Opposition”. In: *Journal of Hand Therapy* 5.2 (Apr. 1992), pp. 102–106. DOI: 10.1016/S0894-1130(12)80265-1.
- [52] M. Tonkin. “Thumb Opposition: Its Definition and My Approach to Its Measurement”. In: *Journal of Hand Surgery (European Volume)* 45.3 (Mar. 2020), pp. 315–317. DOI: 10.1177/1753193419889504.
- [53] T. Buchner et al. “Replicating Human Anatomy with Vision Controlled Jetting – A Pneumatic Musculoskeletal Hand and Forearm”. In: *2024 IEEE 7th International Conference on Soft Robotics (RoboSoft)*. Apr. 2024, pp. 183–189. DOI: 10.1109/RoboSoft60065.2024.10522043.
- [54] T. Feix. *Human Grasping Database*. URL: <http://grasp.xief.net/> (visited on 12/13/2024).
- [55] H. Yang et al. “A Lightweight Prosthetic Hand with 19-DOF Dexterity and Human-Level Functions”. In: *Nature Communications* 16.1 (Jan. 2025), p. 955. DOI: 10.1038/s41467-025-56352-5.
- [56] S. Taniguchi et al. “Thumb Pronation Angle in Thumb Opposition Evaluated by the Nail Tip Angle of Thumb-Ring Finger Opposition”. In: *HAND* (Mar. 2024), p. 15589447241236249. DOI: 10.1177/15589447241236249.
- [57] Anti-Vibration Methods (Rubber) Co Ltd. *Stress-Strain Characteristics of Rubber & Elastomers*. June 2023. URL: <https://avmr.com/how-do-rubber-and-elastomer-compounds-deform-mechanically/> (visited on 11/12/2024).
- [58] S. Özgün. *Ansys Contact Types and Explanations*. Mar. 2021. URL: <https://www.mechead.com/contact-types-and-behaviours-in-ansys/> (visited on 04/25/2025).

- [59] *Overview of Materials for Silicone Rubber*. URL: <https://www.matweb.com/search/datasheet.aspx?matguid=cbe7a469897a47eda563816c86a73520%5C&ckck=1> (visited on 11/27/2024).
- [60] *Aluminum, Al*. URL: <https://www.matweb.com/search/datasheet.aspx?bassnum=AMEAL00> (visited on 04/28/2025).
- [61] T. Feix et al. “A Metric for Comparing the Anthropomorphic Motion Capability of Artificial Hands”. In: *IEEE Transactions on Robotics* 29.1 (Feb. 2013), pp. 82–93. DOI: 10.1109/TR0.2012.2217675.
- [62] Q. Zhang et al. “Finite Element Analysis of Silicone Rubber Based on Yeoh Constitutive Model and Ogden Constitutive Model”. In: *IOP Conference Series: Earth and Environmental Science* 714.3 (Mar. 2021), p. 032078. DOI: 10.1088/1755-1315/714/3/032078.
- [63] M. Arns, T. Laliberté, and C. Gosselin. “Design, Control and Experimental Validation of a Haptic Robotic Hand Performing Human-Robot Handshake with Human-like Agility”. In: *2017 IEEE/RSJ International Conference on Intelligent Robots and Systems (IROS)*. Sept. 2017, pp. 4626–4633. DOI: 10.1109/IROS.2017.8206333.
- [64] M. Chalon et al. “The Thumb: Guidelines for a Robotic Design”. In: *2010 IEEE/RSJ International Conference on Intelligent Robots and Systems*. Taipei: IEEE, Oct. 2010, pp. 5886–5893. DOI: 10.1109/IROS.2010.5650454.
- [65] M. Grebenstein et al. “A Method for Hand Kinematics Designers”. In: *1st International Conference on Applied Bionics and Biomechanics ICABB-2010*. Venice, Italy, 2010.
- [66] R. Hamilton and R. A. Dunsmuir. “Radiographic Assessment of the Relative Lengths of the Bones of the Fingers of the Human Hand”. In: *Journal of Hand Surgery* 27.6 (Dec. 2002), pp. 546–548. DOI: 10.1054/jhsb.2002.0822.
- [67] A. Aydinlioglu, F. Akpinar, and N. Tosun. “Mathematical Relations between the Lengths of the Metacarpal Bones and Phalanges: Surgical Significance”. In: *The Tohoku Journal of Experimental Medicine* 185.3 (1998), pp. 209–216. DOI: 10.1620/tjem.185.209.

Appendix

A Kinematic Model - Design and Construction

The purpose of the model was to investigate the thumb kinematics, specifically regarding the TMC, therefore most of the design focus was put on this joint. The conceptual basis for the model was the above-mentioned paper model by Kapandji, who described the TMC as a cardan joint, providing 2 DoF. The goal was to investigate the necessity of a more complex joint variant, i. e. which functionalities can and cannot be achieved by a 2-DoF joint. Therefore, the TMC in the kinematic model was also implemented as a cardan joint. Several key insights on how the TMC should be positioned were already available thanks to the extensive kinematic study carried out in [13]: Firstly, it should be displaced from the plane of the flat hand in palmar direction. To this was added from personal observation that it should be positioned, for lack of a more scientific description, “below” the index finger when the hand is shown in palmar view with the fingers pointing upwards. Further, Grebenstein [13] found that the first axis should be oriented towards the palm, but not intersect it anywhere close to the long finger MCPs. With this information, it was placed 10 mm from the palmar plane and at a shallow 3° angle, so that it would intersect the plane of the hand far distal to the MCPs (fig. 3.4b). The TMC’s second axis was chosen to be orthogonal to the first, with the MCP and IP axes parallel to that. These latter three are the parameters where twist and inclination could be fine tuned, but since that was not the aim of this study and the kinematic model was supposed to start out as general as possible, the three axes were left at their simplest version, i. e. orthogonal to the first TMC axis. The variations could be added back in to coordinate all parameters together in later stages.

With that information, the TMC placement was constrained around two spatial axes, leaving rotation around the third axis for variation. The component for the TMC can be screwed on and off for easy adjustment of the orientation or replacement by a different version. It is mounted on a gauge disk that locks in rotation steps of 15° . Its geometric neutral, as opposed to anatomic neutral position (cf. [1, p.271]), was set as shown in fig. 3.4c. This orientation is quite obviously poorly suited for opposing all fingers or performing a variety of grasps, so it was not one of the variations examined. Instead, as an educated guess, the rotation was set to $+30^\circ$, which matches Kapandji’s description that pure flexion from the anatomic neutral position brings the tip of the thumb in contact with the base of the little finger. From there, the joint was rotated one step upwards and one downwards to demonstrate the effects of either direction on the results of the evaluation metrics.

The carpus was approximated as a solid ellipse with a ratio of 1.5 of major to minor axis, so as to have a stable base for the rest of the hand. Since, in the biological hand, the movements of the carpal bones against each other are mainly relevant for wrist motion, this simplification should not affect the in-hand kinematics. To this base, the MCs of the long fingers are attached by a capsule made of the “Elastic 50A” resin. The capsule could be described as a double-sided ball-and-socket joint, a cross-section is shown in the bottom

left insert in fig. 3.4a. This design was mainly relevant to provide appropriate mobility in the HMC for palm flexion. Physiologically, the CMCs of the other long fingers decrease in mobility from slight in the ring finger to negligible in the index finger [1]. For the ring finger, the soft joint allows the MC to follow the palm flexion motion and thus create a continuous, natural arch. For the remaining two fingers, it was then merely a convenient attachment for easy assembly and disassembly of the model, the mobility aspect being subordinate here.

The lengths of the finger links and their exact ratios vary from person to person, as emphasised repeatedly in [13] and associated publications [16, 64, 65]. While studies on hand proportions can be found for specific groups of people, this grouping by profession or nationality introduces a bias for certain characteristics, e. g. army recruits likely tend to have more robust hands, whereas the physiology typical for Southeast-Asian women comes with more slender hands. Finding a universally representative average for human hand size, much less for specific parts of the hand, is all but impossible. However, optimisation of specific link lengths or exact joint locations is not productive, as emphasised by [13, p. 92], since the exact dimensions cover a wide range among human individuals without impairing functionality. More important than the absolute values are the proportions between the different parts. Two studies that at least did not explicitly concern themselves with specific groups of people are [66] and [67]. The data from [66] has previously been used for reference in [64], but provides information on neither the MCs nor the thumb, which can instead be gained from [67]. From their combined data, the approximate relations between the parts of the long fingers can be set up as follows:

$$\begin{aligned} PP &\approx MP + DP \\ MP &> \approx 0.5 \cdot PP \\ \frac{DP}{MP} &\approx \frac{3}{4} \\ PP + MP + DP &\approx 1.5 \cdot MC \end{aligned}$$

For the sake of modularity, all long fingers were modelled with the same length, which is not physiologically accurate, but will serve the purpose for a first approach and can be iterated upon in future versions of the model. Since these are only approximate relations, they cannot be solved as an equation system. Instead, an initial value was decided upon and then the relations were followed through to find all other values. The results were rounded to multiples of 5 for usability in model construction. For the initial value, the PP length was chosen to be 60 mm, which is a plausible value for a larger male hand, based on personal observation. With that starting point, the following set of values satisfies all relations:

$$\begin{aligned}
DP &= 25 \text{ mm} \\
MP &= 35 \text{ mm} \\
PP &= 60 \text{ mm} \\
MC &= 80 \text{ mm}
\end{aligned}$$

The thumb, having a different anatomy, requires a different set of relations, which can be derived from [67, tab. 5]. In the following notation, the index f is used for *long finger* and t for *thumb*:

$$\begin{aligned}
PP_f &\approx 1.5 \cdot PP_t \\
\frac{PP_t}{DP_t} &\approx \frac{4}{3} \\
PP_t + DP_t &\approx 1.15 \cdot MC_t
\end{aligned}$$

With the long fingers' PP length from above, this set is satisfied by the values:

$$\begin{aligned}
DP_t &= 30 \text{ mm} \\
PP_t &= 40 \text{ mm} \\
MC_t &= 60 \text{ mm}
\end{aligned}$$

Furthermore, the PP length of the long fingers was also used for the major axis of the carpal ellipse.

All hinge joints as well as the flexion axis of the MCPs were designed with a ratchet mechanism, so that they would keep their position passively without actuation. Being 3D-printed, the mechanism becomes loose rather quickly, but it does still help in making the model easier to handle. The hinge joints also include end stops to limit the RoM to roughly the values described in [1]. The abduction axis of the MCPs runs on smaller pins without the ratchet and is limited by the main body of the hinge meeting the top of the bone.

The strip of soft material in the palm has two functions: It keeps the MCs in place when at rest and allows them to form the palmar arch when moved accordingly. The HMC motion and thus the palmar flexion is an integral part of the human hand and occurs almost without deliberate actuation when performing the later stages of the TOT. It is therefore tied intrinsically to the test design, which makes it an important feature to be included in the kinematic model. The flexible resin was also used to print coverings to approximate the shape of fingertips, which makes the visual interpretation of fingertip contact easier and more intuitive.

B Evaluation Metrics

B.1 Kinematic Model

Total Opposition Test

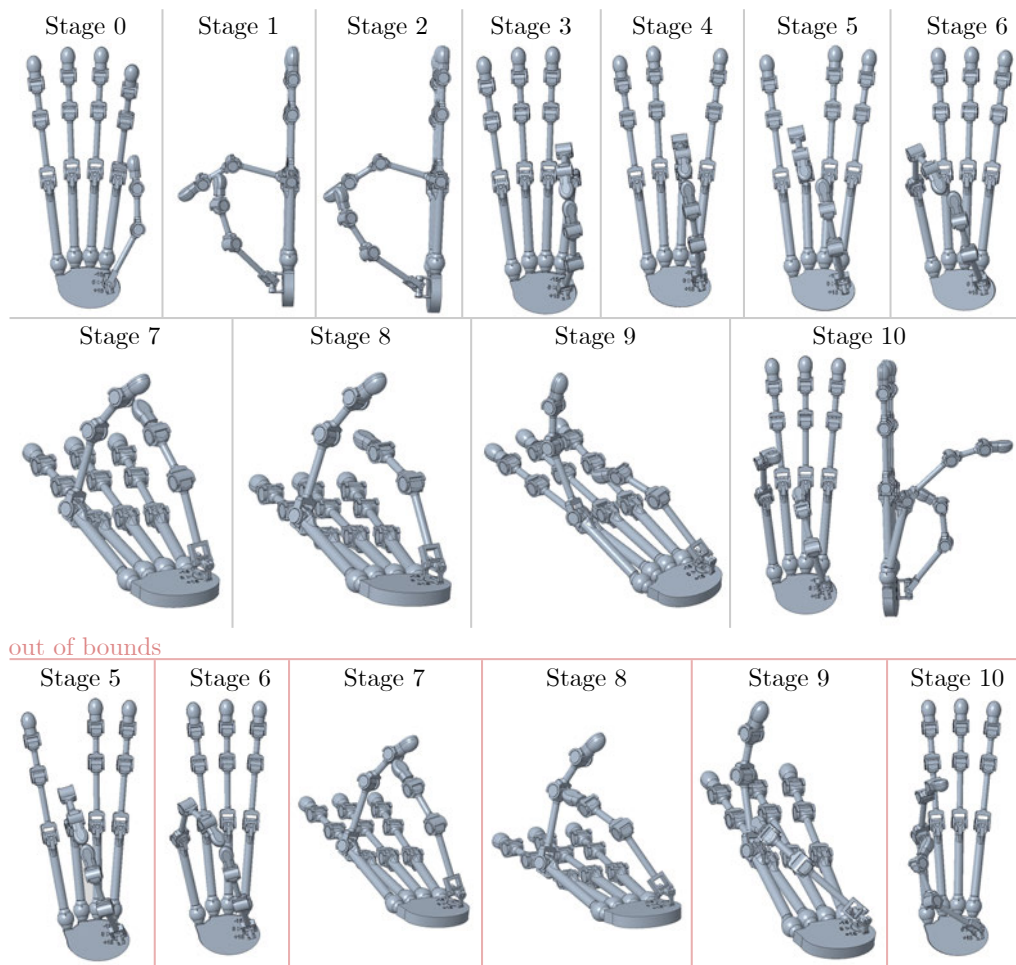


Figure B.1 All 11 stages of the Total Opposition Test performed on the kinematic model, with the TMC in 15° twist, simulated in CAD. Stages 5-10 could not be reached within the physiological joint limits, positions resulting from relaxed joint limits are shown in the bottom row. The postures for at least the last two stages are not anatomically plausible.

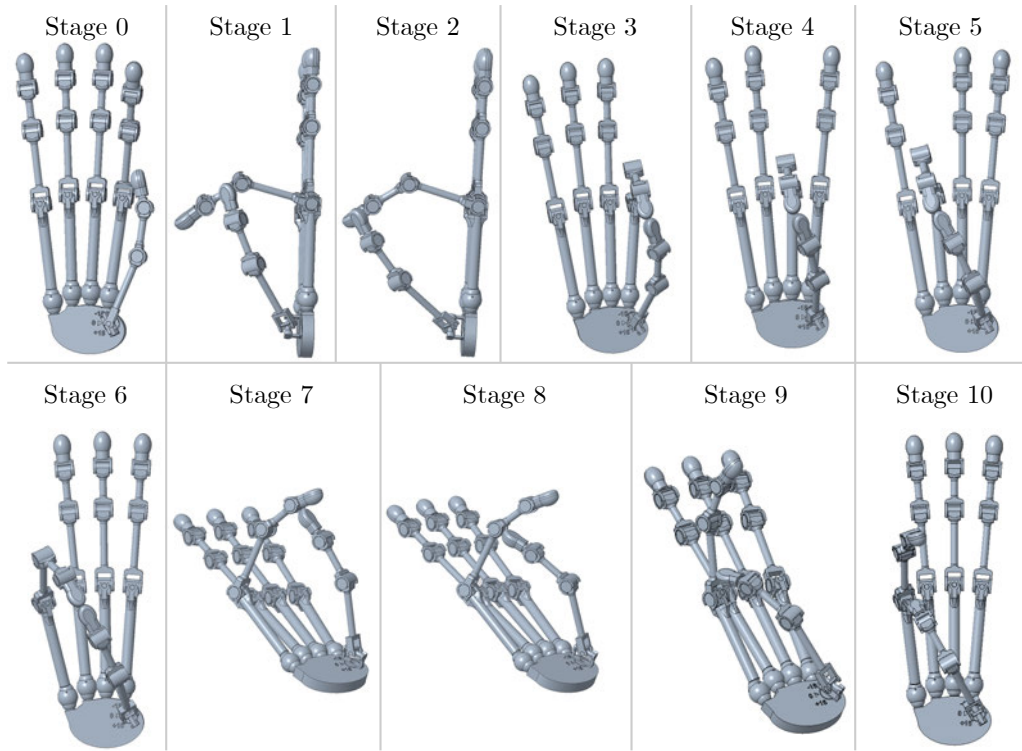


Figure B.2 All 11 stages of the Total Opposition Test performed on the kinematic model, with the TMC in 30° twist, simulated in CAD.

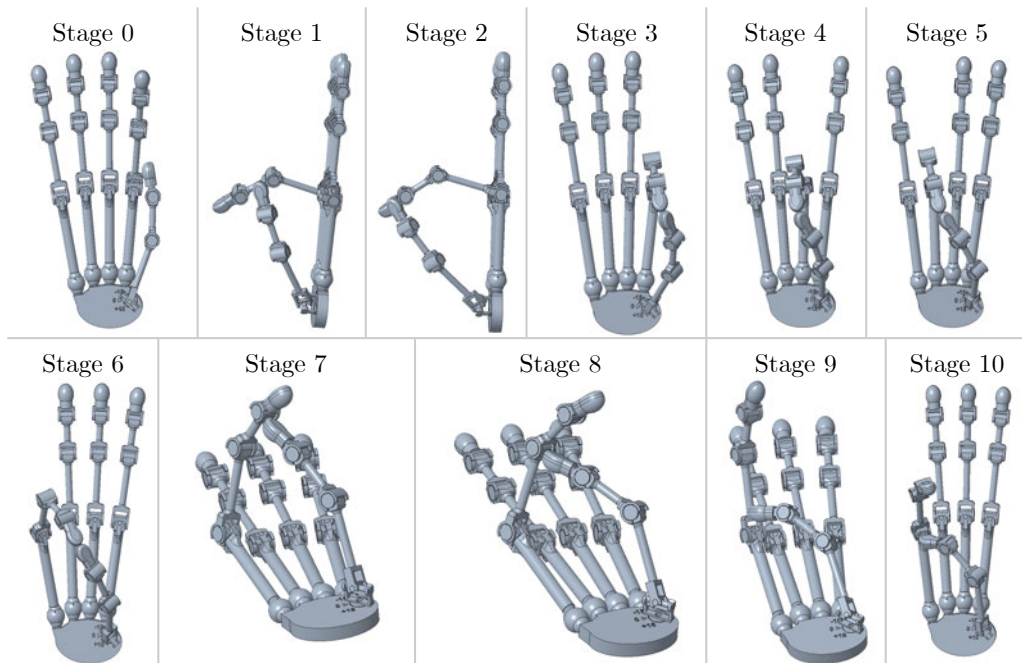


Figure B.3 All 11 stages of the Total Opposition Test performed on the kinematic model, with the TMC in 45° twist, simulated in CAD.

Automatic rotation Kapandji [1] uses a simple model of two paper strips folded and glued to form a series of hinges, s. fig. B.4 a. The first two hinges are orthogonal to each other and thus form a biaxial joint with axes 1 and 2 labelled in the drawing. If the yellow piece was left flat without any movement on axes 2–4 and only rotated around axis 1, it would be a rotation in plane. The flat side of the yellow piece, representing the pulp of the fingertip, would always face upwards. If the yellow piece was moved slightly upwards around axis 2 and again rotated around axis 1, it would describe a conical motion. The flat side would always be facing point O on the rotation axis, i. e. the tip of the cone, as indicated by the lower pair of white arrows in the drawing. If now the hinges 3 and 4 are taken into play, so that the flat side turns vertical, the motion becomes a full cylinder. The longitudinal axis of the last phalanx always stays parallel to axis 1 of the base joint. This, Kapandji claims, fully accounts for the pronation of the thumb and thus its opposition of the long fingers. The described behaviour was in fact observed in the kinematic model, but the model also makes clear why it is not sufficient to bring the thumb into proper opposition with each long finger. Depending on the orientation of the axis, the opposition works well for certain fingers, but not at all for others. This is exemplarily shown in the model with 15° TMC twist, s. fig. B.4 b. The thumb was underpronated, though within the tolerance limit, for the index finger, almost perfectly opposed the middle finger, and then turned into overpronation for the ring and little finger, for both of which the joint limits had to be exceeded. Especially for the little finger, it becomes clear that the thumb starts to turn away from the target once it passes the summit of its arc. In conclusion, Kapandji's model and corresponding explanation are not wrong, but also not sufficient to explain the thumb's opposition motion.

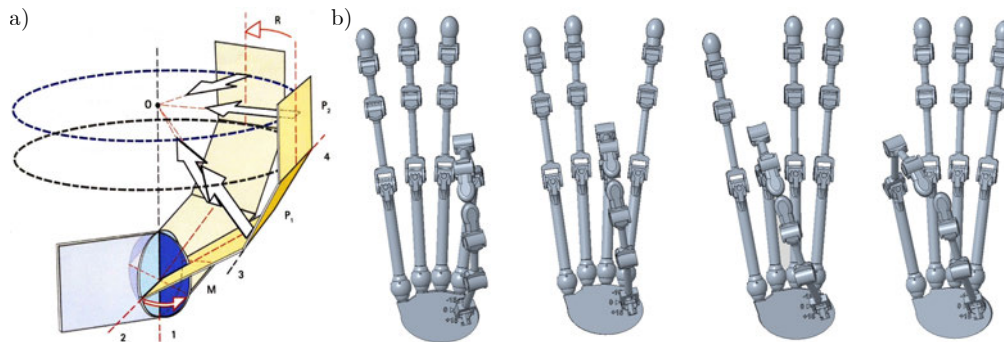


Figure B.4 Automatic rotation of the fingertip as an accessory movement of a biaxial joint, which Kapandji regards as the source of pronation in the thumb (left, drawing taken from [1]). This rotation was, in fact, observed in the Cardan joint of the kinematic model (right). But since the fingertip always faces the joint's rotation axis, as indicated in Kapandji's drawing, this motion is not sufficient to bring the thumb into proper opposition with all long fingers.

GRASP taxonomy

Object specifications:

- card: $85 \times 54 \times 1$ mm
- bottle cap: $d = 30$ mm, $h = 15$ mm
- coin: $d = 20$ mm, $h = 2$ mm
- pencil: $d = 10$ mm, $l = 150$ mm
- golf ball: $d = 43$ mm
- tennis ball: $d = 67$ mm

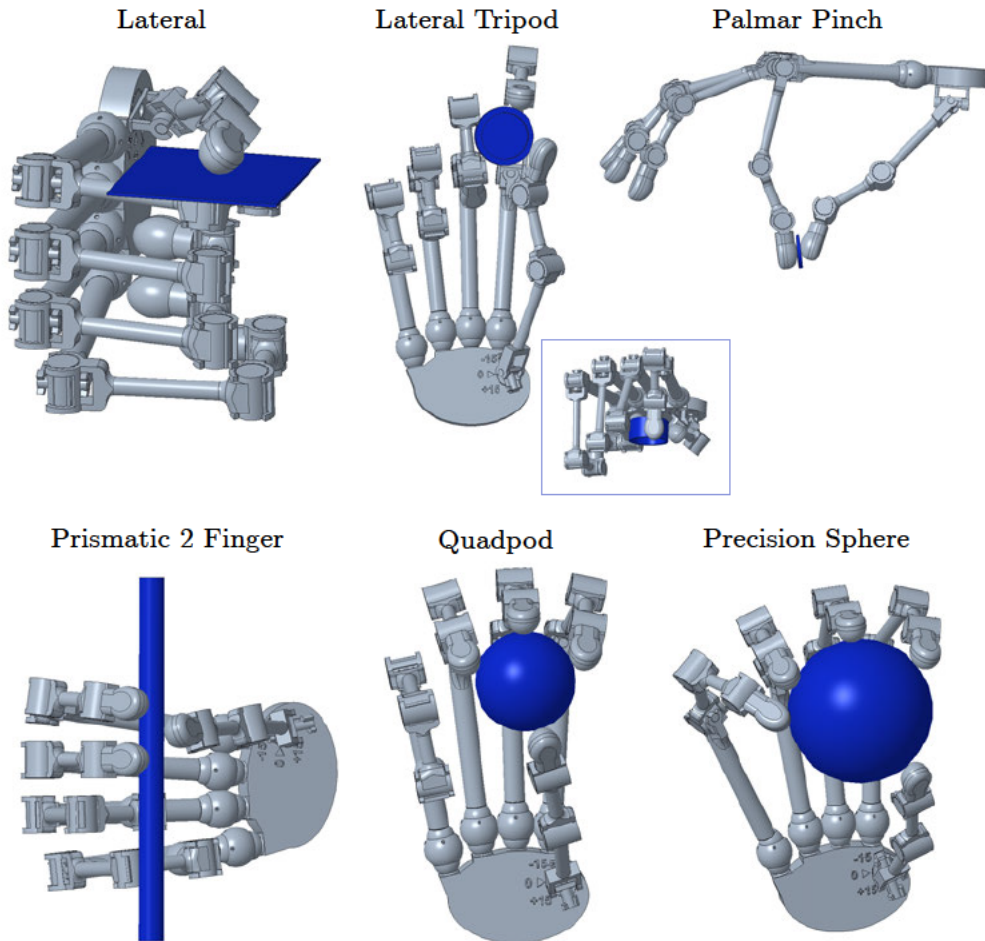


Figure B.5 Subset of the GRASP taxonomy performed on the kinematic model, with the TMC in $+15^\circ$ twist, simulated in CAD.

B.1 Kinematic Model

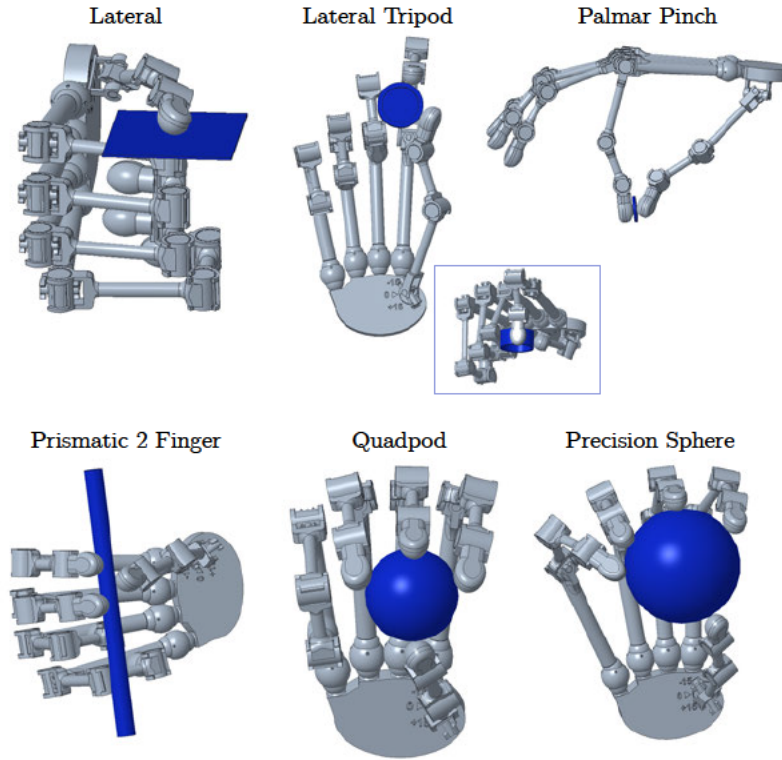


Figure B.6 Subset of the GRASP taxonomy performed on the kinematic model, with the TMC in $+30^\circ$ twist, simulated in CAD.

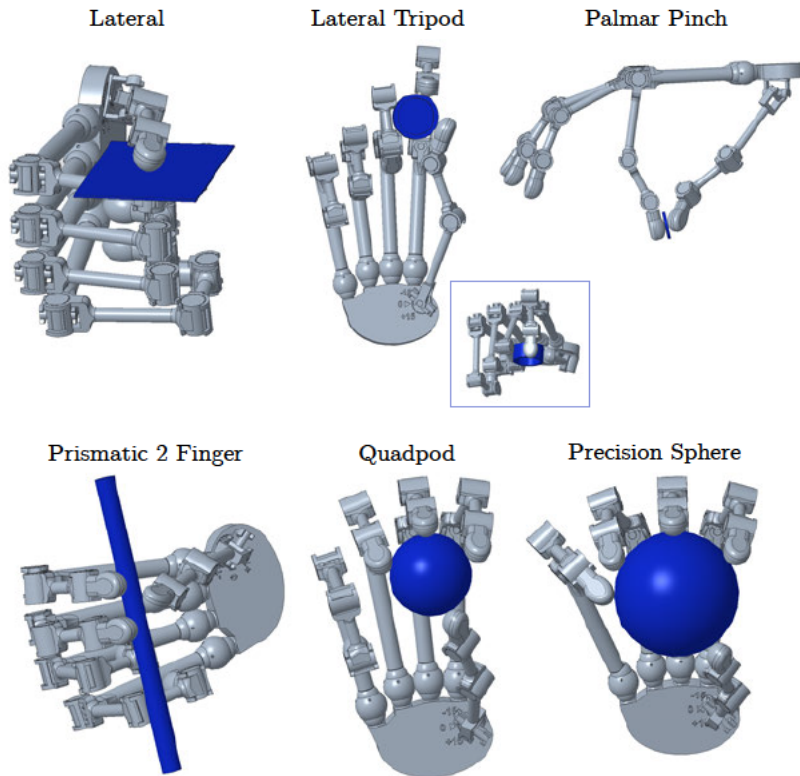


Figure B.7 Subset of the GRASP taxonomy performed on the kinematic model, with the TMC in $+45^\circ$ twist, simulated in CAD.

B.2 Prototype

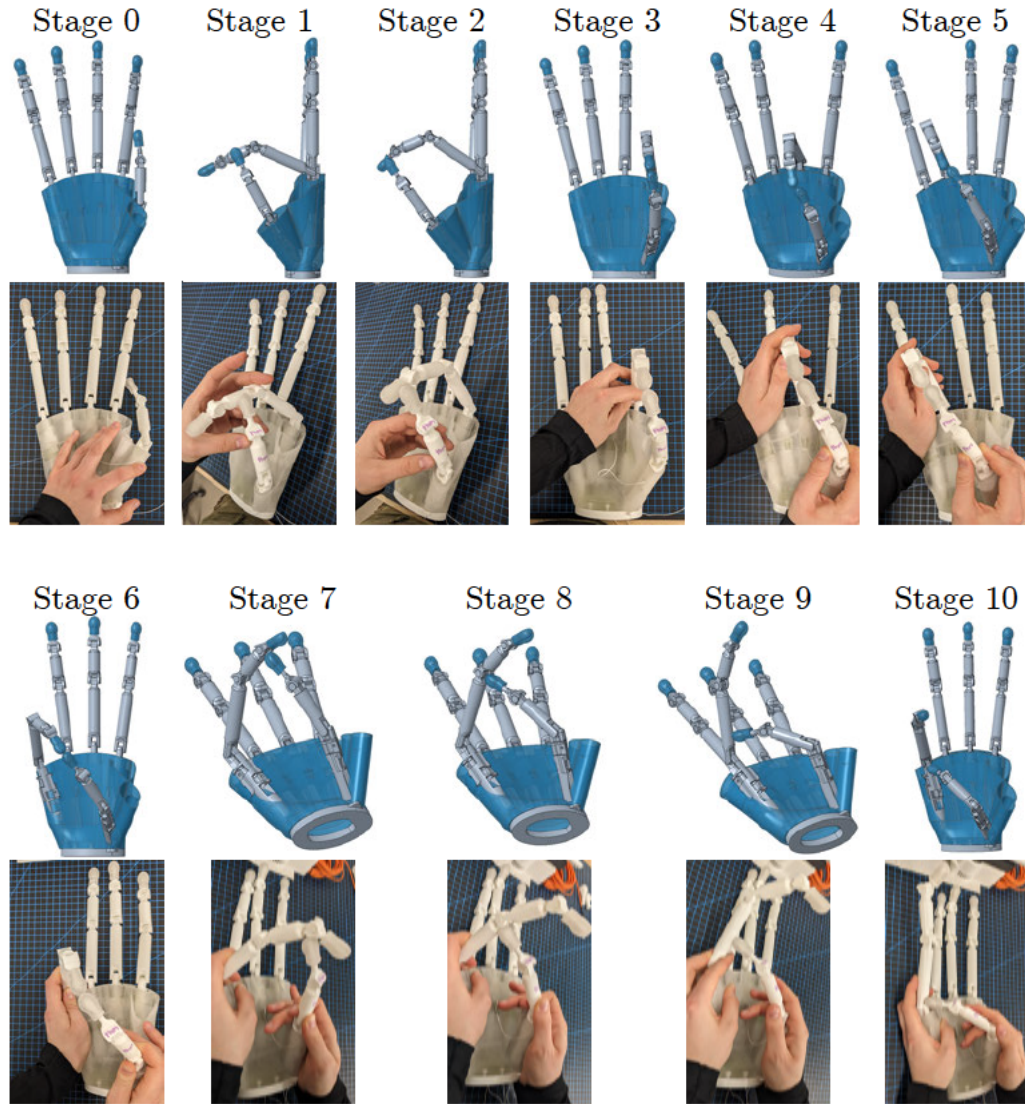


Figure B.8 All 11 stages of the Total Opposition Test performed on the final prototype, with the digital twin shown on top and the physical model on the bottom for each stage respectively. The simulation used for the digital model was limited to joint angles between bodies assumed as rigid and did not encompass deformation simulation, which is why the thumb and little finger move out of the blue part representing the soft material.

B.2 Prototype

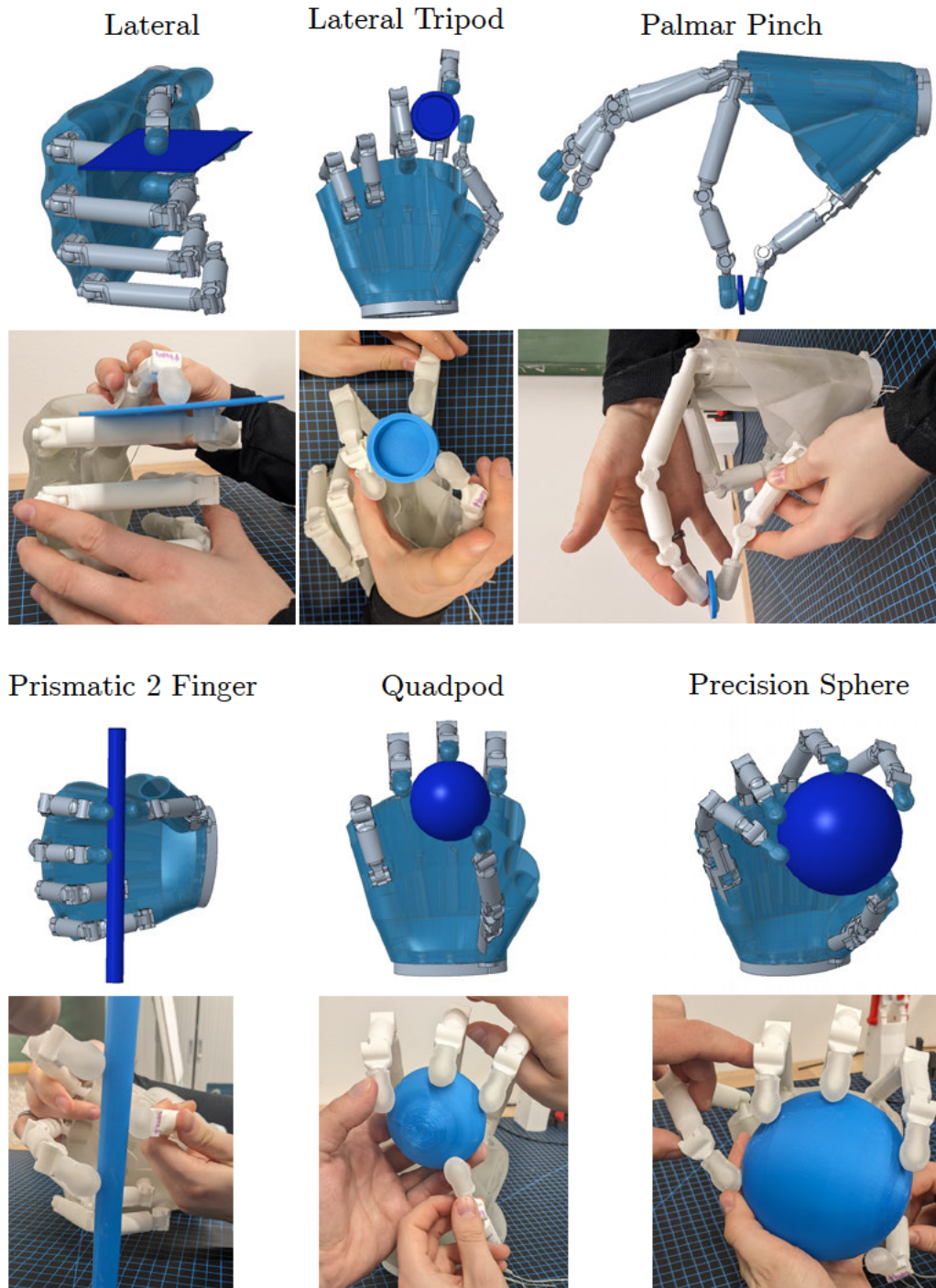


Figure B.9 Subset of the GRASP taxonomy performed on the final prototype, with the digital twin shown on top and the physical model on the bottom for each grasp respectively. The simulation used for the digital model was limited to joint angles between bodies assumed as rigid and did not encompass deformation simulation, which is why the thumb and little finger move out of the blue part representing the soft material.

C FEM - Ansys Settings

s. next page

Table C.1 Ansys simulation settings for the two partial studies on material and structural behaviour.

| setting | specification | pressure contact model | soft palm model |
|-----------------------|---------------|--|--|
| analysis type | | Static Structural, 2D | Static Structural, 2D |
| constant thickness | | 10 mm | 80 mm |
| material | soft | $E = 1.5 \text{ MPa}$ $\mu = 0.49$ $\sigma_{max} = 5 \text{ MPa}$ $\sigma_{y,tens} = 4.9 \text{ MPa}$ $\sigma_{y,comp} = 4.9 \text{ MPa}$ | <i>s. left</i> $\rho = 1.23 \text{ g cm}^{-3}$ |
| | rigid | $E = 10^9 \text{ MPa}$ $\mu = 0.49$ $\sigma_{max} = 460 \text{ MPa}$ $\sigma_{y,tens} = 250 \text{ MPa}$ $\sigma_{y,comp} = 250 \text{ MPa}$ | <i>s. left</i> $\rho = 2.6989 \text{ g cm}^{-3}$ |
| remote point | location | top edge of soft body | ring finger: (20 3.9) little finger: (40 3.9) |
| | behaviour | rigid | rigid |
| contact | type | frictionless | shared edges (bones) frictionless (ext. object) |
| | contact body | bottom edge of soft body | top edge(s) & arc of soft body |
| | target body | both arcs and flat line of rigid body | arc of ext. object |
| mesh | element order | automatic | linear |
| | element size | automatic | 0.7 mm |
| | edge sizing | 0.2 mm | 0.2 mm |
| nonlin. adapt. region | | — | on soft body, criterion “Mesh” |
| analysis settings | | 10 steps, large deflection on | 10 steps, large deflection on |
| boundary conditions | fixed support | face of rigid body | left vert. edge face of ext. object |
| | remote point | fixed in X & Z, remote displacement (<i>var.</i>) in Y, ramped linearly | remote force (-100 N) in X on little finger |

D Mechanical Drawing Tendon Spindle

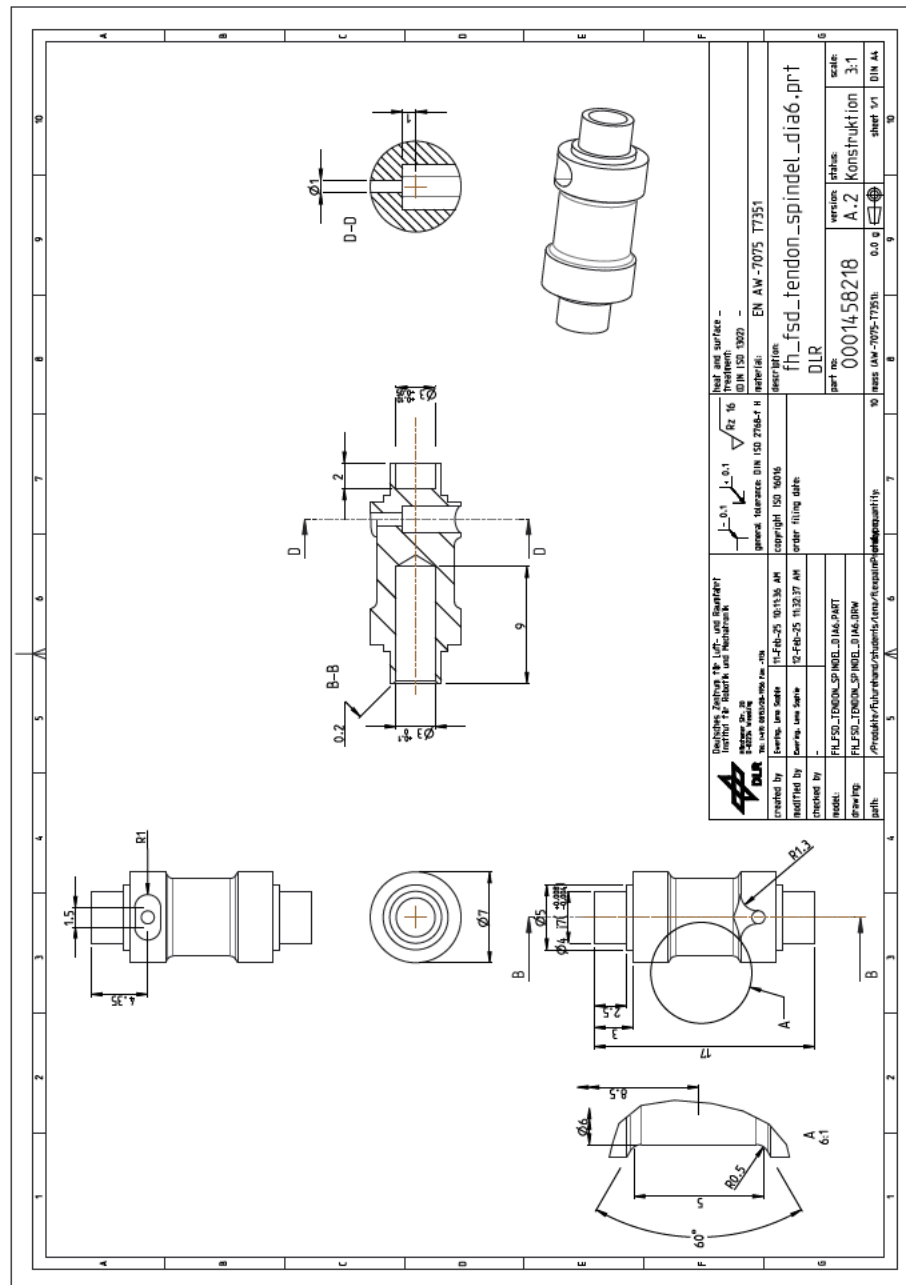


Figure D.1 Mechanical drawing of the custom tendon spindle.

E Digital Appendix

The supplementary material provided with the digital version of this thesis comprises:

- folder “datasheets”:
 - Elastic50A_resin_datasheet.pdf
 - Silicone40A_resin_datasheet.pdf
- folder “JupyterNotebooks”:
 - PyCB_Prototype.ipynb
 - PyCB_Stabmodell.ipynb
- folder “MatlabScripts”:
 - FlexiResin_materialdata.mlx
 - HertzianContact.mlx
 - HertzianCylinder.m
- folder “Prototype”:
 - Prototype_Demo_FingerAbduction.mp4

Affidavit

I hereby confirm that I am the author of the Master's thesis presented. I have written the thesis, as applied for previously, unassisted by others, using only the sources and references stated in the text.

May 30, 2025

LENA SOPHIE EWERING